Laboratory Bentonite Erosion Experiments in a Synthetic and a Natural Fracture

NWMO TR-2010-16 **July 2010**

Peter Vilks

Neil H. Miller

Atomic Energy of Canada Ltd.

nwmo
NUCLEAR WASTE MANAGEMENT ORGANIZATION
SOCIÉTÉ DE GESTION DES DÉCHETS NUCLÉAIRES

Nuclear Waste Management Organization
22 St. Clair Avenue East, 6th Floor
Toronto, Ontario
M4T 2S3
Canada

Tel: 416-934-9814
Web: www.nwmo.ca

Laboratory Bentonite Erosion Experiments in a Synthetic and a Natural Fracture

NWMO TR-2010-16

July 2010

Peter Vilks
Neil H. Miller
Atomic Energy of Canada Ltd.

ABSTRACT

Title: **Laboratory Bentonite Erosion Experiments in a Synthetic and a Natural Fracture**
Report No.: **NWMO TR-2010-16**
Author(s): Peter Vilks and Neil H. Miller
Company: Atomic Energy of Canada Ltd.
Date: July 2010

Abstract
A scenario being addressed as part of the long-term performance assessment for a Deep Geological Repository is the penetration of dilute glacial meltwater to depth followed by the possible erosion of bentonite from repository sealing systems and subsequent transport of colloids to the geosphere. Such a scenario also includes the presence of an adjacent, water-bearing fracture into which the bentonite can swell, forming a gel with an expanded structure. If this gel is able to release mobile bentonite colloids at a significant rate, the buffer may lose substantial mass and sorbed contaminants may be transported into the geosphere. A laboratory experimental program was initiated to address these issues. The initial experimental phase consisted of a series of mock-up tests in which bentonite erosion was studied in a synthetic transparent fracture. Sodium and calcium rich bentonite samples, spiked with fluorescent latex tracers, were used to make round 37 mm diameter plugs, which were installed in a borehole that intersected the fracture. When water (deionized or synthetic glacial meltwater) was introduced into the fracture, the expansion of the clay into the fracture was monitored under stagnant conditions and under the influence of two different flow rates. Colloid generation and transport was studied by monitoring the concentrations of bentonite and latex colloids eluted from the fracture. These tests investigated the effects of water chemistry, clay composition, fracture aperture, flow rate and fracture slope. In the second experimental phase a longer term bentonite erosion test was performed in a natural fracture within a Quarried Block to build on the results of the previous tests and to investigate the role of aperture variability on erosion and transport. This phase provided a link between a simple laboratory system and a field-scale natural system.

The results of the mock-up and Quarried Block tests found that bentonite erosion and colloid generation were affected by water composition, bentonite composition, fracture dip and fracture aperture. Significantly higher bentonite erosion and colloid generation rates were observed with deionized water than with synthetic glacial meltwater. Transported bentonite colloids formed erosion resistant deposits that altered flow properties within the fracture. Increasing flow rate did not affect the erosion rate of bentonite when stabilized by the presence of millimolar salt concentrations in the synthetic glacial meltwater. Fracture slopes had a significant influence over bentonite colloid transport and deposition, notably under no flow conditions. Under the influence of gravity, swelling bentonite migrated to the lower part of the fracture and larger colloids became trapped leaving transport mainly to the very small, 10 nm colloids.

The results of the Quarried Block tests indicate that in waters containing millimolar amounts of dissolved salts (representative of glacial melt water) the bentonite that expands into an open fracture is likely to form stable deposits that do not readily erode and release significant concentrations of bentonite colloids.

TABLE OF CONTENTS

LIST OF TABLES

Page

LIST OF FIGURES

Page

1. INTRODUCTION

When the compacted bentonite used in sealing systems of a Deep Geologic Repository (DGR) comes into contact with groundwater it will begin to swell and develop a swelling pressure because clay expansion is restricted by the geologic matrix. Without volume for expansion the compacted bentonite will likely remain stable. However, if open fractures are present the bentonite could expand into these openings without restrictions and reduce the local swelling pressure. The bentonite could continue to swell, until clay layers and particles begin to separate. The extent of swelling will depend upon the ionic strength of the groundwater, frictional resistance along fracture planes, and the balance between repulsive and attractive forces within the clay itself. Eventually, depending up these circumstances, the separation could be large enough to allow bentonite colloids to be released into suspension (SKB, 2006). These could be transported away by diffusion or advection, depending upon groundwater velocity.

In the presence of divalent and monovalent salt concentrations that exceed critical coagulation concentration (CCC) values, bentonite expansion is more limited than in dilute water and bentonite colloids are not stable. This would effectively reduce the release of mobile bentonite colloids. Fortunately the bentonite buffer in a DGR of spent nuclear fuel will likely be in contact with old saline groundwater, which is commonly present at depth in many geologic formations. However, recently there has been a concern that during periods of glacial retreat, dilute, low ionic strength glacial melt water could recharge a deep geologic formation. If the saline water surrounding the bentonite-based buffer and backfill material of the DGR was replaced with dilute water, the bentonite buffer may swell into adjacent fractures and incorporate so much water that the repulsive forces exceed the attractive forces between the montmorillonite sheets. This would release montmorillonite colloids for further transport. The continuous release of these colloids could eventually result in mass loss from the buffer and the transport of contaminants that could be attached to the released colloids. This issue has attracted previous interest and research efforts (Missana et al., 2003). Bentonite erosion studies have found that the potential of bentonite erosion is high when Ca^{2+} is depleted from the groundwater and clay system (Liu and Neretnieks 2006), and proposed that the mass loss from the buffer can be substantial if glacial melt water reaches a DGR. However, these studies were performed with deionized water as an approximation of glacial melt water. This may be a conservative approximation since glacial melt water (Brown, 2002) is likely to contain millimolar concentrations of monovalent and divalent cations which are likely to destabilize bentonite colloids and reduce colloid generation. Therefore, the understanding of colloid generation from bentonite buffer materials requires experimental conditions that include water with salinities more representative of natural conditions.

In 2008, an experimental program was initiated to gain understanding of the processes that would occur when compacted bentonite is contacted with relatively dilute water and allowed to expand into an open fracture. The processes of interest include bentonite expansion, the formation of a gel, colloid release from the gel, and subsequent transport of bentonite colloids. The extent of bentonite expansion would be determined by the swelling capacity of the clay, countered by frictional resistance, gel stabilization and the filling of the fracture aperture with erosion resistant mineral deposits from the expanding bentonite. The initial phase of the experimental program included a series of mock-up tests performed with a borehole intersecting a transparent synthetic fracture. A compacted bentonite plug was

installed in the borehole and allowed to expand into the fracture when water was introduced to the system through the fracture. These tests were designed to provide insight on plug expansion, gel propagation and erosion mechanisms, and to determine if fluorescent latex colloids mixed in the bentonite plug could serve as a suitable indicator of bentonite colloid behaviour in a fracture. The mock-up tests also investigated the effect of water composition, bentonite composition, water flow rate, and the effect of gravity induced by adding a slope to the fracture. The findings of the mock-up test were used for planning the second and final phase of the experimental program in which bentonite erosion was studied in a natural fracture in the Quarried Block. The Quarried Block experiments provided a link between the simple laboratory mock-up tests and the significantly more complicated field-scale tests associated, for example, with the Colloid Formation and Transport Project at the Grimsel Test Site in Switzerland (www.grimsel.com). The Quarried Block experiments improved on what was learned in the simpler mock-up tests by introducing complexities associated with the geosphere in the form of natural fracture geometries and larger scales. This report presents the results of the mock-up experiments and the more complex tests in the Quarried Block, aimed at evaluating the potential for bentonite erosion and colloid generation when dilute glacial melt water contacts a clay-based buffer.

2. MOCK-UP EXPERIMENTS IN SYNTHETIC FRACTURE

2.1 METHODS

The bentonite erosion tests were performed in a simple experimental system designed to study the behaviour of bentonite without the complications introduced by fracture aperture variability associated with a natural fracture. The experimental system (Figure 1) consisted of a clay plug installed within a transparent Lexan tube (38 mm ID) intended to simulate a borehole. Known quantities of fluorescent latex colloids (1 µm or 200 nm) were added to a slurry of bentonite to help quantify bentonite erosion. The clay was then dried and homogenized. The clay plugs were prepared by compressing dry bentonite in a form using a pressure of 15,000 psi. Each plug had a thickness of 1.0 cm and a diameter of 3.7 cm. The dry density of the compacted bentonite plugs was 2 g/cm^3 The Lexan tube was attached to a transparent synthetic fracture with an aperture of either 1 or 5 mm. The fracture dimensions were roughly 22 x 22 cm. The bentonite was emplaced in the borehole with its exposed surface approximately flush with the upper fracture surface. A rubber packer was used to stabilize the bentonite and prevent it from expanding upward into the borehole. Therefore, the swelling pressure generated during hydration was accommodated by bentonite movement into the fracture.

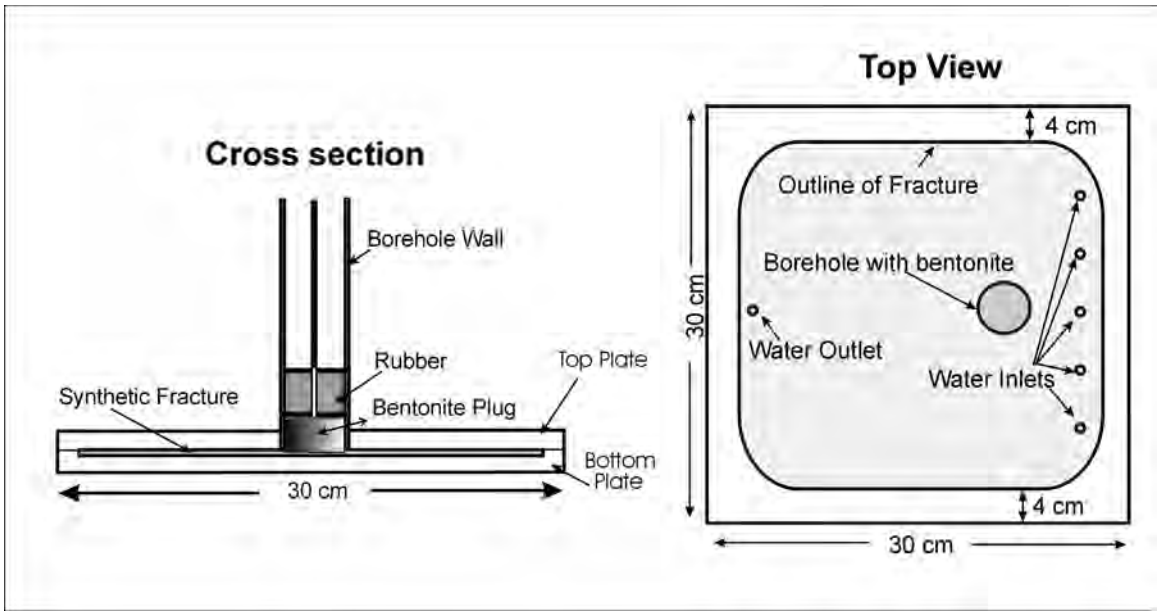

Figure 1: Schematic Diagram of the Synthetic Fracture and Bentonite Emplacement

The fracture system contained five water inlet holes close to the bentonite borehole and one outlet hole near the other side of the fracture. These holes were used to fill the fracture with water and to induce a flow through the system when required.

The waters used in the tests included deionized water and synthetic Grimsel water (Möri et al., 2003), with a composition of 0.001 mol/L NaCl and 0.0002 mol/L $CaCl_2$. In several tests the pH of the synthetic Grimsel water was maintained at 9.6, while in other tests it was not controlled to reduce the addition of extra salts. The bentonite compositions included a Wyoming bentonite (Osage), and Na-exchanged and Ca-exchanged bentonites prepared by Clay Technology, AB. The bentonites were spiked with fluorescing latex microspheres (either 1μm diameter blue or 220 nm diameter yellow-green), to act as a conservative indicator of bentonite erosion as these have been shown to be less susceptible to retention in fractures than bentonite colloid (Vilks and Miller, 2009). Latex microsphere concentrations varied between 0.5 and 4 mg latex per g clay for different plugs. After spiking, the bentonite was compacted to a density of 2 g/cm^3 to form a circular plug with a diameter of just under 38 mm, and a thickness of 10 mm.

Tests were initiated by filling the fracture with water. Progress of bentonite saturation and swelling was visually monitored from the top and bottom of the fracture by observing bentonite expansion into the fracture. The initial experimental conditions consisted of no flow for periods ranging from 23 to 430 h depending on the test. A low flow of 6 mL/h was then started for periods ranging from 72 to 170 h. During this time the bentonite was visually monitored and eluted water was sampled for bentonite and latex colloids. The flow rate was then increased to 44 mL/h for periods ranging from 24 to 50 h to test for flow velocity effects on bentonite erosion and transport. The 44 mL/h flow rate is the same rate that was used in the Quarried Block bentonite erosion test, and corresponds to flow

conditions that likely exceed what can be expected to occur at depth in fractured rock. The tests were terminated by stopping flow and opening the fracture for examination of the bentonite deposits on the bottom surface of the fracture.

The concentration of bentonite colloids eluted from the fracture was determined by light scattering using a Cary Eclipse fluorescence spectrophotometer (Varian) with the wavelength set to 280 nm. The detection limit of this technique was 0.01 mg/L bentonite. The concentrations of the latex colloids were determined by fluorescence. The Series 9200 MICROTRAC Ultrafine Particle Size Analyzer (UPA), manufactured by Leeds & Northrup and sold by Honeywell, was used to measure eluted bentonite colloid size distributions and to provide an additional estimate of colloid concentration. The UPA is a laser based instrument that quantifies particle sizes between 0.0038 and 6.5 μm by dynamic light scattering. The Doppler shift in the wavelength of light scattered from sample particles is measured and used to determine particle Brownian motion, which is related to particle size.

Once the fracture was opened for post-test analyses the clay extruded from the borehole and the clay deposits on the bottom fracture surface were examined under UV light to characterize the distribution of fluorescing latex colloids in the clay deposits. Clay samples were taken from various locations and analyzed by X-ray diffraction to determine the extent of mineral redistribution during the bentonite swelling and erosion processes
.

2.2 RESULTS

2.2.1 Bentonite Expansion in the Fracture

Table 1 gives a summary bentonite erosion tests performed in the synthetic fracture, along experimental parameters. The parameter(s) in bold highlight the change from the previous test. Figure 2 provides an example of the visual appearance of a bentonite erosion experiment at the time of its conclusion. This example shows the top view of Test 2, performed with Wyoming bentonite using a 5 mm fracture aperture and deionized water as the saturating solution. Figure 2A shows the view at the end of the test through the top of the fracture (bentonite plug and packer still in place), while Figure 2B shows the same view with the fracture top removed. In this test the bentonite plug was fully saturated with water and was still firm enough to keep its form after the synthetic borehole was removed. During the water saturation period the bentonite had expanded into the fracture, filling the entire 5 mm fracture aperture close to the borehole. The edge of the expanded bentonite is clearly visible as a shoulder. This shoulder was elongated in the direction of water flow, implying preferential upstream erosion. The elongation only became apparent after a flow field had been established. The shoulder of the expanded clay was characterized by an erosion slope containing a light coloured region which was bordered by a dark ring. The distribution pattern of darker minerals radiating outward from the dark ring suggests that bentonite was eroded by gravity from the edge of the shoulder, and was transported away by density flows, resulting in mineral separations. The dark ring is depleted in montmorillonite, leaving a residual enriched in muscovite and biotite.

Table 1: Summary of Bentonite Erosion Tests in Synthetic Fracture

Test	Parameters
Test 2	Wyoming bentonite with 1 μm blue latex Deionized water 5 mm aperture
Test 4	Wyoming bentonite with **220 nm yellow-green latex** **Grimsel water** 5 mm aperture
Test 5	Wyoming bentonite with 220 nm yellow-green latex Grimsel water **1 mm aperture**
Test 6	**Ca montmorillonite** with 220 nm yellow-green latex Grimsel water 1 mm aperture
Test 7	Wyoming bentonite with 220 nm yellow-green latex Grimsel water 1 mm aperture **fracture dips 15^0**
Test 8	**Na montmorillonite** with 220 nm yellow-green latex Grimsel water 1 mm aperture latex fracture dips 15^0

N.B. Test 1 is not listed as it was a trial run for the test set-up. Test 3 is not listed as it was abandoned due to placement problem with the bentonite plug leading to anomalous behaviour.

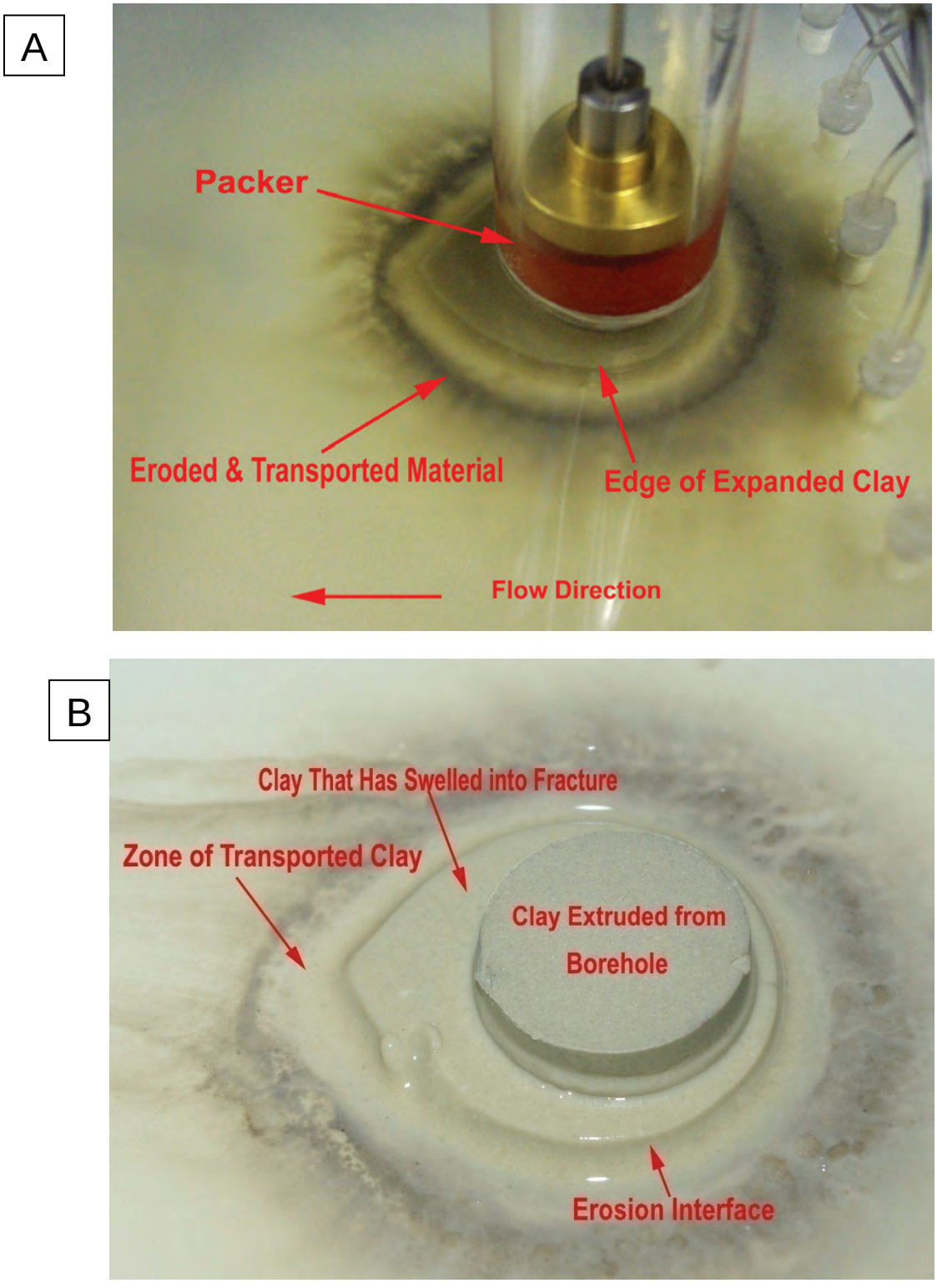

Figure 2: Top View of Bentonite Plug at the Completion of an Experiment Showing the View (A) Before the Fracture is Opened and (B) After Fracture Top is Removed.

Figure 3 shows the views of Test 2, at various times, through the bottom of the fracture. The advantage of the bottom views is that it is easier to monitor and quantify bentonite expansion and erosion by using the borehole outline as a reference. A red ring in each photo marks the dimensions of the clay plug before saturation with water. The dimensions and orientation of the ring were established before bentonite expansion began. The top four images (for times of 6, 23, 30 and 120 h since the test start) illustrate the progress of bentonite expansion during no flow conditions. The last two images illustrate the effects of low flow and high flow conditions, respectively. The expansion behaviour in Test 2 and in the subsequent tests are discussed later and illustrated in Figure 11. The features visible in Figure 2 are also apparent in the bottom view of the last image in Figure 3. The edge of the expanded clay shoulder appears as a dark green region bounded by a light ring which corresponds to a relatively thin layer of bentonite. The ring of dark residual minerals is significantly broader on the right side, close to the water inlet ports. During the period of no flow the bentonite appeared to expand uniformly in all directions, displaying the shoulder surrounded by the light ring of thin bentonite deposits. As flow was initiated the montmorillonite in the expanded clay was preferentially eroded on the side close to the inlet ports. The asymmetric pattern of the expanded bentonite is thought to be caused by differences in upstream and downstream erosion rates. The fracture outside of the dark residual ring appears cloudy due to the dispersion of bentonite colloids throughout the fracture.

Test 3 was performed in a 5 mm aperture fracture with Wyoming bentonite spiked with 220 nm yellow-green latex. However, the deionized water was replaced with a synthetic Grimsel water, with millimolar concentrations of NaCl and $CaCl_2$. Unfortunately, in this test the bentonite plug did not make a tight fit within the borehole and slipped out while the fracture was being closed. This left a gap between the bentonite and the borehole wall which allowed faster access of water to the entire bentonite mass. As a result the experiment was repeated as Test 4, using a bentonite plug with much better fit that did not fall out of the borehole. The expansion behavior of Test 4 is illustrated in Figure 4. Test 4 displayed a stable border that was not affected by flow. The expanded bentonite shoulder was symmetrical and was bordered by a rim of a white, relatively thin bentonite deposit (Figure 4). A very thin ring of residual dark mineral deposits and the symmetrical form of the expanded bentonite indicate minimal bentonite erosion. This is supported by the lack of suspended bentonite in the fracture waters, which appeared remarkably clear, compared to Test 2.

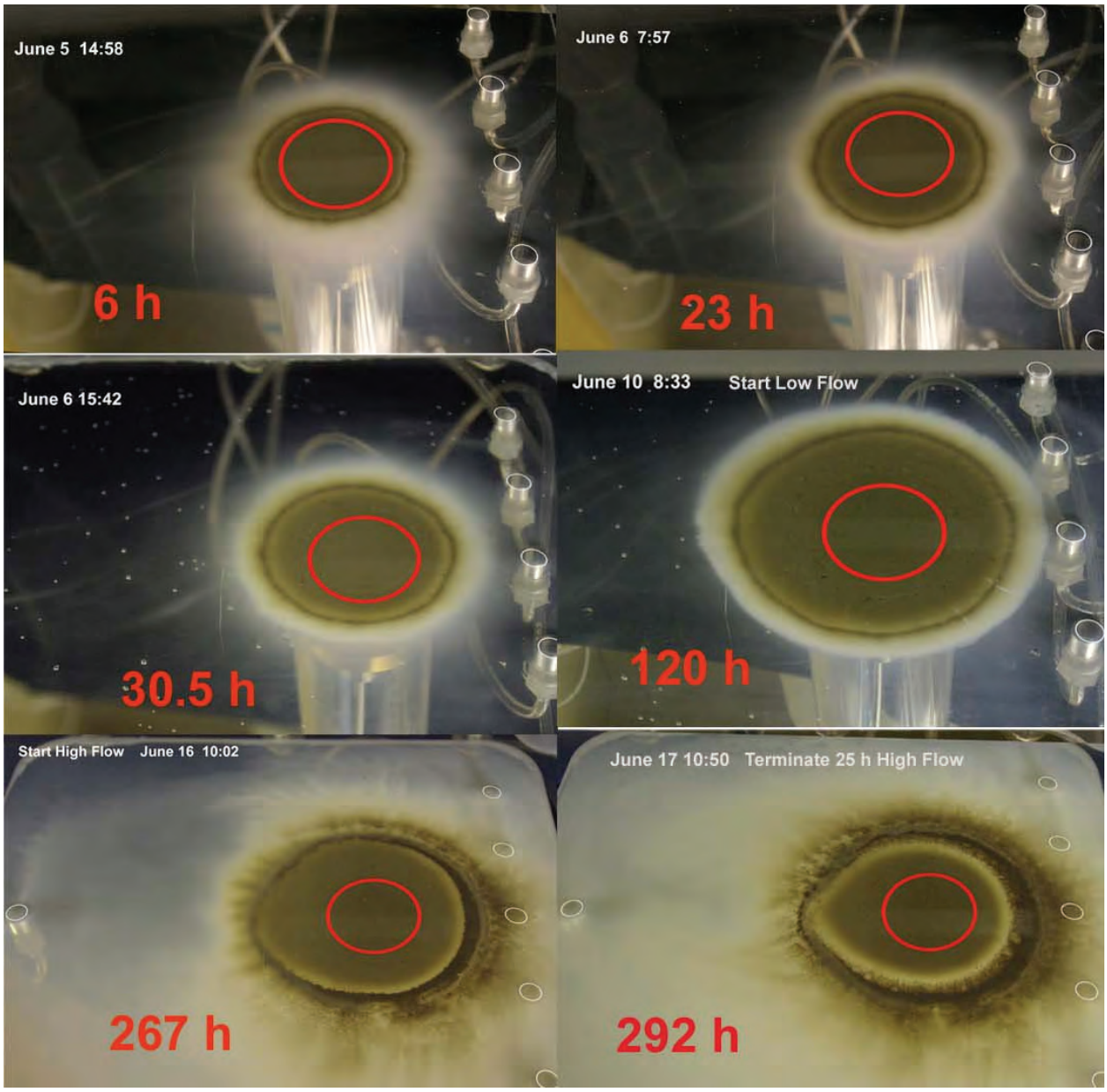

Figure 3: Underside Views of Test 2 at Various Times

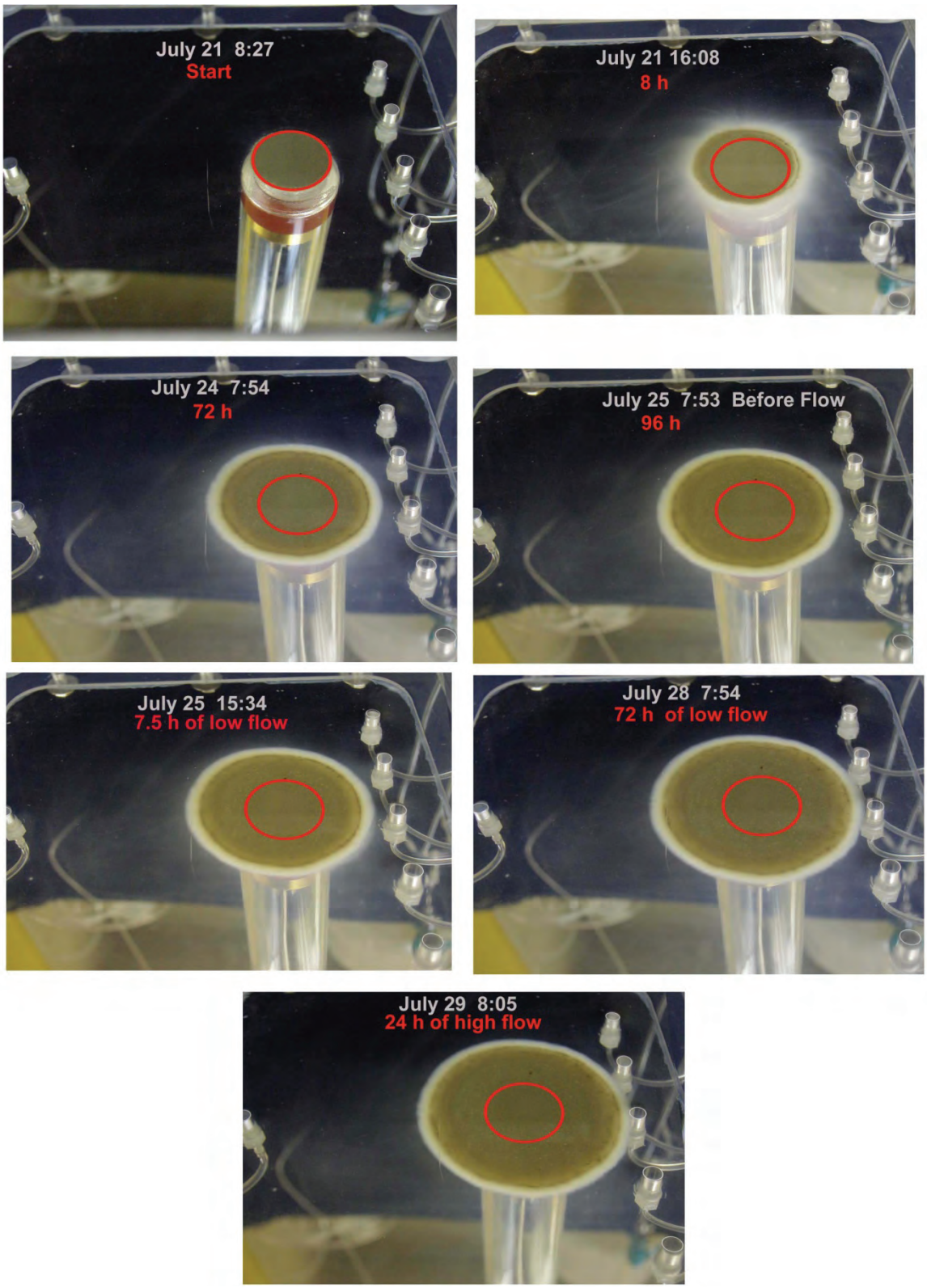

Figure 4: Underside Views of Test 4 at Various Times.

Test 5 was similar to Test 4, except that the fracture aperture was reduced from 5 mm to 1 mm. With a smaller aperture one would expect more resistance to bentonite expansion from the fracture walls. However, with a smaller aperture the same flow rate would produce a higher flow velocity within the fracture. This could increase the potential for colloid transport and bentonite erosion by exposing bentonite to higher hydraulic shear forces . The experimental progress of Test 5 is illustrated in Figure 5. Bentonite expansion appeared to be symmetrical, but was not as extensive as for the experiment with a 5 mm aperture (Figure 4). Within 7.5 hours of starting the low flow phase, the white rim on the downstream side began to develop a jagged appearance indicative of the onset of erosion. Bentonite erosion continued to progress throughout the test, producing clear signs at the finish in the form of a thin line of residual minerals on the left side and cloudy streams being focused on the outlet port. Despite evidence of bentonite erosion, the water throughout most of the fracture remained clear and apparently relatively free of colloids.

Test 6 was performed with similar conditions to Test 5, except that the Wyoming bentonite was replaced with a Ca-exchanged montmorillonite. Since the divalent Ca reduces the negative, repulsive charge on the faces of the clay sheets more effectively than monovalent Na, one can expect that the physical properties of the Ca-montmorillonite would be different from those of Wyoming bentonite. For example, after compaction with the same force, the density of the Ca-montmorillonite was lower by 9 percent, and the Ca-montmorillonite released small sand sized particles when contacted with water. This became readily apparent when the fracture was filled with water. At the time of filling the fracture was in a vertical position and was filled from below via the inlet ports. A downward cascade of particles toward the inlet ports was observed as soon as the montmorillonite was immersed in the filling solution. This behavior was not observed in previous tests with Na-rich bentonite. Figure 6 illustrates the progress of Test 6. Note on the right side the cascade and accumulation of fallen montmorillonite particles which were deposited at the time of fracture filling. The Ca-montmorillonite did not expand into the fracture as a cohesive mass. Instead, the clay expansion into the fracture appeared to be more in the form of a debris flow. In Figure 6 one can see several radiating grooves in the expanded clay that suggest the existence of empty spaces surrounded by debris flows. These grooves may have started to form at the end of the no-flow period and became distinct after flow was initiated. When the fracture was opened at the end of the experiment the distinct shoulder of the expanded bentonite (seen in the previous tests) was absent. The clay in the borehole was not held together as a continuous mass, and did not display the well defined extruded form visible following Test 2 with Wyoming bentonite (Figure 2B). If it was not for the sedimentation of clay particles while the fracture was filled with water, the expansion of clay around the borehole would have been symmetrical. The clarity of the water in the fracture and the lack any residual mineral separations suggest that colloid generation from the Ca-montmorillonite was minimal.

In Test 7 the fracture was tilted 15 degrees perpendicular to the flow direction to evaluate the effect of fracture dip on bentonite erosion and transport. Since the dip was perpendicular to flow direction, down-slope movement of bentonite is likely to reduce the mass of colloids reaching the outlet port. Had the dip been in the direction of flow, one would expect enhanced transport to the outlet port. Note that the fracture dip in the Quarried Block is also 15 degrees. The fracture aperture was 1 mm and the clay plug was made from Wyoming bentonite. The results are illustrated in Figure 7, with the fracture dipping to the top of the photo. Small amounts of bentonite erosion and transport down

slope were noted after 21 hours of no flow saturation and continued for up to 72 h of no flow conditions. The extensive pattern of bentonite erosion and deposition down slope was developed during the period of low flow. The erosion pattern was characterized by montmorillonite loss from the bentonite shoulder, leaving behind a residual band of dark minerals on the down slope side. The downward migration of bentonite is evidenced by fingering clay deposits that are orientated down slope with an influence from flow direction. After 96 h of low flow conditions a significant portion of the bentonite deposits appeared to be fixed on the fracture surface. When the flow was increased the erosion pattern was modified to a minor extent, mainly in the form of erosion from the up slope side of the bentonite shoulder. The observation that more than half of the down slope deposits were fixed during high flow conditions was rather surprising, and prompted an investigation of flow properties in the fracture using a coloured dye (Figure 8). The results of the dye study revealed that flow was concentrated in the upslope region of the fracture that was free of bentonite deposits.

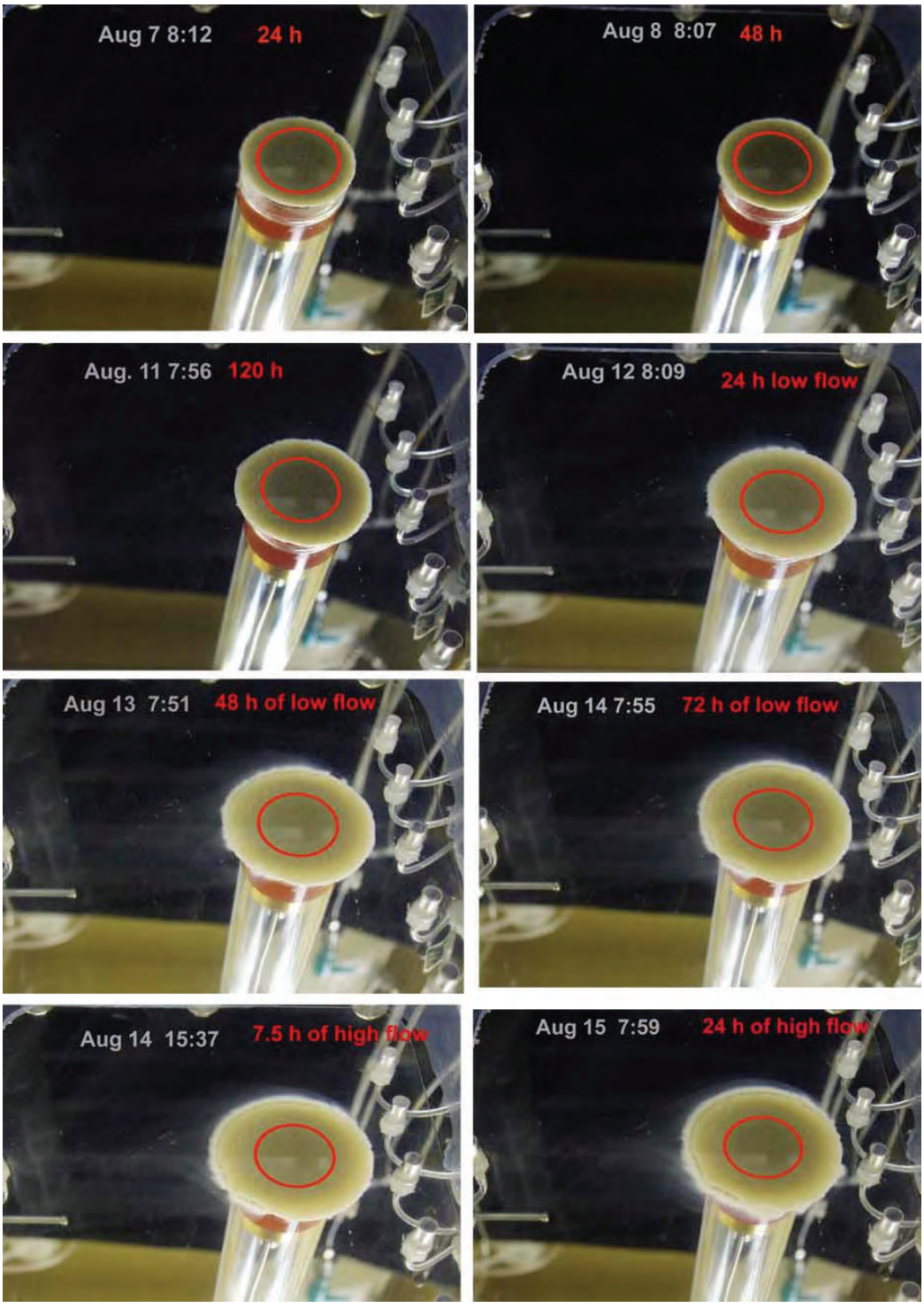

Figure 5: Underside View of Test 5 at Various Times.

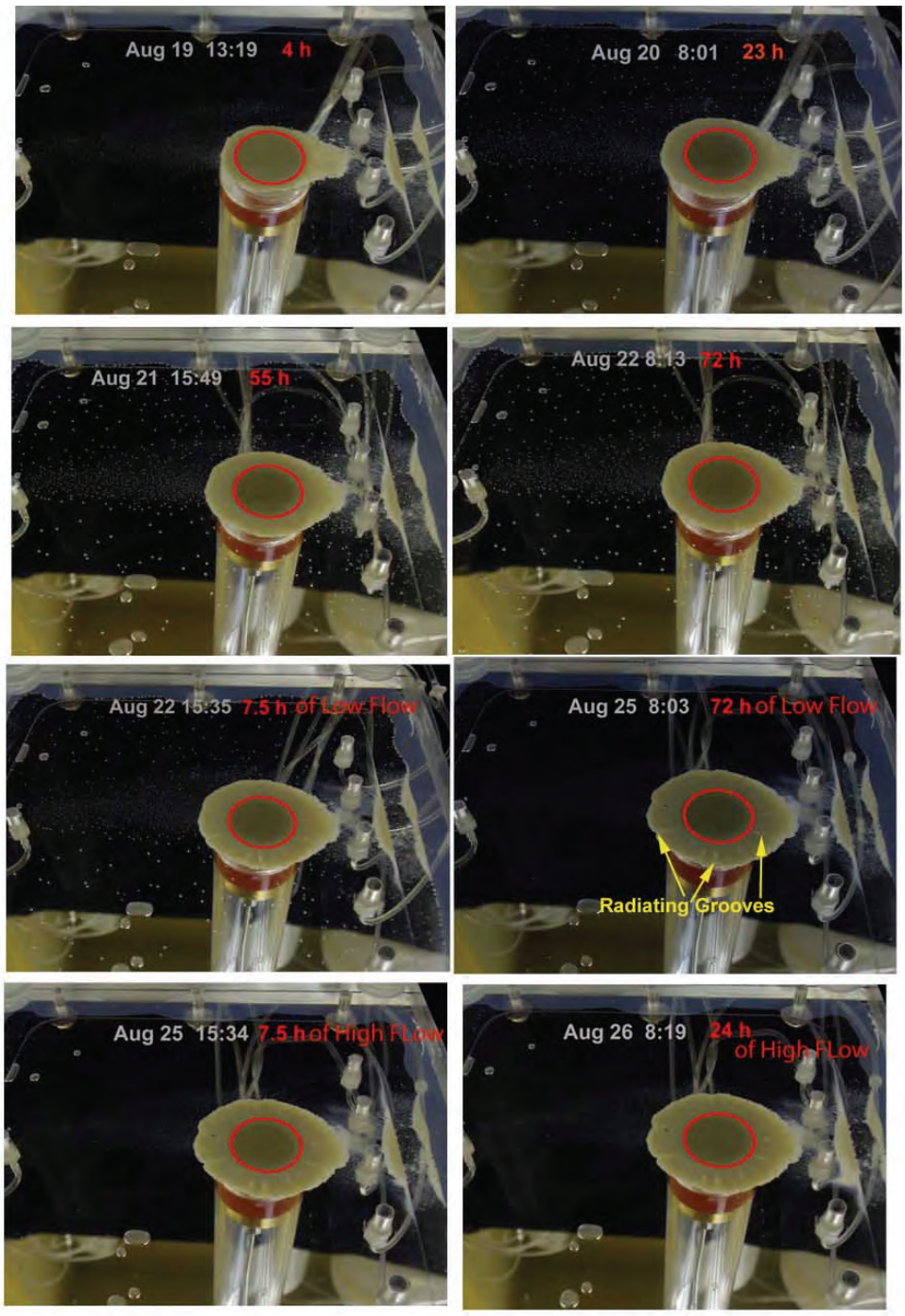

Figure 6: Underside View of Test 6 at Various Times.

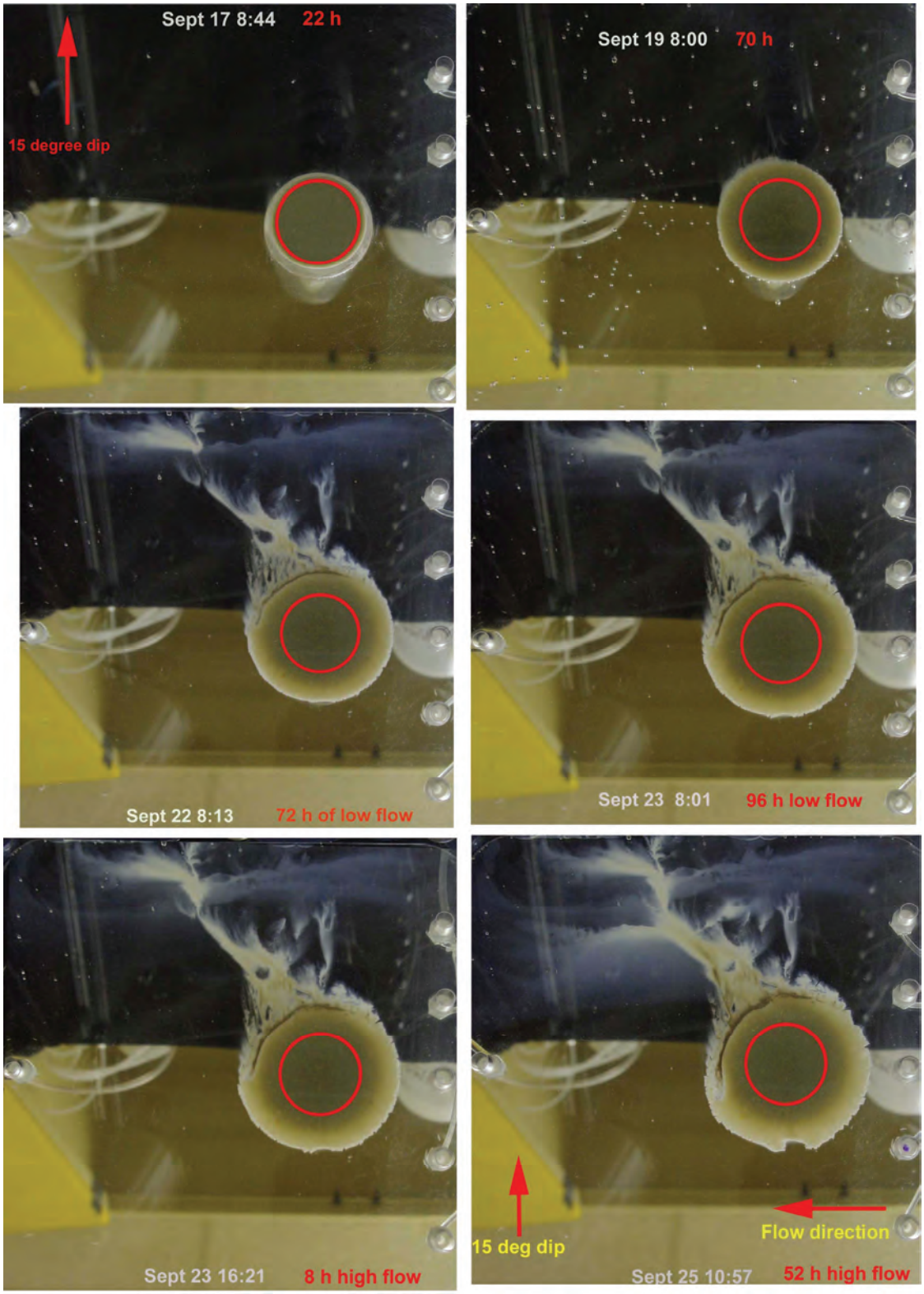

Figure 7: Underside View of Test 7 at Various Times.

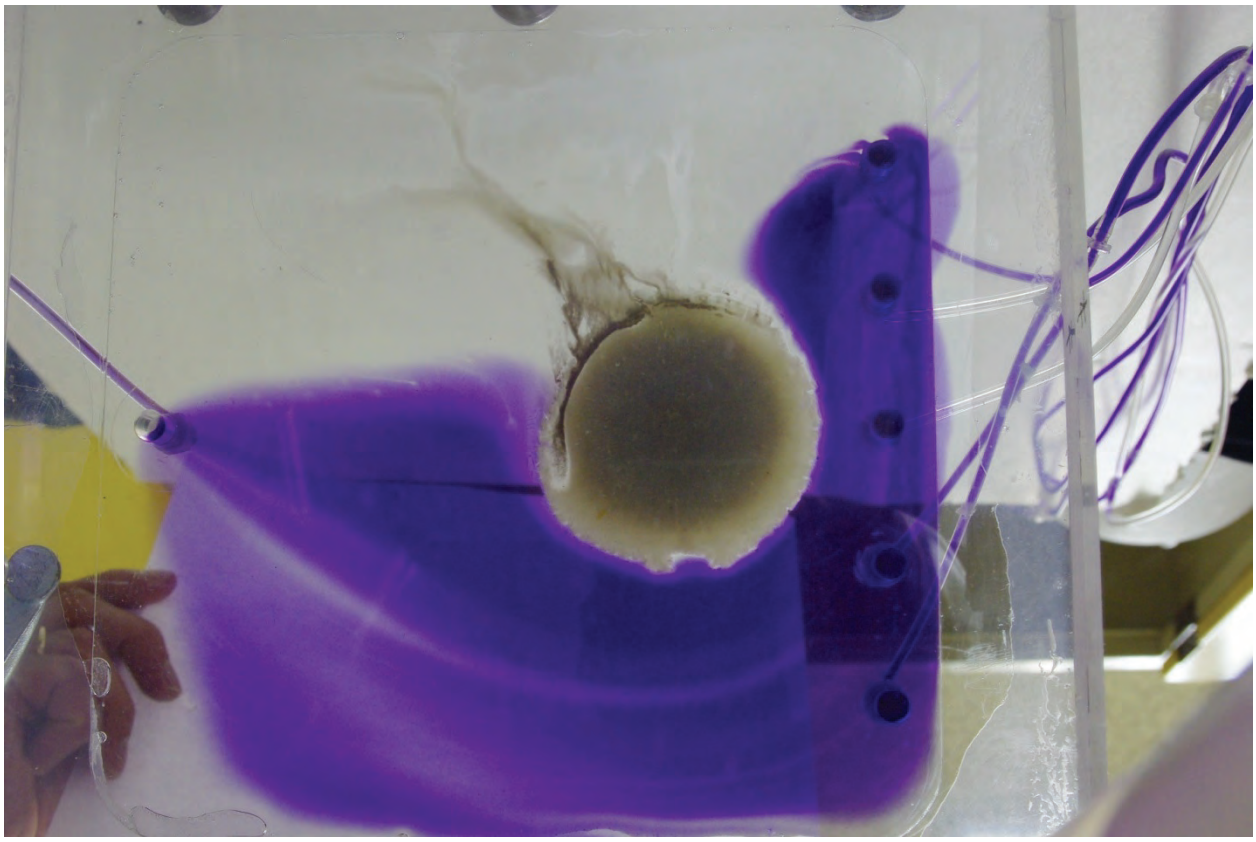

Figure 8: Dye Test at the Completion of Test 7 Showing that the Down Slope Bentonite Deposits Have Diverted All Flow to the Up Slope Part of the Fracture.

Test 8 was also performed by applying a 15 degree dip to the fracture. Synthetic, Na-exchanged montmorillonite was used and the experimental time period was twice that used in Test 7. The behaviour of the Na-exchanged bentonite was expected to be similar to that of Wyoming bentonite as the latter's composition includes 75% Na-montmorillonite as well as 15% quartz, 5% to 8% feldspar and 1% calcite (Lajudie et al., 1995. Figure 9 illustrates clay behaviour in Test 8. Montmorillonite erosion and transport down the fracture dip under the influence of gravity was observed after 21 h of no flow conditions. The transport was evidenced in the form of thin streamlines, coming mainly from the left side of the bentonite plug. After 117 h of no flow conditions, small clay strips with lengths of 1 to 6 mm were also observed moving down slope. At this point bentonite build up began to occur along the bottom edge of the fracture. By 360 h the clay build up along the bottom fracture edge continued, but most of the clay strips were fixed. Clay strips close to the expanding clay were fixed firmly enough not to be moved by the expanding clay. After 432 h of no flow conditions, most of the clay deposits appeared to be fixed. The establishment of low flow and high flow conditions had virtually no impact on the montmorillonite deposition pattern established during stagnant conditions, which lasted 4 times longer than in the previous test. At the end of the test a dye tracer (Figure 10) was used to show that flow was occurring preferentially in the up slope part of the fracture. This again indicates that bentonite deposition had altered flow conditions, directing most of the flow to more open regions of the fracture that were free of clay deposits. Residual mineral deposits were not observed in this test because the starting clay was a purified montmorillonite lacking the darker accessory minerals.

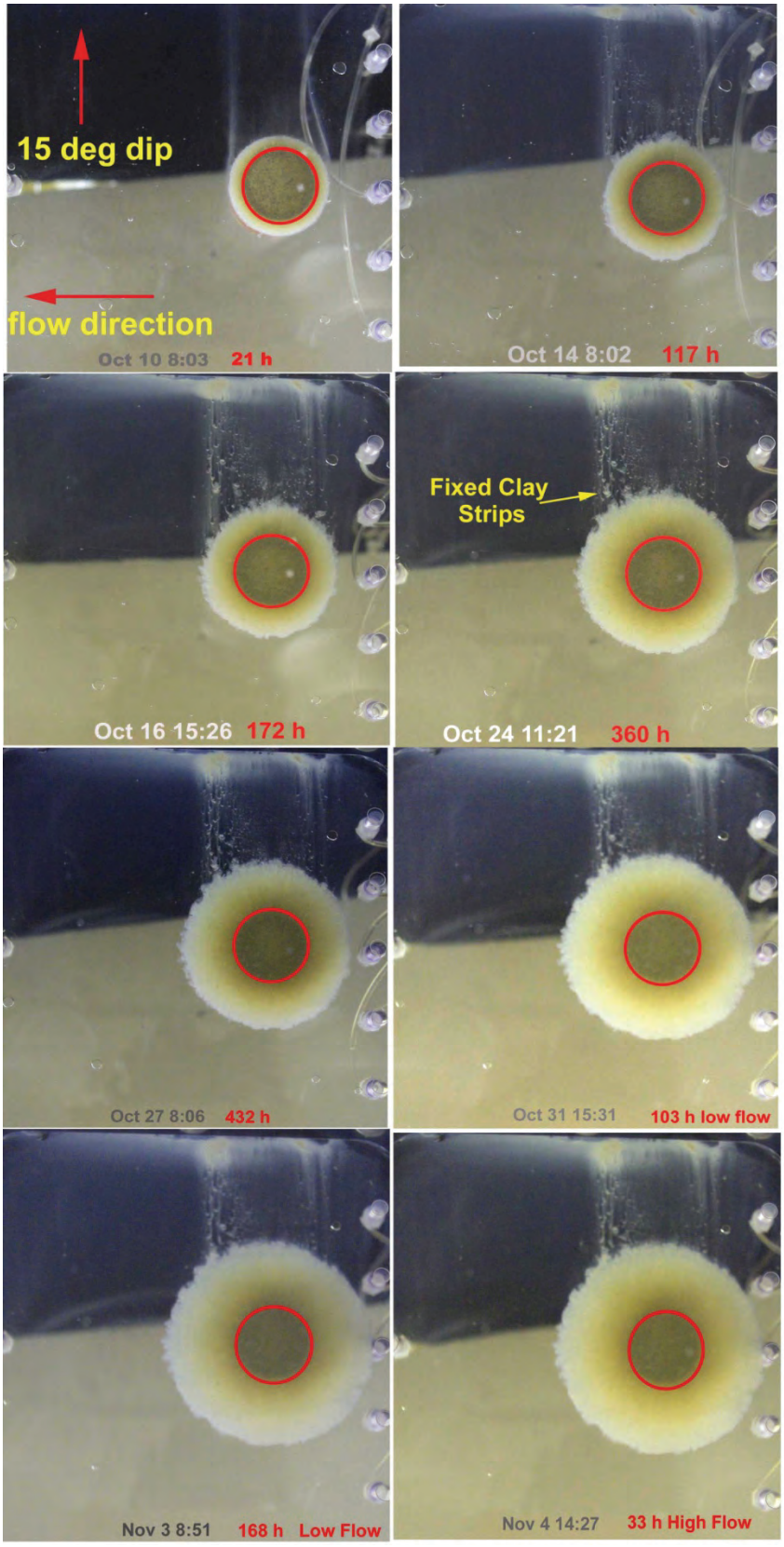

Figure 9: Underside Views of Test 8 at Various Times.

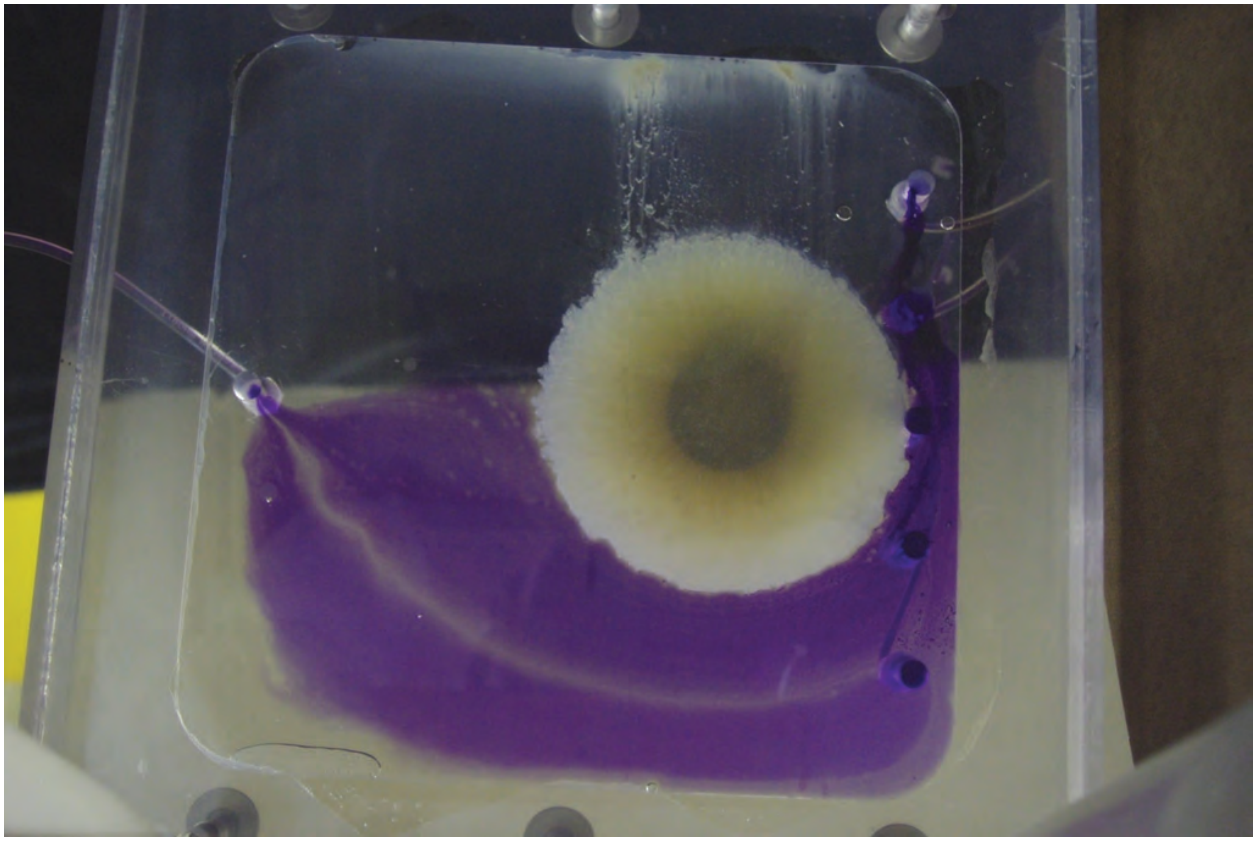

Figure 10: Dye Test at the End of Test 8 Showing that the Down Slope Bentonite Deposits Have Concentrated Flow in the Up Slope Part of the Fracture.

The expansion behavior of bentonite was characterized to better understand expansion and gel formation over time, and to provide an estimate of the bentonite expansion that is likely to occur in the Quarried Block. This helped the decision making process for the Quarried Block experiment, in which bentonite expansion could not be seen until after the test was completed. Figure 11 summarizes the expansion behavior of compacted bentonite as a function of time for the different tests. Using photos, such as those in Figure 3 and the other underside views, taken at various times, the outline of the expanded clay shoulder was identified and its diameter in the x and y direction measured. In each photograph the projected diameter of the borehole was also measured in the x and y directions. The measured diameters of the clay shoulder in the x and y directions were divided by the respective borehole diameters to obtain ratios that describe the extent of clay expansion into the fracture. The expansion ratios in the x and y directions were averaged and plotted in Figure 11 as a function of time. In addition, the expansion ratio was determined for the outer white rim, marking the maximum extent of visible clay erosion and deposition. These ratios were also plotted in Figure 11. Arrows point to measuring points which were either the start of or under the influence of conditions of low flow (LF) or high flow (HF).

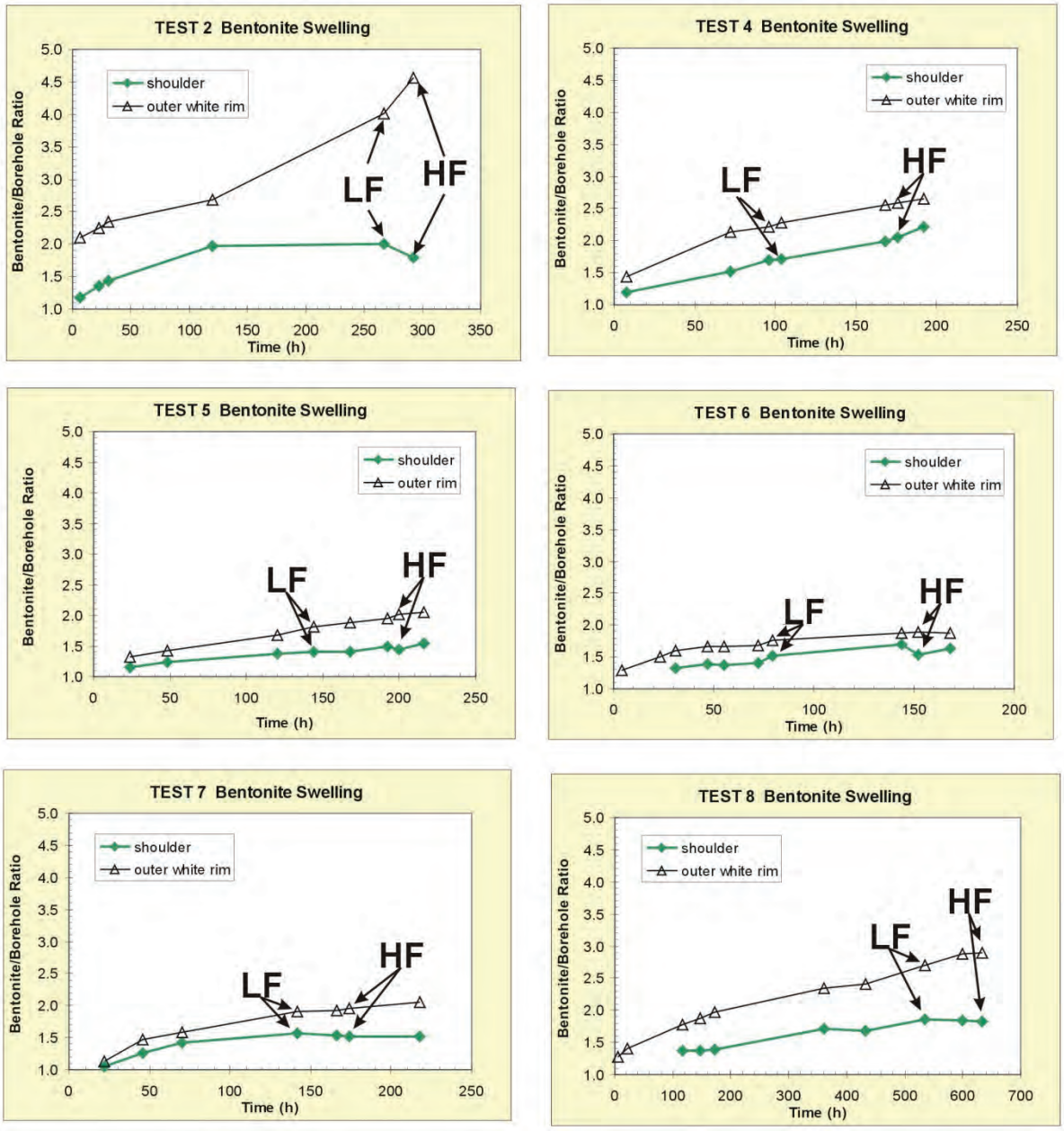

Figure 11: Compare bentonite expansion as a ratio of the diameter of expanded clay to the borehole diameter (38 mm). LF represents the start of low flow and HF marks high flow conditions.

The plots in Figure 11 show that the maximum clay expansion occurred when the fracture was filled with deionized water (Test 2). In Test 2 the expansion of the clay shoulder appeared to be complete after 100 h, while the outer rim continued to grow, particularly under conditions of low and high flow. In this test the maximum extent of erosion and deposition was difficult to estimate after flow had started because bentonite appeared to be dispersed throughout the fracture. The replacement of deionized water with synthetic

Grimsel water (Test 4) reduced the extent of expansion of the clay shoulder and the outer white rim. The clay shoulder in Test 4 continued to expand without reaching a plateau over the 200 h experimental time span, and the expansion of the outer white rim appeared to run in parallel with that of the shoulder. The expansions in Test 4 were not affected by flow rate. The reduction in fracture aperture to 1 mm (Test 5) further reduced the expansion rates of the shoulder and outer rim by a factor ~1.5. The expansion of the outer rim was slightly faster than that of the inner rim. Neither expansion was affected by flow rate. In the case of the Ca-montmorillonite (Test 6) the expansion rates were similar, although not directly comparable since the expansion mechanism of the Ca-montmorillonite appeared to be different. The addition of a fracture slope to Test 7 (Wyoming bentonite) and Test 8 (Na-montmorillonite) produced expansion curves that were not significantly different from Test 5 with Wyoming bentonite in a horizontal fracture. After 200 h the expansion rate in Test 8 dropped by a factor 2, and remained constant till the end of the experiments. The longer time span expansion curves of Test 8 are a reasonable approximation of bentonite expansion in a 1 mm fracture for up to 650 hours.

2.2.2 Latex Fluorescence as a Marker for Bentonite

The compacted bentonite used in the mock-up experiments was spiked with fluorescent latex spheres to test the usefulness of fluorescent colloids for assisting the visualization of bentonite expansion and deposition, and for assessing the extent of bentonite erosion. The latex colloids provide a useful comparison to bentonite colloids since the carboxylate-modified latex spheres are almost perfectly spherical, resistant to biodegradation and are more stable in saline water through a combination of hydrophilic and negatively charged (at pH>5) surfaces (Becker et al., 1999). Previous tests in the Quarried Block (Vilks and Miller, 2009) showed that with low ionic strength water and high flow velocities, typical of forced-gradient field-scale tracer tests (10's cm/h), bentonite colloids and 100 nm latex colloids are mobile and have similar transport behaviour. Differences in transport behaviour between the two colloid types became evident as flow velocity was reduced to cm/h and then mm/h, the latter being more typical of certain natural flow conditions. Differences in their transport properties can be attributed to the higher specific gravity and more heterogeneous charge density of bentonite colloids. This section focuses on using fluorescent colloids to visualize bentonite behaviour during expansion into an open fracture. Figure 12 illustrates bentonite plugs from Test 2 and Test 4, under visible and UV light after the fracture has been opened. Fluorescent blue (1 µm) latex spheres were used in Test 2, while fluorescent yellow-green (220 nm) latex spheres were used in Test 4. The yellow-green was the better colour because it was easier to distinguish from the background blue cast by the UV light. The blue colloids (Test 2) appear as evenly distributed specs in the bentonite that had remained in the borehole during the experiment. However, the bentonite that was eroded and transported displayed blue streaks elongated in the direction of clay movement. In Test 4 the yellow-green latex spheres were also evenly distributed in the bentonite plug that was in the borehole, and displayed yellow-green streaks in the expanded shoulder and in the clay that had migrated away from the shoulder.

Figure 13 illustrates the bentonite at the termination of Test 6 (Ca-montmorillonite). In this test the Ca-montmorillonite did not hold together as well as the Na dominated clays and consequently was not recovered from the borehole in a solid form as in all of the other tests. Furthermore, the clay surrounding the borehole took on the appearance of a shallow

dipping slope containing sand-sized lumps. Under UV light the yellow-green fluorescence had a granular appearance throughout the clay, without any streaks that would suggest flow.

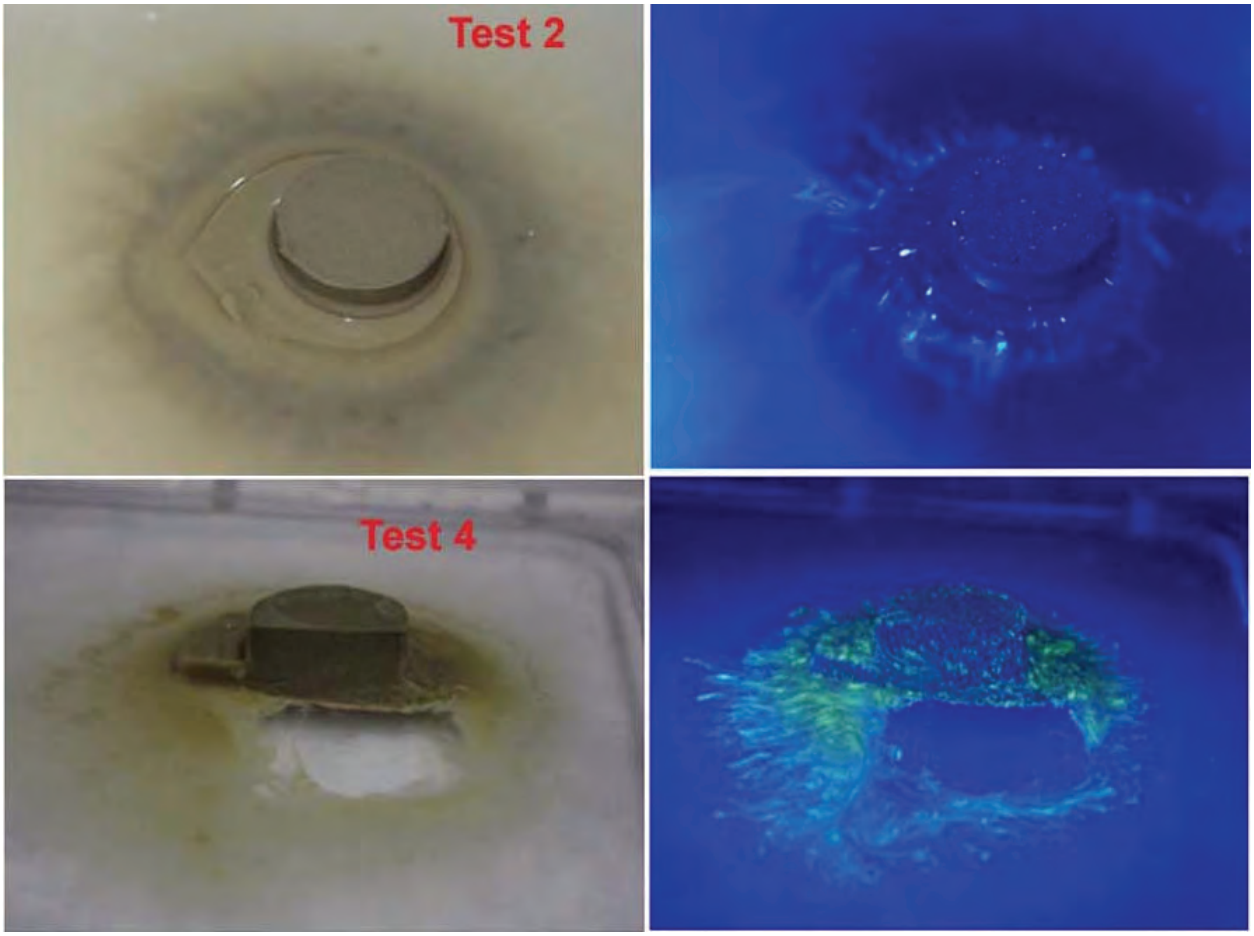

Figure 12: Test 2 and Test 4 Images Under Visible and UV Light After Fracture Was Opened.

Figure 14 shows several images taken after the termination of Test 8. This test had more time to expand into the fracture and develop a distinctive shoulder. The shoulder contained very distinct yellow-green streaks, indicative of outward clay expansion into the fracture. The down slope clay deposits (in the upper part of the photo) did not have a strong fluorescence, suggesting a possible separation of latex and bentonite during down slope movement in this test. The separation could be attributed to the greater impact of gravity on the denser bentonite colloids. The image of the clay section that was sliced in half, again illustrates a uniform latex distribution within the clay that remained in the borehole. The cross section of the shoulder shows some streaking and separate movement of latex and bentonite.

In summary, under UV light the fluorescence associated with latex colloids appears as specs or as streaks in regions where clay movement has taken place. Although the fluorescence imparted by the latex colloids is not intimately associated with each clay

particle, and does not move exactly the same as the bentonite, it is still a useful marker for visualizing the expansion behaviour of bentonite.

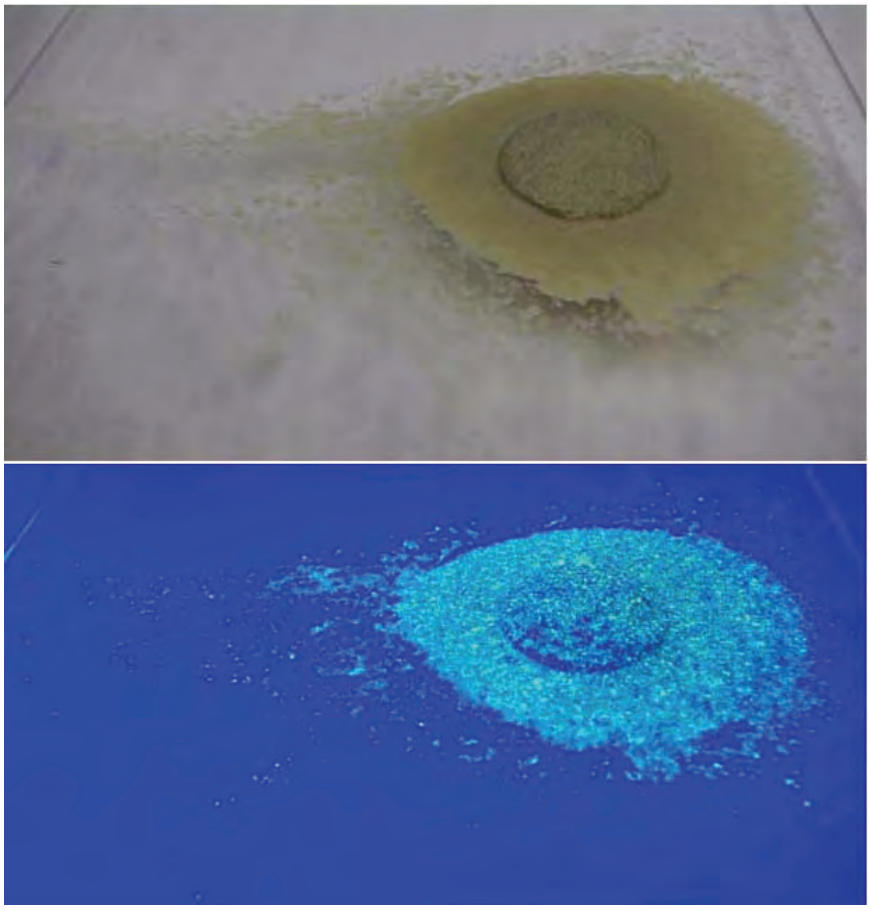

Figure 13: Test 6 Images Under Visible and UV Light.

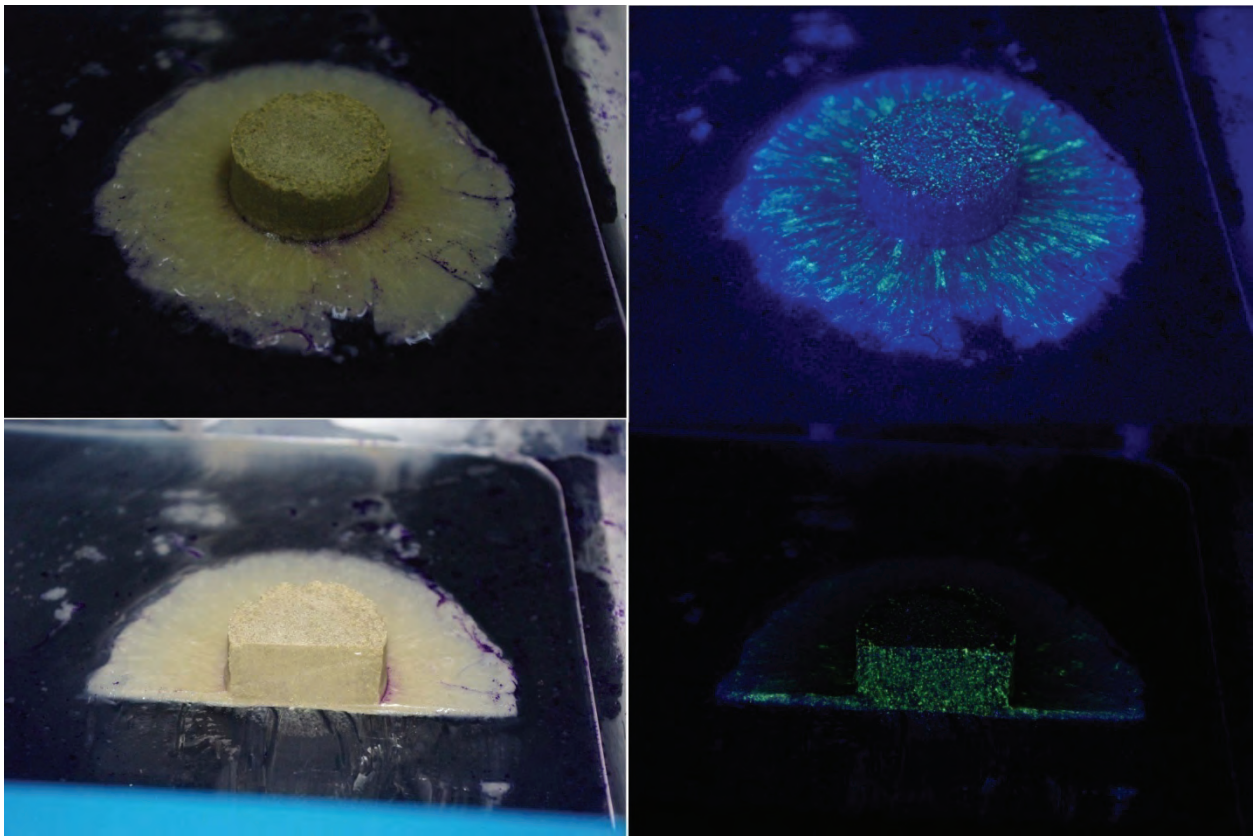

Figure 14: Test 8 Images Under Visible and UV Light.

2.2.3 Bentonite and Latex Transport

The concentrations of bentonite and latex colloids eluted from the water from the withdrawal port as a function of elution volume are presented in Figure 15. These concentrations are a measure of colloids that were transported and do not provide a direct measure of colloid concentrations in close vicinity to the clay or those released during the period of no flow.

Bentonite colloids: As predicted from the visual behavior of bentonite, the highest colloid concentrations were observed in the presence of deionized water (Test 2). Measured colloid concentrations continued to increase during the period of low flow, and jumped sharply when the flow rate was increased from 6 to 44 mL/h. When deionized water was replaced with synthetic Grimsel water (Test 4) measured colloid concentrations dropped by about an order of magnitude. These concentrations were similar to colloid concentrations reported to be in equilibrium with Na-montmorillonite in the presence of 0.001 mol/L NaCl (García-García et al., 2009). Colloid concentrations decreased with increasing elution volume and flow velocity. This suggests that for Test 4 the rate of colloid transport away from the bentonite was faster than the generation rate at the bentonite surface.

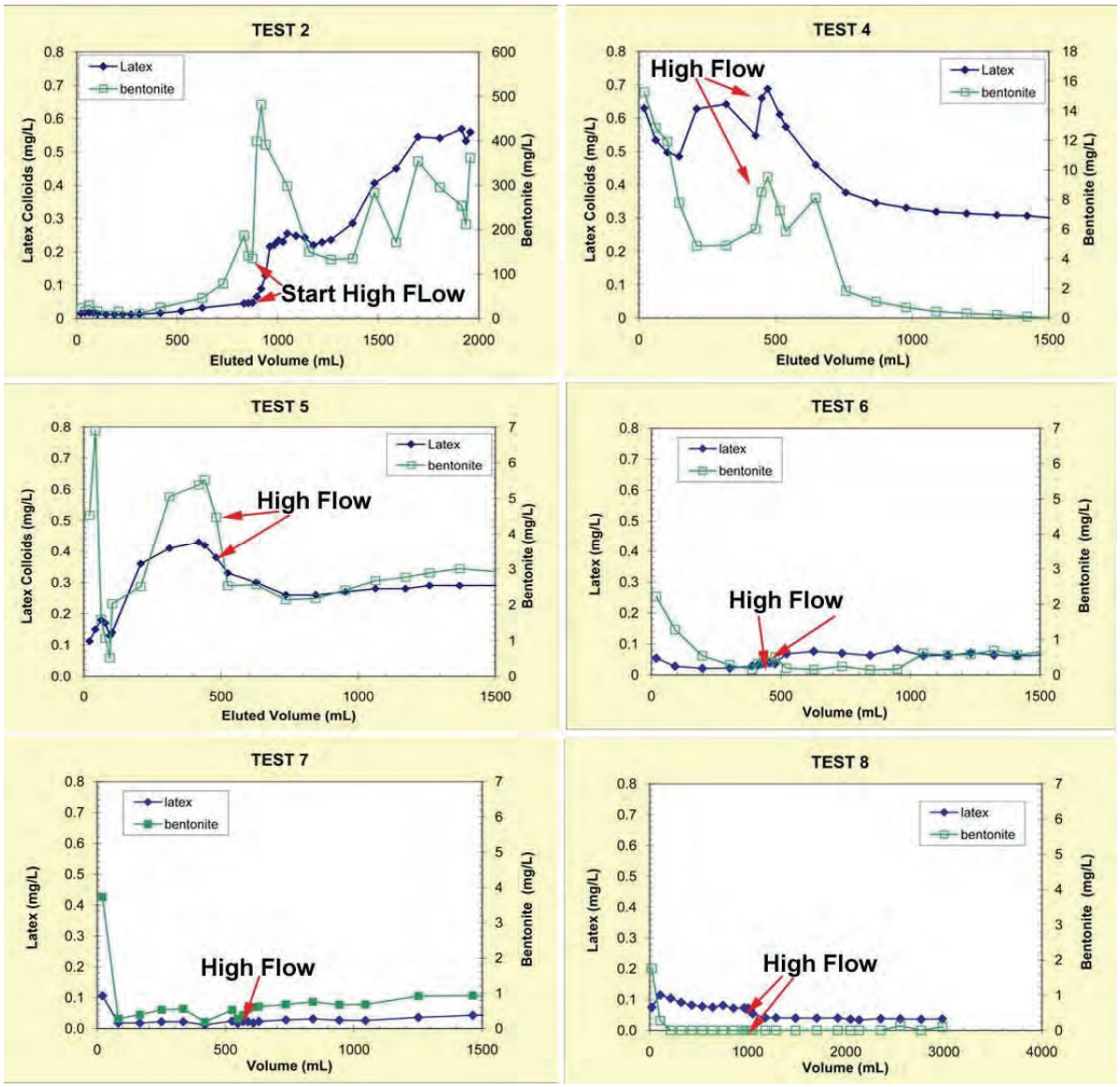

Figure 15: Bentonite and Latex Colloid Concentrations Eluted from the Synthetic Fracture. Note that the Bentonite Colloid Concentration Scale is Different in Tests 2 and 4.

When the fracture aperture was reduced to 1 mm in Test 5 initial bentonite colloid concentrations reaching the outlet port were lower by about a factor 2. During low flow colloid concentrations dropped and then increased before the start of high flow, reflecting a stabilization of the erosion and transport rates following initiation of flow. At the start of high flow colloid concentrations initially declined but then reached a steady-state as colloid generation was able to keep up with the rate of colloid removal. Ca-montmorillonite (Test 6) produced lower concentrations of mobile colloids compared to Wyoming bentonite. During the period of low flow, colloid concentrations decreased with elution volume, as the rate of removal exceeded the colloid generation rate. Increasing the flow rate did not significantly change colloid concentrations, although after 1000 mL, colloid concentrations increased slightly and reached a steady-state. These concentrations were similar to the average colloid concentration reported to be in equilibrium with Ca-montmorillonite in contact with 0.001 mol/L NaCl (García-García et al., 2009).

With the introduction of a sloping fracture (Test 7), the concentrations of colloids transported to the outlet port from Wyoming bentonite were lower than observed in Test 5, particularly after the initial sampling point. The increase in flow rate did not make a significant difference in colloid concentrations, although a steady-state was achieved, as colloid generation was able to match removal at the outlet port. Visual inspection of the fracture had shown a significant bentonite accumulation in the down slope section of the fracture, so a change in sampling location within the fracture would have made a huge difference in measured colloid concentration. In this test the down slope section of the fracture behaved as a colloid trap. When the sloping fracture experiment was repeated with Na-montmorillonite and longer experimental times (Test 8), colloid concentrations dropped to below detection limits very soon after the initiation of low flow conditions. The increase in flow rate was not able to supply new montmorillonite colloids. Explanations for the low colloid concentrations could include several factors: (1) Eroded montmorillonite colloids moved down dip during the period of no flow, and when flow was initiated it was diverted to the top side of the fracture and away from the bentonite (Figure 9 and Figure 10). (2) The period of no flow was significantly longer than in previous tests, allowing more time for the clay to form a stable gel that was less resistant to erosion.

Bentonite colloid size distribution: Figure 16 illustrates typical size distributions of bentonite colloids eluted from the synthetic fracture. Note that these distributions represent the dominant sizes determined from Brownian motion. The presence of larger particles may mask the presence of smaller particles, and the 1.0 and 0.2 μm latex sizes are masked by the much higher bentonite colloid concentrations. The transported bentonite colloid size distributions are variable, ranging from a narrow distribution of small colloids around 0.01 μm to a broad distribution from 0.1 to 1.0 μm, which may or may not be accompanied by suspended particles larger than 1 μm. These larger particles are likely to be flocs of smaller colloids. The particle size distributions can be converted to average sizes to facilitate comparison between experiments. Averages based on particle volume will be weighted to larger sizes, while averages based on particle numbers will be weighted to smaller sizes.

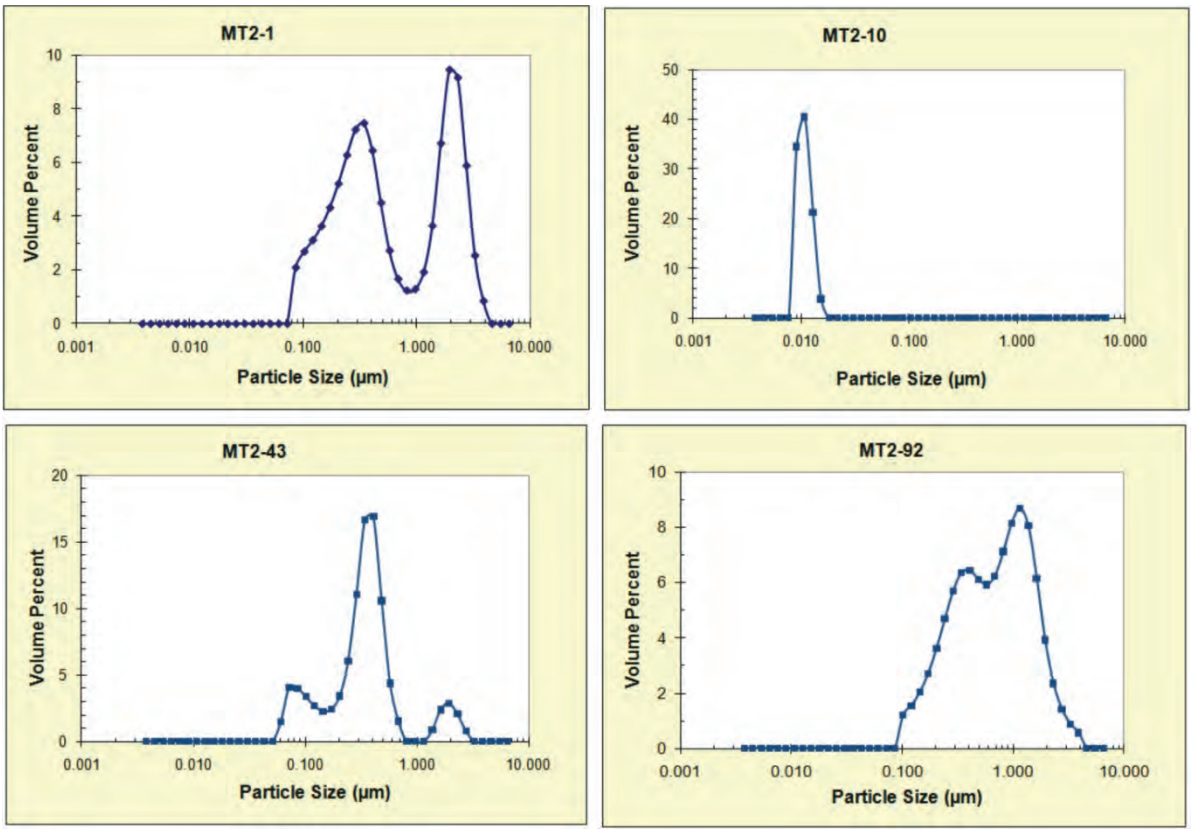

Figure 16: Examples of bentonite colloid size distribution from Test 2.

The average values using these two approaches are plotted in Figure 17 as a function of eluted volume. The size of the error bars in Figure 17 is determined by the difference between the average values based on particle volume and the smaller sizes based on particle number. In Figure 17 the average particle sizes for the size distributions shown in Figure 16 are labeled in the Test 2 plot. In Test 2 the initial colloids reaching the outlet port under low flow conditions tended to be small (~ 0.01 μm). Eventually, even before the start of high flow, larger colloids reached the outlet port with average sizes between 0.2 and 0.5 μm. The error bars show that these size distributions were rather broad. When deionized water was replaced with Grimsel water in Test 4, the average particle sizes increased to between 0.3 and 1.4 μm, with no appearance of 0.01 μm colloids. The higher ionic strength of the Grimsel water likely induced flocculation of the 0.01 μm colloids, leading to higher average particle sizes. The reduction of fracture aperture from 5 to 1 mm did not have a significant effect on average particle size (Test 5). The particles generated from Ca-montmorillonite (Test 6) had higher average sizes (0.7 to 3.7 μm) compared to colloids produced from Wyoming bentonite, probably because Ca reduced repulsive forces within the montmorillonite. Fracture slope had a significant effect on the size distributions of colloids arriving at the outlet port. For the most part these colloids were small (around 0.01 μm), probably because the larger colloids had moved down slope, where they were effectively trapped. In summary, the average size of bentonite colloids depends upon water chemistry and bentonite composition. The smaller colloid sizes are more easily transported, and become apparent when the larger sizes have become trapped.

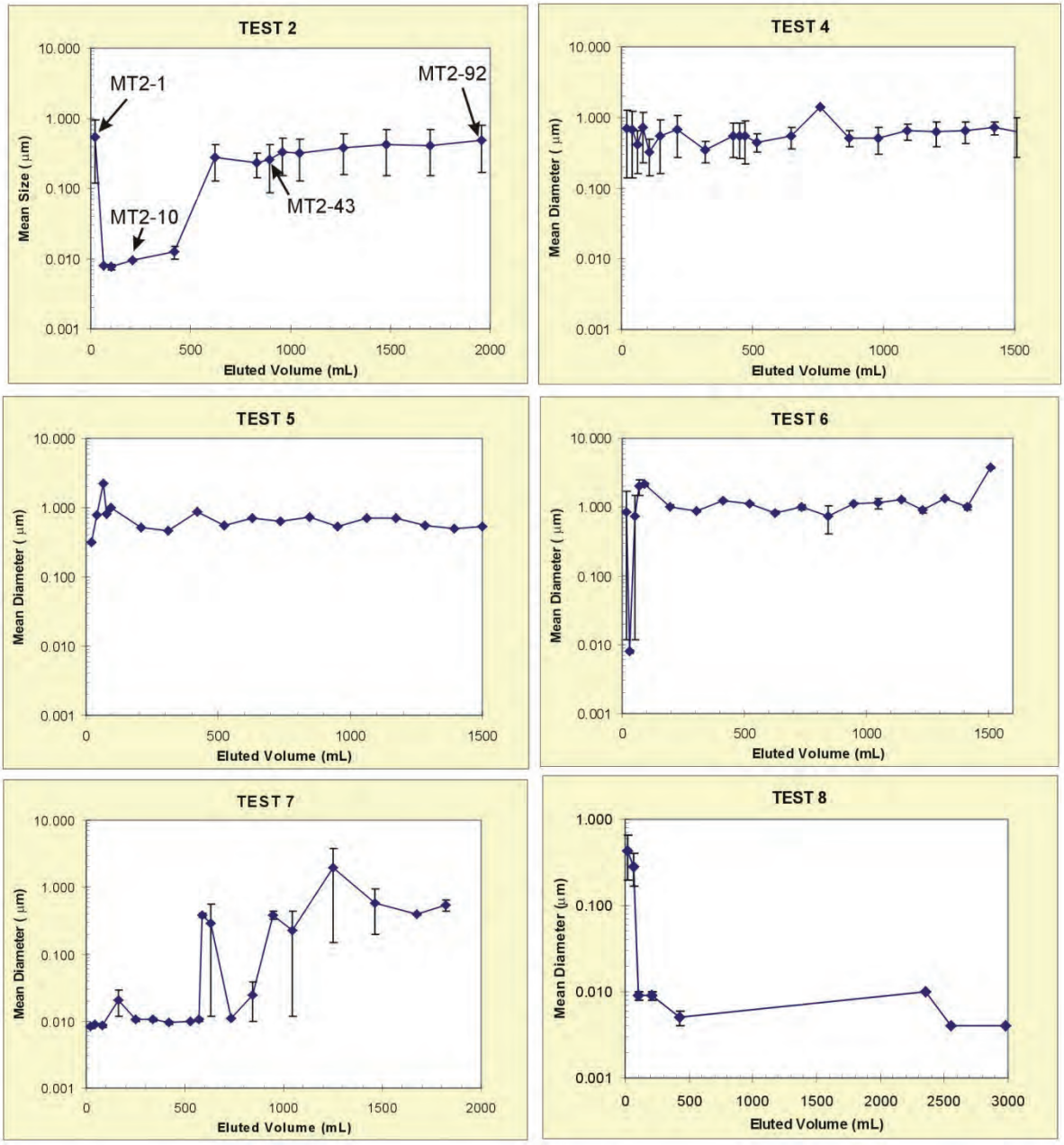

Figure 17: Variations in average bentonite colloid size with eluted volume. The Labels in Test 2 Refer to the Size Distributions Shown in Figure 16.

Latex Colloids: In compacted bentonite the latex/bentonite mass ratio was 0.0005 for the clay spiked with 1 μm blue latex and 0.004 for the clays spiked with 220 nm yellow-green latex. In the experiment spiked with 1 μm blue colloids (Test 2) the latex/bentonite ratios in mobilized colloids were higher than in the original clay by a factor 0.4 to 5. However, in the experiments with 220 nm yellow-green colloids the latex/bentonite ratios in mobilized

colloids were higher by a factor 2.5 to 750. Using tests with a 5 mm aperture for comparison, the concentrations of 220 nm latex (Test 4) were higher than 1 μm latex (Test 2) despite the fact that significantly more bentonite had eroded in Test 2. This indicates that 1 μm colloids are less mobile than 220 nm colloids. Although the larger latex colloids have migration properties that are closer to bentonite, the smaller colloids may be more useful as markers for bentonite erosion in an experiment where one cannot visualize what is happening to the bentonite during the erosion phase.

In many cases there was correlation between the trends in latex and bentonite colloid concentrations, suggesting that latex colloid concentrations were related to the rate of bentonite erosion. Test 6 appeared to be an exception since at high flow rate there was a significant increase in measured latex concentration, with only a small or delayed response in bentonite concentration. When bentonite colloid concentrations dropped below detection in Test 4 and Test 8 latex was still easily detectable. Since latex and bentonite colloids come from the same source, the observation of latex colloids must be attributed to the higher mobility of latex. Latex colloids also have a better detection limit due to their fluorescence, but this was not a factor in these tests.

2.2.4 Summary of Experimental Results

The results of the mock-up experiments are summarized in Table 2. Some of the main observations are as follows. Water containing millimolar amounts of dissolved Na, Ca and Cl significantly reduced bentonite erosion and colloid transport compared to what was observed in deionized water. The presence of these salts also appeared to stabilize the bentonite gel with time, leading to reduced colloid formation. These results confirm the need to utilize water chemistries that are more representative of natural conditions when investigating the potential for bentonite erosion and colloid transport. Reducing fracture aperture from 5 mm to 1 mm decreased bentonite expansion and colloid generation. Comparing the results of Tests 5 and 6 performed under identical fracture geometries, it was apparent that, compared to Na-dominated montmorillonite, Ca-montmorillonite behaved differently during water saturation and clay expansion, and released lower colloid concentrations. The presence of fracture slopes promoted down slope gravity driven bentonite movement, and the entrapment of bentonite colloids in low spots. However, with time the down slope movement of bentonite stopped as bentonite deposits became fixed to the fracture surfaces. These bentonite deposits were stable enough to modify the hydraulic regime in the fracture. Fluorescing yellow-green latex colloids are useful for visualizing bentonite behaviour during expansion and erosion, and for acting as a measure of bentonite erosion.

Table 2: Summary of Expansion Ratios and Colloid Concentrations

Test	Parameters	[(1)]Clay Expansion	Bentonite Colloids (mg/L)		Latex Colloids (mg/L)	
			6 mL/h	44 mL/h	6 mL/h	44 mL/h
2	Wyoming bentonite DIW 5 mm aperture 1 μm blue latex	1.86 (2.60)	20 to 200	150 to 480	0.02 to 0.04	0.04 to 0.55
4	Wyoming bentonite **Grimsel water** 5 mm aperture **220 nm YG latex**	1.71 (2.25)	4 to 16	0 to 9	0.48 to 0.65	0.30 to 0.70
5	Wyoming bentonite Grimsel water **1 mm aperture** 220 nm YG latex	1.34 (1.62)	0.3 to 7	2.0 to 4.7 reached steady-state at 3	0.10 to 0.43	0.25 to 0.38
6	**Ca montmorillonite** Grimsel water 1 mm aperture 220 nm YG latex	1.59 (1.80)	0.2 to 2.2	0.2 to 0.6 reached steady-state at 0.5	0.02 to 0.06	0.04 to 0.08
7	**Wyoming bentonite** Grimsel water 1 mm aperture 220 nm YG latex **fracture dips 15^0**	1.48 (1.72)	0.2 to 3.7	0.5 to 1.0 reached steady-state at 1	0.01 to 0.11	0.02 to 0.04
8	**Na montmorillonite** Grimsel water 1 mm aperture 220 nm YG latex fracture dips 15^0	1.38 (1.72)	0 to 1.8	0 to 0.15	0.07 to 0.12	0.04 to 0.07

[(1)] Clay expansion at 100 h – shoulder
- (outer white rim)

2.3 DISCUSSION

Bentonite erosion can be conceptualized as consisting of several parts. The first part involves bentonite swelling and gel formation, followed by colloid release, diffusive or advective transport away from the clay, and aggregation/sedimentation of released colloids (Degueldre et al., 2009a). Bentonite swelling depends upon the availability of volume for expansion, bentonite composition and water chemistry. In the initial stages of hydration, the bentonite undergoes intracrystalline swelling (Boek et al., 1995) in which limited amounts of water, up to 3 water molecule layers, are adsorbed in the interlayer spacing. When the volume for expansion is very limited, high expansion pressures can be generated by the structural rearrangement of water in the interlayer. If there is volume for expansion and a sufficient supply of water, the montmorillonite will expand by osmotic swelling (Boek et al., 1995), driven by the difference in salt concentration at the clay surface and the hydrating water. During osmotic swelling complex electrostatic repulsions may push swollen montmorillonite flakes apart to distances that may exceed 1 µm (Zbik et al., 2008). This may produce an expanded cellular network in which water is encapsulated in cellular voids with dimension up to 0.5 or 2 µm.

Bentonite composition and water chemistry influence the nature of bentonite swelling and the nature of the resulting gel structure by determining which cations are influencing repulsive forces between clay sheets (Liu et al., 2009). The repulsive forces between clay sheets are stronger if the exchangeable cations in the interlayer have a lower valence and higher hydrated radii (Rao and Mathew, 1995). For example, since K^+ has a smaller hydrated radius than Na^+, it is more effective at shielding the repulsive forces between clay sheets, reducing the ability of bentonite to expand when K^+ has replaced Na^+ in the interlayer (Boek et al., 1995). In suspensions with a high ionic strength and high Ca^{2+} to Na^+ ratio, the repulsive forces are reduced such that the primary clay grains associate in a face to face pattern to form relatively compact agglomerates (Sjöblom et al., 1999). If the suspensions have low ionic strength and a low Ca^{2+} to Na^+ ratio, the primary clay particles form aggregates with a face to edge pattern. Although these aggregates are more prone to release primary clay particles, they also form more voluminous gels that plug the porosity in compacted bentonite (Sjöblom et al., 1999).

In gels fromed by Na-montmorillonite the stacks of montmorillonite sheets, referred to as tactoids, form thin walled cells with average distances between sheets of 940 nm (Zbik et al.,2008). Ca-montmorillonite produces aggregates containing thick walled cells with distances between sheets of only ~400 nm. The difference in the properties of the two types of montmorillonite is attributed to the influence of the Ca content on repulsive forces between surfaces. The long range repulsive forces between Na-montmorillonite surfaces extended to distances > 1000 nm, while those between Ca-montmorillonite surfaces extended only to ~400 nm (Zbik et al.,2008). The shapes of the decay curves of these repulsive forces with distance resembled double-layer interactions as described by DLVO[1] theory (Derjaguin and Landau, 1941). According to DLVO theory the thickness of the electric double layer is decreased by electrolyte concentration and ion charge. Differences in the hydration of exchangeable ions will also affect the shape of the electric double layer.

[1] The **DLVO** theory is named after Derjaguin and Landau, Verwey and Overbeek and describes the force between charged surfaces interacting through a liquid medium combining the effects of van der Waals and double layer forces.

In addition to influencing the stability of colloids released to water, the composition of water contacting the bentonite can modify the composition and properties of the gel. If bentonite is contacted with relatively dilute water, with a low Ca^{2+} to Na^{+} ratio, Ca^{2+} may be leached from the clay by cation exchange with Na^{+} or the dissolution of soluble Ca^{2+} minerals, such a gypsum. This process would make the gel more likely to erode and release colloids (Liu and Neretnieks, 2006).

With progressive swelling, repulsive forces tend to generate the release of montmorillonite colloids from the gel. These colloids are removed from the clay surface by diffusion (García-García et al., 2009), or can be swept away with the passing groundwater if there is sufficient flow. In the absence of flow colloid concentrations generated from the bentonite will be limited by aggregation and sedimentation (García-García et al., 2009; Bessho and Degueldre, 2009) These colloid concentrations will vary as a function of water chemistry because ionic strength affects colloid generation and the opposing aggregation and sedimentation processes in a similar way. The aggregation and sedimentation processes are also likely to produce new gel deposits that may continue to contribute to colloid generation. Sjöblom et al., 1999, noted that exposure of compacted bentonite to dilute water causes the bentonite to swell and to produce particles by exfoliation. The particles will form gels that can close pores, and limit the influx of more water. Zbik et al., 2008, produced gels from suspensions of Na and Ca montmorillonite. Degueldre et al., 2009b, investigated bentonite colloid aggregates that had been in stable suspension for over a year, using scanning transmission X-ray microscopy. These aggregates, with diameters between 100 and 800 nm, appeared as gel like and porous spheres or ellipsoids that appeared to be made of colloids smaller than 20 nm, and probably had lower densities than the original bentonite. These aggregates could represent the building blocks for gel formation.

In this study compacted bentonite, with a density of 2 g/cm^3, was allowed to saturate with water and to expand, with relatively little confinement, into an open synthetic fracture. During the unconfined expansion into the fracture the structure of the compacted bentonite was altered from water-saturated, moderately expanded clay in the borehole to that of a highly expanded gel close to the bentonite-water interface. Gel formation took place within hours of water contacting the clay, and was followed very closely by apparent colloid release. However, in the initial time after hydration (170 to 430 h) the expanding clay was subjected to mass loss that involved particles larger than colloids. These particles were observed to move under the influence of gravity if there was a sloped fracture or a larger fracture aperture. Depending upon the water composition, as gel formation became more complete this type of particle loss and transport was arrested, as indicated by the fixation of gel deposits within the sloped fracture. After this period, bentonite erosion was controlled by colloid release from gel.

The water composition that comes into contact with compacted bentonite has a major impact on clay behaviour. When bentonite was allowed to saturate with deionized water significant amounts of colloids were released. Colloid release was accelerated when flow was introduced. However, when the bentonite was saturated with synthetic Grimsel-type water the released colloid concentrations decreased by about an order of magnitude. The gel expansion rate was lower, and increasing flow rate did not increase colloid release.

These observations indicate that when bentonite gel is formed in contact with deionized water, the composition of the water within the gel becomes dilute enough to allow the repulsive forces between like-charged montmorillonite sheets to develop to a sufficient

distance to overcome the attractive forces holding the gel together. This weakens the gel and triggers the release of colloids. This gel was also too weak to resist the hydraulic shear forces created when flow was initiated. In addition, the input of fresh deionized water during flowing conditions may further dilute the salt content of the bentonite gel. However, when contacted with water with mM salt concentrations, the water inside the gel was not sufficiently diluted to produce repulsive forces that were as effective in overcoming forces of attraction. This resulted in a stronger gel structure that released lower colloid concentrations and was able to resist the shear forces of moving fluid. In addition to having lower colloid generation from bentonite, the colloids in the system with mM salts were more likely to agglomerate and contribute to gel formation.

In this study bentonite was observed to continuously expand at various rates for the duration of the experimental time frame (200 to 650 h). This means that the clay masses had not yet achieved their maximum possible degree of expansion. The expansion rates were very sensitive to water composition and were influenced to a lesser extent by fracture aperture.

As predicted, the Ca-montmorillonite produced a gel that appeared to consist of small granules, giving the gel a less cohesive structure. The observed presence of granules is consistent with the observations of Zbik et al., 2008. The Ca in the gel reduced the range of repulsive forces to about one half that in Na-montmorillonite, producing a gel structure with a shorter range structure. Granules were released from the gel as soon as the fracture was filled with water, cascading downward while the fracture was vertical. This suggests that if the subsequent experiment had been performed with an inclined fracture, these particles may have moved down slope. However, the fracture was orientated in the horizontal position after it was filled with water, and the subsequent release of colloids is about a factor 3 to 6 lower than from Na-montmorillonite, under similar conditions.

The reduction in fracture aperture from 1 to 5 mm decreased the bentonite expansion ratio into the fracture, as well as the initial release of colloids. The gel expansion in the 1 mm fracture may have been limited by more resistance from fracture walls due to the higher surface area to volume ratio of the gel in the fracture. The sloped morphology of the clay water interface suggests that gravity played a role in the initial stages of bentonite erosion and later colloid transport. When the fracture aperture was reduced to 1 mm, the elevation differential at the clay-water interface was reduced by a factor 5. In addition to reducing the driving force of gravity affecting erosion in the initial stages of expansion, the reduced surface area of the water clay interface would reduce the colloid flux to water later on. When flow was initiated the actual water velocity and shear were higher in the smaller aperture fracture. This increase in shear was sufficient to increase colloid generation within the 1 mm aperture fracture. The morphology of the gel in the 1 mm fracture displayed evidence of erosion created by the high flow, which was not seen in the larger fracture.

After the initial contact with water and expansion into the fracture the properties of the bentonite appear to evolve with time, depending upon the water composition. In deionized water colloid release started in the absence of flow and was accelerated with increasing flow rate. In Grimsel water bentonite erosion was observed in the early stages of no flow conditions, but then appeared to slow down, suggesting a stabilization of bentonite gel. If the fracture was sloped, bentonite transport down slope would begin during this period of initial colloid release. During the first 120 hours, the down slope transport would accelerate. However, after about 150 h of contact with Grimsel water the gel becomes more “sticky”, to the point where erosion and transport cease after about 430 h. The

resulting gel deposits resisted erosion by fluid flow and changed the hydraulic properties of the fracture. These observations indicate that bentonite in contact with water containing mM concentrations of mono and divalent salts will eventually form stable gels that are more resistant to colloid generation. This suggests that short term experiments, using deionized water overestimate the potential for colloid generation from a deep geologic repository because even glacial melt water that recharges to the depth of a DGR is likely to pick up mM concentrations of salts.

The size distribution of bentonite colloids measured at the outlet port depended upon water chemistry, bentonite composition, and fracture geometry. In dilute water, bentonite colloid size distributions tended to be broad, with average sizes between 200 and 500 nm. The average colloid sizes increased (300 to 1400 nm) in Grimsel water, and the size distributions were somewhat narrower. This suggests a higher level of coagulation in the presence of salt, as would be expected from DVLO theory (Derjaguin and Landau, 1941). The thicker walled Ca-montmorillonite produced larger colloids with average sizes between 700 and 3700 nm. When a fracture slope was present the larger colloid were collected in the lower part of the fracture leaving mainly the smaller 10 nm colloids to be transported to the outlet port. This suggests that in natural systems the larger colloids are likely to be trapped in low spots, leaving transport mainly to the smaller colloids.

The colloid concentrations released from Wyoming bentonite in the presence of deionized water were consistent with the results reported by Jansson, 2009, for his tests using distilled water in a synthetic 1 mm aperture fracture. Both studies confirm that in the presence of dilute water, significant bentonite erosion will take place, leaving behind deposits of non-clay minerals. When water with mM salt concentrations was used, the release of colloids from Wyoming bentonite in a 5 mm fracture varied from 4 to 16 mg/L under low flow, while in the 1 mm fracture (horizontal) colloid concentrations varied between 0.3 and 7 mg/L under low flow, and reached a steady state concentration of 3 mg/L at high flow. Colloid concentrations from Ca-montmorillonite varied between 0.2 and 2.2 mg/L at low flow, and reached a steady state of about 0.5 mg/L at high flow. These results are fairly close to the pseudo-equilibrium colloid concentrations observed 7 cm above a clay bed in batch tests with no flow (García-García et al., 2009), which were 5.2 ± 0.5 mg/L for Na-montmorillonite, and 0.4 ± 0.2 mg/L for Ca-montmorillonite. In the batch tests colloid concentrations increased above these values with proximity to the bentonite bed. The similarities are remarkable, given the differences in basic experimental design. In this study the maximum sedimentation distance (horizontal fracture) was only 1 to 5 mm. If colloids are not trapped, this should promote higher colloid concentrations in the fracture. However, as shown by the results with the inclined fracture and by transport experiments in a granite fracture (Vilks and Miller, 2009), the larger bentonite colloids that are affected by sedimentation are trapped by irregularities in fracture surfaces. This study also showed that the development of pseudo-equilibrium colloid concentrations can be disturbed by the removal of colloids by flow.

Grimsel water is a proxy for glacial melt water. The average Ca and Na concentrations in 18 glacial melt waters, sampled from around the world, (Brown, 2002) were 0.20 ± 0.15 and 0.17 ± 0.30 mmol/L, respectively. These waters also contained an average of 0.24 ± 0.17 mmol/L of other divalent cations and 1.05 ± 0.85 mmol/L other monovalent cations. While the ionic strength of new ice melt is ~ 0.01 meq/L (Brown, 2002), the average ionic strength of the 18 glacial melt waters was 1.05 ± 0.85 meq/L. By interactions with minerals over relatively short time spans, new ice melt water can increase its ionic strength by two orders of magnitude, particularly through the acquisition of divalent cations (Brown, 2002). Since

for bentonite the CCC values for Ca are in the range 0.1 to 1 mmol/L, and those for Na are 10 to 100 mmol/L, Ca and other divalent cations are a key factor governing bentonite stability in glacial melt waters and the synthetic Grimsel water used in this study. The synthetic Grimsel water used in this study has a similar ionic strength (0.90 meq/L) and Ca concentration to average glacial melt water, and is therefore a reasonable representation of the salt concentrations that may be achieved by recharge of glacial melt water. Since ice melt waters acquire salt concentrations relatively rapidly, the deionized water is not a very reasonable representation of dilute groundwater chemistry that could result from glacial recharge. The results of Test 2 could be considered as a low probability, worst case scenario.

3. BENTONITE EROSION IN A NATURAL FRACTURE

The goal of the block-scale bentonite erosion experiment is to determine whether bentonite erosion and transport are significant in a natural system, mimicked by a 1 x 1m fracture with a known aperture distribution. The experimental objectives are

- Characterize the transport properties of the Quarried Block (QB) fracture, with solute tracer, to provide a benchmark for the modelling of colloid transport.
- Perform the bentonite erosion test in the Quarried Block by allowing two bentonite plugs to swell and expand into a variable aperture fracture in the presence of synthetic Grimsel groundwater, first under conditions of no flow and then in the presence of a dipole flow field.
- Repeat selected solute tracer tests after the bentonite erosion experiment to determine whether eroded bentonite has altered transport within the QB.
- Demonstrate the use of fluorescent latex colloids as tracers to (1) identify the source(s) of colloids being sampled at a particular location, (2) provide a reference with which bentonite colloid transport can be compared to a mobile colloid, and (3) test the usefulness of fluorescence during post-test analyses to help visualize possible bentonite erosion and subsequent transport.

3.1 METHODS

3.1.1 The Quarried Block

The Quarried Block is a 1m x 1m x 0.7 m block of granite containing a single, well characterized, through-going variable aperture fracture. The Quarried Block was previously excavated from Subvertical Joint Zone 2 (JZ2), also known as the “Room 209 Fracture,” at the 240 level of AECL’s Underground Research Laboratory (URL). This Joint Zone originates from Fracture Zone 3 and terminates just below and to the south east of the 240 level. It is the only hydraulically active fracture at the 240-level. The Quarried Block was coated with a silicone material to prevent loss of moisture from the fracture and from the interconnected pore space in the rock matrix. The block was also fitted with stainless steel frames on the top and bottom sides to help facilitate the opening and closing of the fracture. The Quarried Block was placed in such a way that the fracture plane was sub-horizontal to

the support frame. This orientation, rather than the original sub-vertical orientation, would facilitate the instrumentation and testing of the fracture. To support a set of previous transport experiments, the Quarried Block was opened up to expose the fracture surfaces in order to develop a fracture aperture distribution model using an optical digitizing technique based on white light triangulation. The digital fracture aperture model formed the basis for a 3D colloid transport model. Reassembly of the upper and lower fracture surfaces was aided by four keys located on the sides of the Quarried Block that were used as reference points and guides. The Quarried Block was previously used for colloid transport experiments with latex and bentonite colloids (Vilks and Miller, 2006, Vilks and Miller, 2009)

The fracture, which can be accessed from the top via thirteen S-series (6 mm) holes, and five L-series (38 mm) holes (Figure 18). The fracture can also be accessed on two sides via four mini-plena. The L-series holes, labeled as L1 to L5 in Figure 18, contain mechanical packers that are removable, allowing the emplacement of a 2-cm thick bentonite plug (Figure 19). The bentonite plugs were made by compressing MX-80 bentonite to a dry density of 2 g/cm^3 to approximate that likely to be used in a DGR. MX-80 was chosen for the bentonite erosion test in the Quarried Block because it was used most often in the previous tests with the synthetic fracture, and is representative of Na bentonite that may be used in a DGR. The bentonite plug was stabilized by the presence of the packer on one side, while the other side was exposed to water within the fracture. The bentonite was emplaced from the top of the borehole. Bentonite plugs were spiked with fluorescing latex tracers as outlined in Table 3.

Boreholes L1 and L3 (Figure 18) were chosen as locations for bentonite plugs to investigate the role of fracture aperture variability on bentonite erosion and colloid transport. L1 is in a region of relatively larger aperture and L3 is located in a region of relatively lower aperture that may be more restrictive for clay expansion. The MX-80 bentonite at each location was labelled with a characteristic fluorescent latex colloid to help identify the source of colloids recovered during the bentonite erosion experiment. The flow regime for the bentonite erosion test was established by the borehole pair S3 and L4. The straight line between these boreholes passes between L1 and L3.

Table 3. Latex Tracer and Bentonite Borehole Assignments

Borehole	Latex Colour	Latex Concentration g latex/g clay	Excitation/Emission	Bentonite
L1	Yellow-green	0.0023	477/527 (nm)	MX80-bentonite
L3	Red	0.0023	580/605 (nm)	MX80-bentonite

The Quarried Block was reassembled by using four keys on sides B and D as guides. The lifting yoke was then removed from the upper frame, and the Quarried Block was returned to the location, where the bentonite erosion test is to be performed. The four mini-plena (B1, B2, D1 and D2 in Figure 18) were reattached to the edge of the fracture. The fracture edges and any exposed bolt holes were sealed with silicon cement. The fracture was filled with distilled water from the point of lowest elevation (B1). Any leaks revealed by rising water levels were sealed with silicon cement.

Once all leaks were sealed, the Quarried Block was drained and refilled with synthetic Grimsel water. The L-series boreholes have open spaces above the packers, which are accessible to water from possible intersecting fracture splays. Therefore, the openings of these boreholes were sealed at the top of the Quarried Block and sample lines were installed to permit monitoring of hydraulic heads and water sampling. In order to ensure that the QB was fully saturated and free of air pockets, standpipes were installed on each borehole. The purpose of the standpipes was to vent trapped air and to enable the measurement of hydraulic head throughout the fracture in the Quarried Block. In order to establish a reference hydraulic pressure to which all observed heads can be compared, a constant head system was set up to input water into the Quarried Block. Once the Quarried Block was fully saturated and free of air bubbles, the hydraulic heads in each standpipe were checked to be the same and match the level of the constant head system.

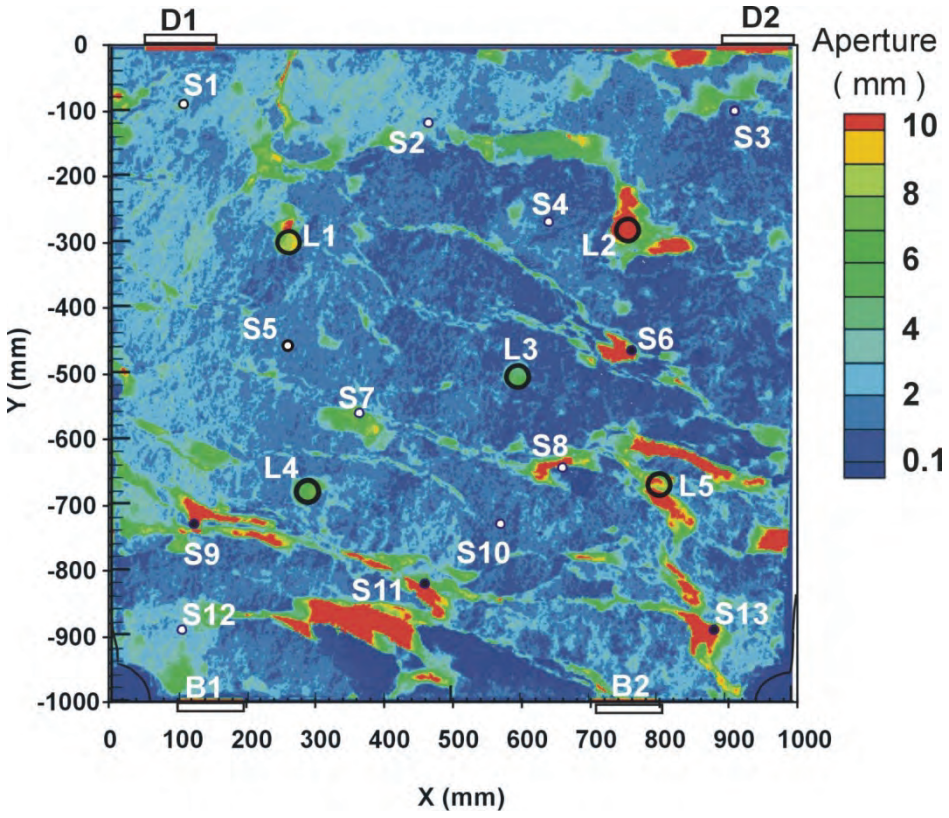

Figure 18. Borehole Locations and Aperture Distribution.

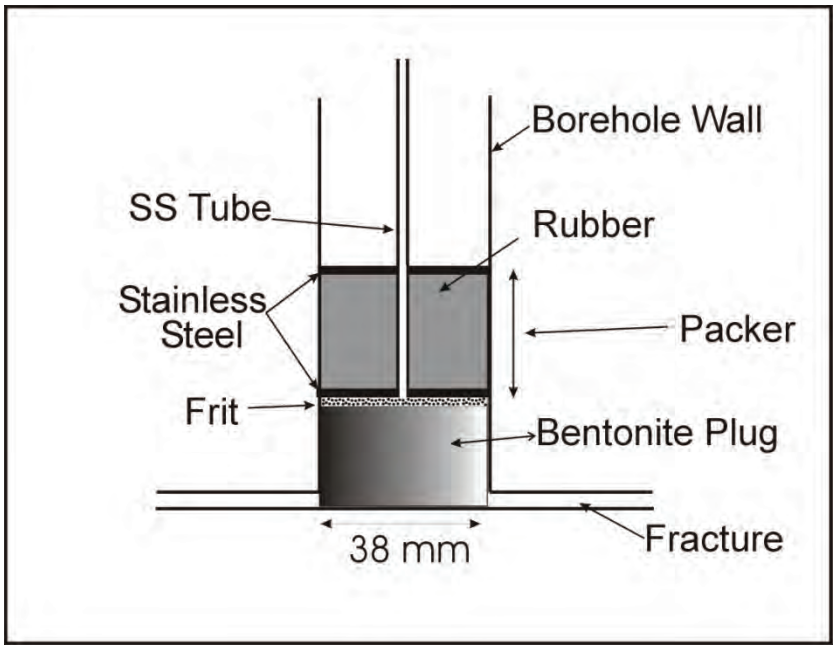

Figure 19: Emplacement of Bentonite Plug in 38 mm Diameter Borehole, Showing Packer, Stainless Steel Tube to Hold Packer in Place, and a Stainless Steel Frit.

3.1.2 Analyses

Concentrations of suspended bentonite colloids were determined by light scattering using a fluorometer. The UPA was used to determine the size distribution of mobilized bentonite colloids. The concentrations of latex colloids released from bentonite plugs were also determined by the fluorometer, taking advantage of the different excitation/emission wavelengths characteristic to particular colours. The concentrations of fluorescent dye tracers (uranine, orange and red) were determined with the fluorometer. Bromide was measured by ion chromatography and iodide was determined with an ion selective electrode.

3.1.3 Experimental Method

3.1.3.1 Solute Tracer Tests

Solute tracer tests were initiated after the Quarried Block was reassembled, tested for leaks, and fully saturated with water. Synthetic Grimsel water (at neutral pH) was used as the ionic medium for the solute tracer tests and the bentonite erosion experiments in the Quarried Block. A number of borehole pairs were selected for dipole tracer tests (Figure 20). L4 was the recovery hole for each tracer test. Note that L1 and L3 were used as injection holes during this phase because they did not yet contain bentonite. The solute tracer tests are summarized in Table 4, which gives their order of execution and tracer types. Note that the purpose of the first two tracer tests (B1 and B2) was to characterize

transport from the locations of the two bentonite plugs to L4 to serve as a reference for future colloid transport modelling. Also note that the first test provided a comparison to previous experiments performed in the Quarried Block (Vilks and Miller, 2009). Tests BE3 to BE6 were used as a benchmark to evaluate the effects of bentonite deposition on transport in the fracture. BE7 and BE8 were used to simulate the simultaneous movement of tracer from boreholes L1 and L3 within a flow field established by boreholes S3 and L4. After the flow field between S3 and L4 was established, dye tracers were simultaneously injected into L1 and L3. This was intended to approximate the actual bentonite erosion test in which a flow from S3 to L4 would erode bentonite emplaced in L1 and L3. Towards the end of each tracer test a fracture survey was performed by sampling the other boreholes and the four mini-plena to determine the extent of tracer dispersion within the fracture. The boreholes were sampled by flushing 10 mL of fracture water from each hole and then collecting a 20 mL sample. In addition, the water in the L-series boreholes that is above the packers was sampled to check for possible tracer migration into fracture splays. The solute tracers used for testing purposes were uranine, iodide and bromide. In addition, red and orange fluorescent dyes were obtained from Risk Reactor (www.riskreactor.com) for use as tracers. The red fluorescent dye (IFWB-C7) was a formulated version of rhodamine WT, and the orange fluorescent dye (IFWB-33) was a formulated version of xanthene dye.

The flow rate used for solute tracer tests was 44 mL/h, which is the same flow rate used in the bentonite erosion experiment. A peristaltic pump at the withdrawal borehole was used to establish the flow rate. Water was delivered to the input borehole from a constant head system. Water was circulated between each pair of test boreholes for at least 24 hr before tracer injection. The tracer solutions used for tests BE1 to BE6 contained a nominal 80 mg/L of uranine, bromide or iodide, and had a volume of about 300 mL. In BE7 and BE8 the red and orange tracers were simultaneously injected into L1 and L3 as 10 mL volumes with either 10 mg/L or 100 mg/L tracer concentrations (See Table 4). With the exception of BE7 and BE8, the tracer injections were followed by a volume of tracer-free Grimsel water, which varied between 5 and 6 L, depending upon the total experimental time. Each test was terminated after a time period of one week, which was based on previous experience and the recovery of a reasonable tracer mass. The choice of tracer was alternated between the anions and dyes to reduce background levels at the start of each test.

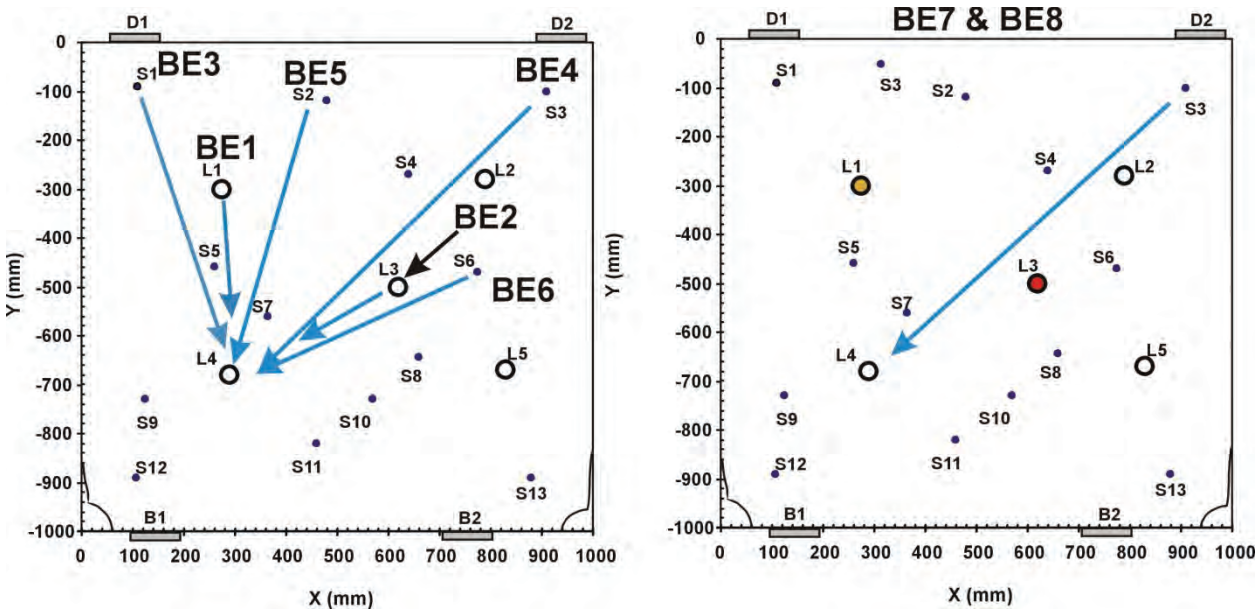

Figure 20: Borehole Pairs That Were Used for Solute Tracer Tests (BE1 to BE8) to Characterize the Fracture's Transport Properties before Bentonite Erosion Test.

Table 4: Solute Tracer Tests Performed Before Bentonite Erosion Experiment

Test	Borehole Pair	Borehole Separation	Tracer(s)	Tracer Volume and Concentration
BE1	L1 to L4	364 mm	Bromide (L1)	296 mL – 79 mg/L
BE2	L3 to L4	373 mm	Iodide (L3)	289 mL – 80 mg/L
BE3	S1 to L4	584 mm	Uranine (S1)	309 mL – 80 mg/L
BE4	S3 to L4	641 mm	Bromide (S3)	305 mL – 82 mg/L
BE5	S2 to L4	565 mm	Iodide (S2)	293 mL – 78 mg/L
BE6	S6 to L4	536 mm	Uranine (S3)	329 mL – 75 mg/L
BE7	S3 to L4	641 mm	Fluorescent Orange (L1), Fluorescent Red (L3)	10 mL – 10 mg/L 10 mL – 10 mg/L
BE8	S3 to L4	641 mm	Fluorescent Red (L1), Fluorescent Orange (L3)	10 mL – 100 mg/L 10 mL – 100 mg/L

3.1.3.2 Bentonite Erosion Test

The two bentonite plugs used in the erosion test (Figure 21) were prepared by compressing MX-80 bentonite in a form using a pressure of 15,000 psi. The dry density of the bentonite plugs was 2 g/cm^3. Each plug had a thickness of 1.94 cm and a diameter of 3.7 cm. Known quantities of fluorescent latex colloids (200 nm) were added to the bentonite before being pressed into plugs to achieve latex to bentonite mass ratio of 0.0023. Yellow-green latex colloids were added to the plug placed in L1, and red latex colloids were added to the plug placed in L3.

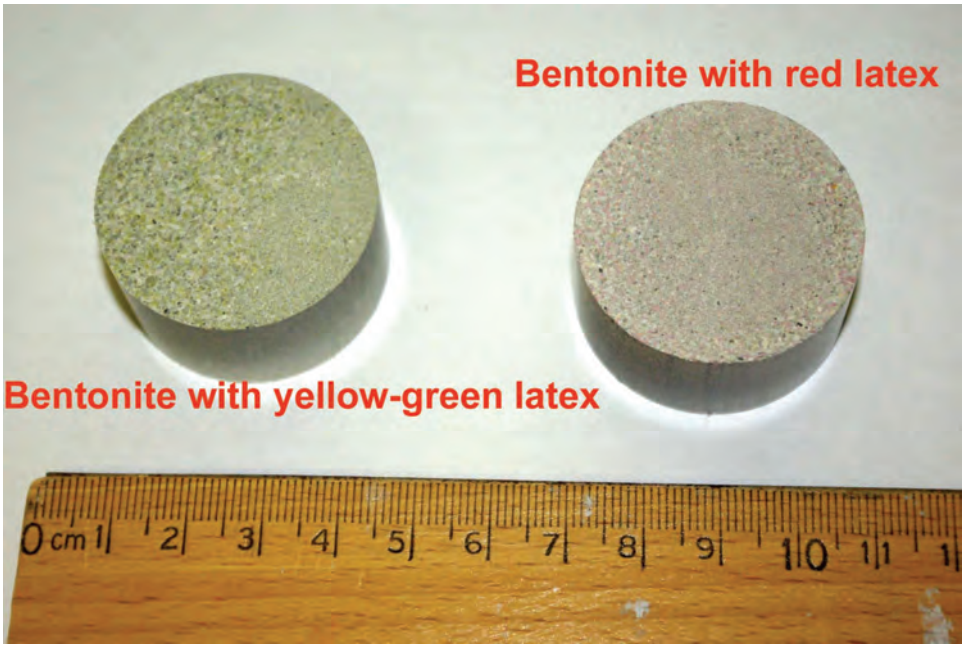

Figure 21: Bentonite Plugs Inserted into Boreholes L1 (Yellow-green) and L3 (Red).

Once the solute tracer tests were complete the Quarried Block was drained. The packers in L1 and L3 were removed and the borehole walls were allowed to dry overnight before installing the bentonite. The fit of the bentonite plugs in a synthetic borehole was tested and their diameters were adjusted to ensure that they fit down the borehole. Once the bentonite plugs were installed at the bottom of the holes, resting on the fracture surface, a stainless steel porous frit was added, followed by packer assemblies, as shown in Figure 22. The Quarried Block was then resaturated with synthetic Grimsel water. The clay was allowed to saturate and swell for 19 days with no flow. During the time of no flow fracture surveys were performed after 8 and 16 days to determine if latex and bentonite colloids had dispersed in the fracture as a function of time. The fracture surveys were performed as with the previous solute tracer tests by flushing 10 mL and collecting 20 mL of water from each available borehole. The appearance of latex and bentonite colloids would provide evidence of bentonite erosion and transport under no flow conditions. Particular attention was paid to boreholes located down-dip from the bentonite plugs since the mock-up tests showed that gravity influences bentonite transport. After the 19 days a flow field was established between S3 and L4, using a flow rate of 44 mL/h. Water collected from L4 was analyzed for latex and bentonite colloids. A borehole survey was performed after 37 days of flow to look for evidence of bentonite and latex colloid transport within the fracture. After 42 days of flow the bentonite erosion phase was concluded by initiating the first of the post-test solute tracer tests.

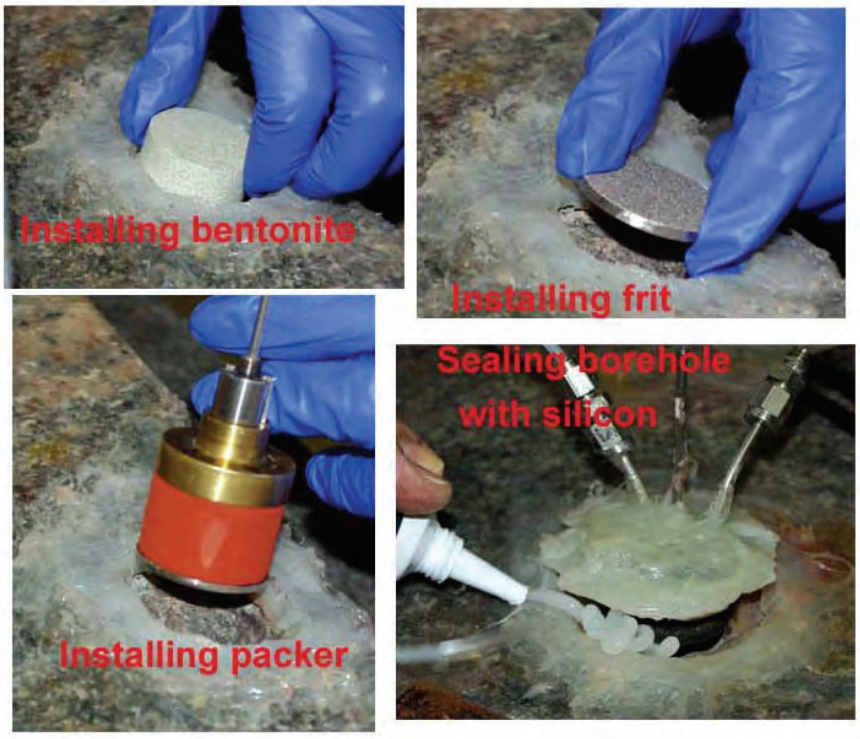

Figure 22: Installation of Bentonite Plugs, Stainless Steel Frits, and Packer Assemblies into L1 and L3 Boreholes.

3.1.3.3 Solute Tracer Tests after the Bentonite Erosion Test

The solute tracer tests performed after the completion of the bentonite erosion test are summarized in Table 5 and Figure 23. The first test (BE10) was performed without interrupting the S3 to L4 flow field that had been used for the bentonite erosion test. In the remaining tests, the flow fields were established in the test boreholes at least 24 h before tracer injection. Fracture surveys were performed for tests BE11, BE12 and BE13.

Table 5: Solute Tracer Tests Performed After Bentonite Erosion Experiment

Test	Borehole Pair	Borehole Separation	Tracer(s)	Tracer Volume and Concentration
BE10	S3 to L4	641 mm	Iodide (S3)	319 mL – 82 mg/L
BE11	S1 to L4	584 mm	Bromide (L3)	369 mL – 92 mg/L
BE12	S2 to L4	565 mm	Iodide (S2)	366 mL – 79 mg/L
BE13	S6 to L4	536 mm	Iodide (S3)	390 mL – 81 mg/L

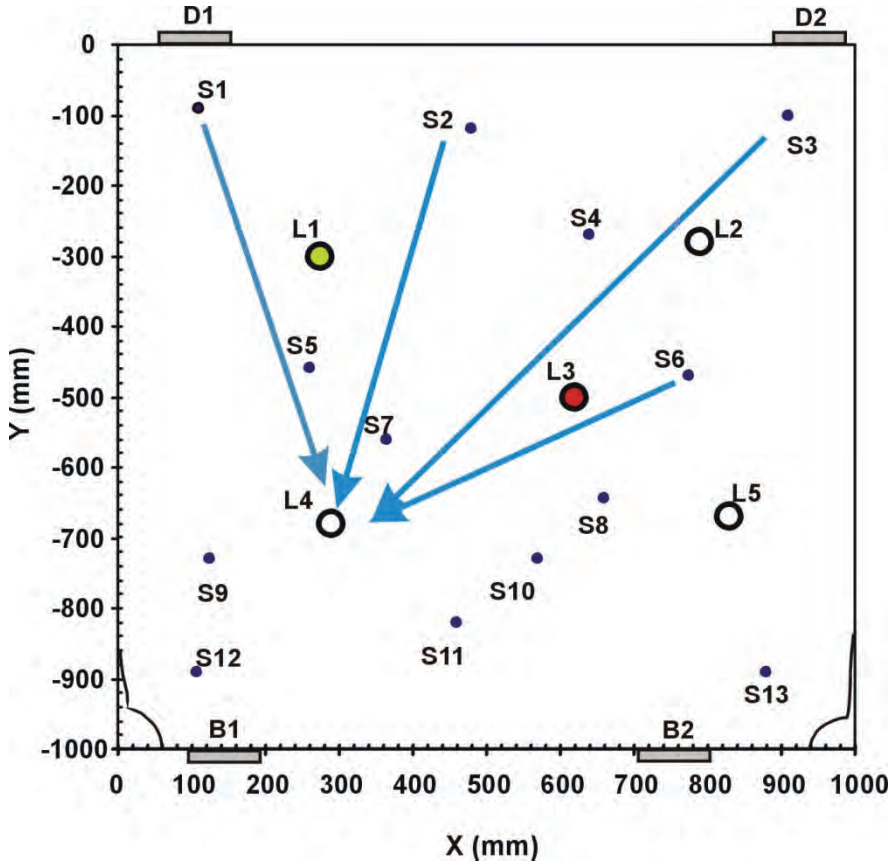

Figure 23: Borehole Pairs That Were Used for Solute Tracer Tests (BE10 to BE13) to Characterize the Fracture's Transport Properties after Bentonite Erosion Test.

3.1.3.4 Post Test Analyses

Post test analysis of possible colloid deposition on fracture surfaces and bentonite erosion from clay plugs was initiated after the completion of the solute tracer tests. The first important step was to carefully drain the water from the block in such a way as to minimize colloid mobilization. The fracture was slowly drained by starting with the boreholes accessing the parts of the fracture with higher elevation to minimize extra flow in those parts of the fracture with lower elevation. The draining operation was progressively switched to boreholes accessing lower fracture elevations. While the fracture was being drained, any water in the upper sections of the L series holes above the packers was pumped out to prevent this water from draining into the main fracture via connecting fracture splays.

After the fluid was drained from the fracture the silicon cement was cut away from the edge of the fracture, and the four mini-plena were removed. A steel frame and lifting yoke were attached to the upper section of the Quarried Block. In order to help reassemble the Quarried Block and reposition the fracture surfaces after post-test analyses, four keys were

attached to sides B and D. Using a hoist, the upper half of the Quarried Block was gently separated from the lower half. The upper half was turned over and placed beside the lower half for post-test analyses.

The upper and lower fracture surfaces were visually inspected and photographed to record the morphology of the bentonite plugs on the upper and lower fracture surfaces, and document evidence of bentonite erosion from clay plugs and subsequent bentonite deposition. A UV lamp, with a spectral range of 310 to 400 nm, was used to induce fluorescence in latex colloids. Although the optimum excitation wavelengths of red and orange colloids are outside of the spectral range of the UV lamps, the UV radiation was able to make these colloids fluoresce. The fluorescence pattern was photographed and matched with bentonite plug locations and the fracture aperture distribution (Figure 18) to help map tracer colloid erosion and deposition patterns.

In order to quantify the distribution of colloids deposited on fracture surfaces, specifically marked surface areas were sampled with a scrubbing technique that involved scrubbing the rock surface with a wet cotton swab. Colloids were recovered from the swab with deionized water and sonification. The scrubbing technique was performed under UV light to ensure to monitor the efficiency of colloid removal. Sampling locations were documented with digital photography, and the locations were plotted on images of the fracture surface. Suspensions of material recovered from fracture surfaces were analyzed for bentonite and latex colloids using the fluorometer. The results were used to estimate the mass of eroded colloids, help to determine erosion rates from the individual bentonite plugs, and identify bentonite transport and deposition patterns in relation to fracture aperture.

3.2 RESULTS

3.2.1 Solute Tracer Tests before Bentonite Erosion Experiment

The breakthrough curves for the simple dipole solute tests (BE1 through BE6) are illustrated in Figure 24, and their recoveries are shown in Figure 25.

The main purpose of these tests was to characterize the transport properties of the fracture before the bentonite erosion test. BE1 and BE2 characterize flow between L4 and the two boreholes where bentonite will be emplaced for the erosion test. BE3 through BE6 will be repeated after the erosion test to determine whether bentonite erosion has influenced flow characteristics within the fracture. The overall results of the tracer tests showed that the breakthrough curves had multiple peaks, indicating the presence of multiple flow pathways within a complex fracture. The mass recoveries were higher from flow paths that started near the top of the fracture (Figure 18), where apertures are larger, compared to recoveries from flow paths starting in the middle part of the fracture (L3 and S6), which have smaller apertures and possibly more complex flow paths.

In tests BE7 and BE8 a flow field was established between S3 and L4, and then fluorescent dyes were injected into L1 and L3. The breakthrough curves for these tests are illustrated in Figure 26, with recoveries shown in Figure 27. The test results showed that a significant fraction of solute tracer originating at L3, whether red or orange dye, is captured by the flow

field established by the S3 to L4 dipole. The dyes injected into L3 displayed similar behaviour in both BE7 and BE8, despite a significant difference in injected tracer mass (Table 3). The tracer recoveries were similar and in both tests the tracers from L3 displayed a rapid breakthrough, consistent with test BE2 (L3 to L4). In test BE7 the amount of orange tracer injected in L1 was too low to produce usable data. In BE8 the red tracer from L1 displayed a good breakthrough curve, with a delayed main peak compared to tracer from L3. Although not tabulated in this report, the tracer from L1 also showed close to 100 % combined recovery from both the breakthrough curve and the fracture survey. Since the tracer injection into L1 in BE7 did not produce usable data, the data sets from BE8 provide the best comparison of transport from L1 & L3 to L4. The transport of tracer from L1 was significantly delayed compared to tracer from L3. Tracer injected into L1 tends to remain in the upper left side of the Quarried Block, while tracer from L3 tends to be in the mid to upper left side (Figure 28). Tracer concentrations above the packers in the L-series holes were not significant. In summary, provided that bentonite erosion occurs, it is possible that bentonite and latex colloids will be transported to L4. Colloids from L3 should arrive first. Due to the longer transport times there is a possibility that bentonite colloid transport from L1 to L4 may be more limited compared to bentonite colloids from L3.

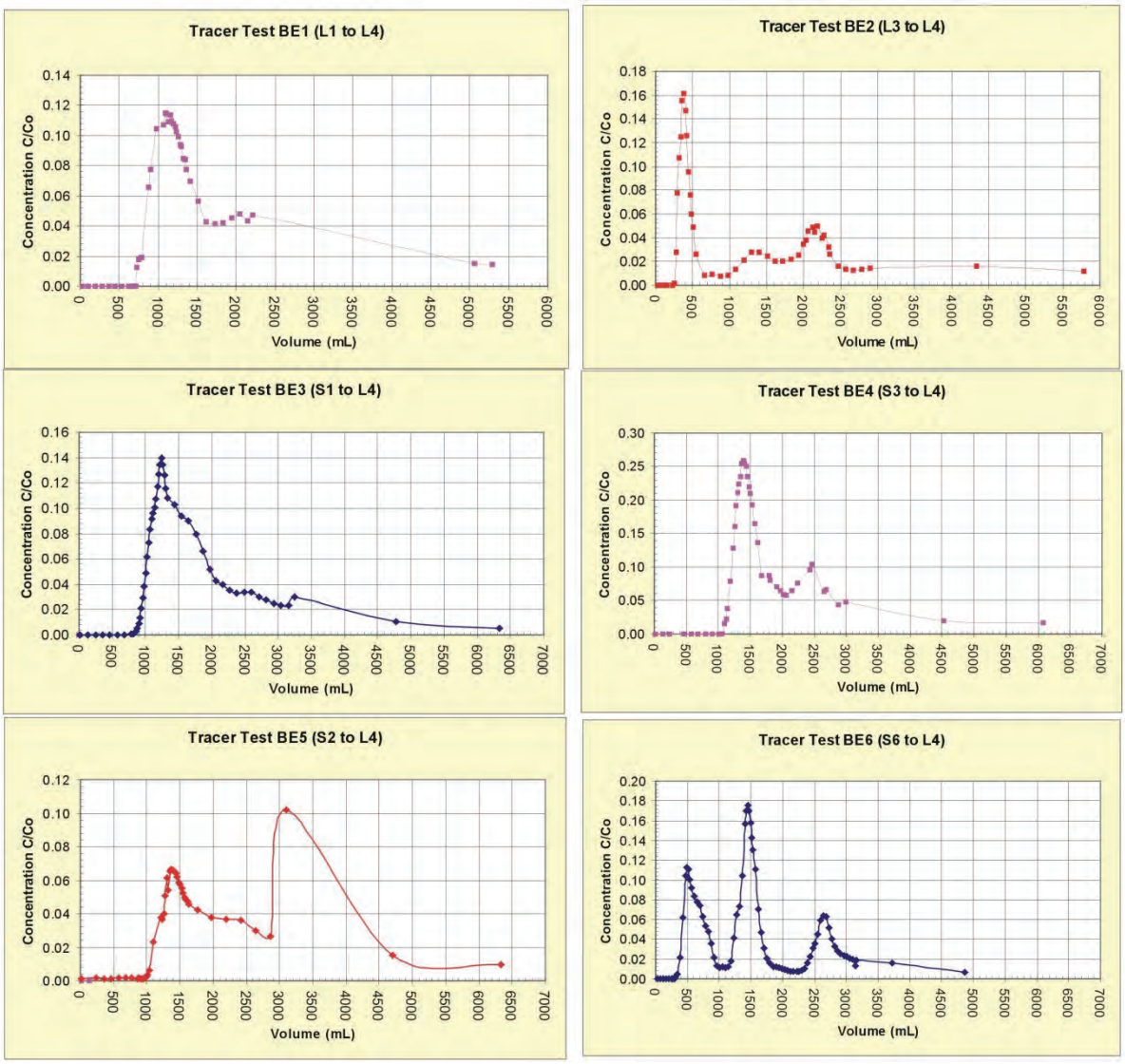

Figure 24: Breakthrough Curves of Solute Tracer Tests before Bentonite Erosion Experiment.

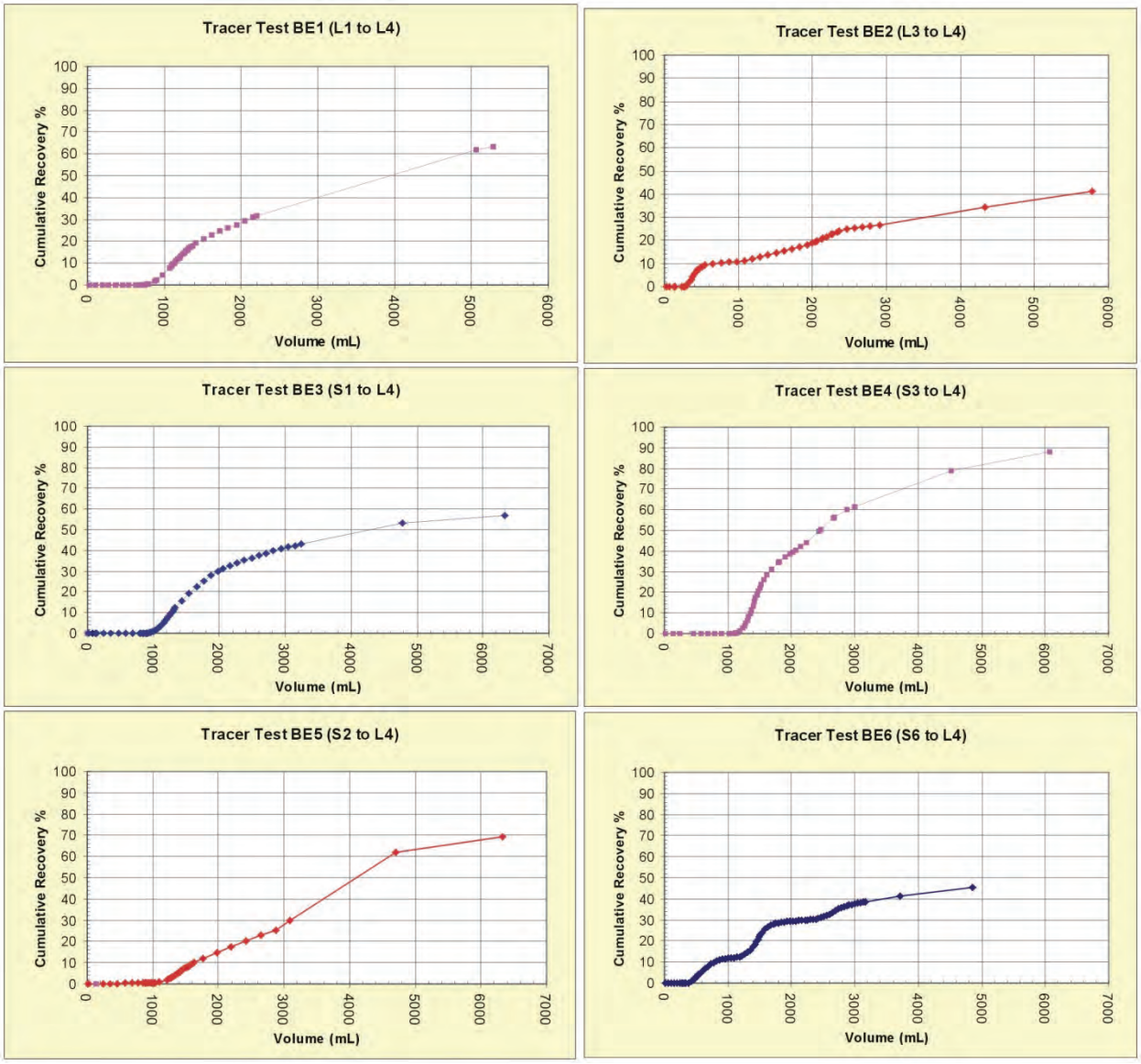

Figure 25: Percent Recoveries of Solute Tracer Tests Performed Before Bentonite Erosion Experiment.

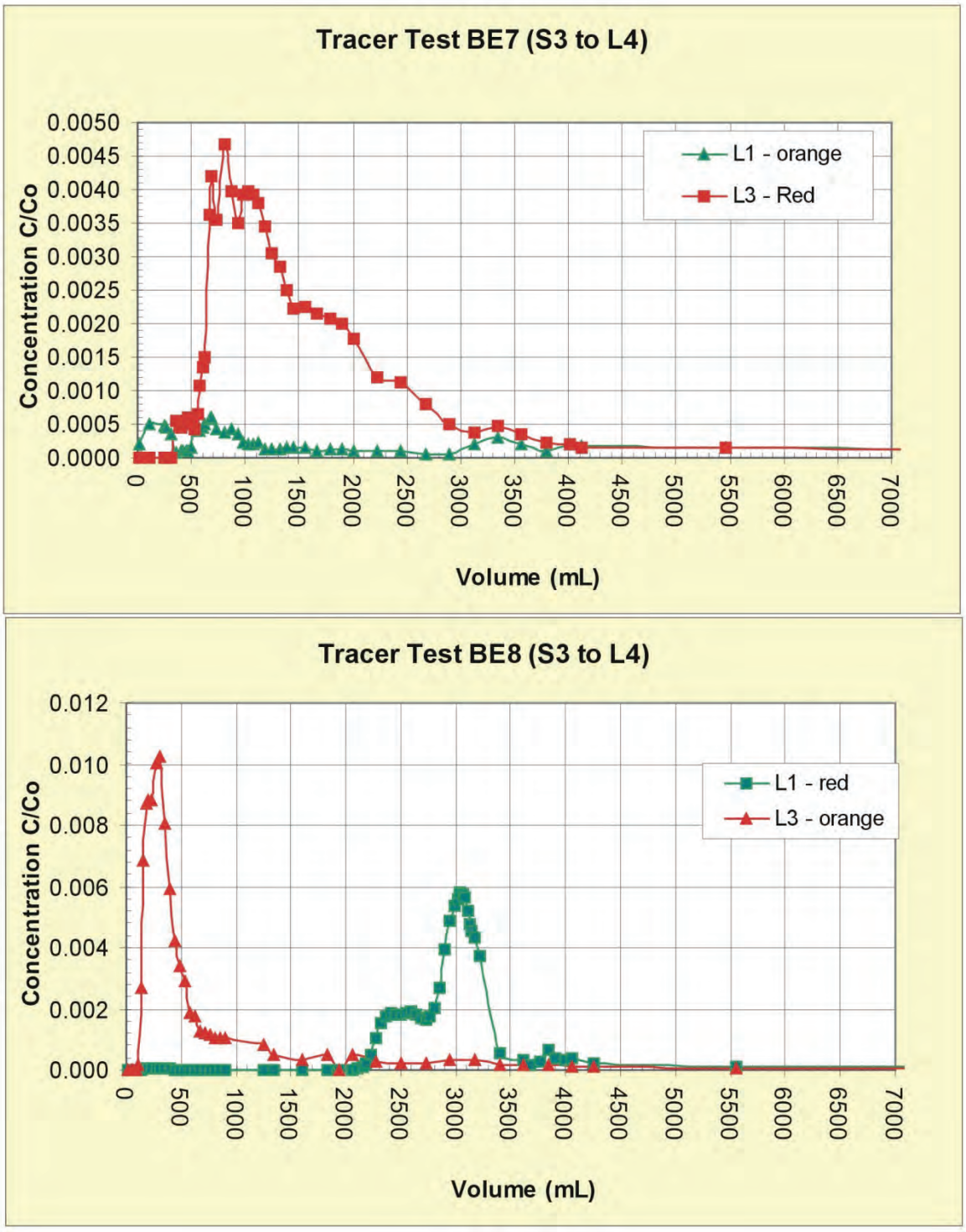

Figure 26: Breakthrough Curves of Solute Tracer Tests with Dye Injections into L1 and L3 in the Presence of the S3 to L4 Flow Field.

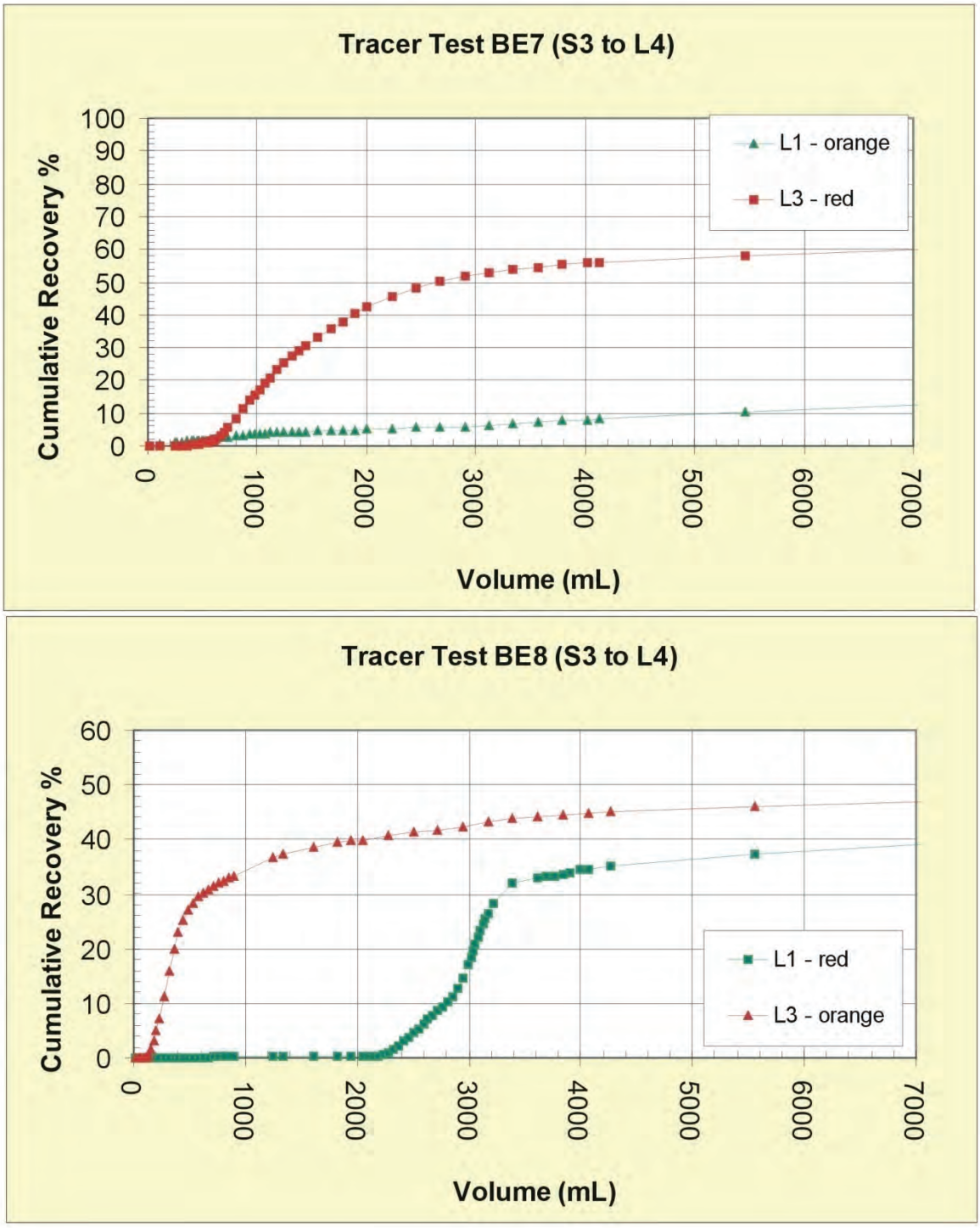

Figure 27: Percent Recoveries of Solute Tracer Tests with Dye Injections into L1 and L3 in the Presence of the S3 to L4 Flow Field.

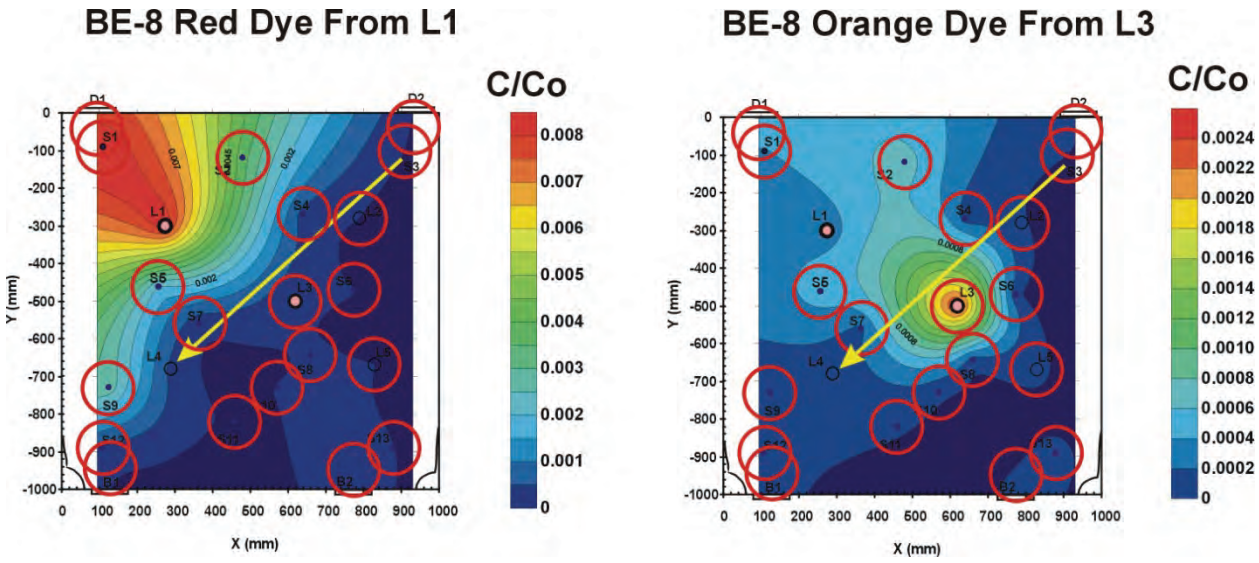

Figure 28: Distribution of Tracers Injected into L1 and L3 within the Fracture after an Elution Volume of 4 Litres.

3.2.2 Bentonite Erosion Experiment

The initial part of the bentonite erosion experiment consisted of a 19 day period of no flow to allow the bentonite to swell and to generate colloids without the influence of hydraulic forces. During this time period the only way to access the progress of any bentonite erosion and colloid generation was through fracture surveys after 8 and 16 days. The observed concentrations of latex colloids in these surveys were at background levels (0 to 0.2 mg/L) and provided no evidence of bentonite erosion. Observed bentonite colloid concentrations (Figure 29) were also very low. The bentonite distributions in Figure 29 do not show a pattern of bentonite transport away from L1 and L3 (both of which could not be sampled for the survey), and likely represent background concentrations. Although later post-test analyses revealed that down-slope movement of bentonite did occur, this movement was not extensive enough to be picked up by the borehole surveys.

Once flow was initiated the concentrations of bentonite and latex colloids were monitored in the water pumped from L4 (Figure 30). Bentonite colloid concentrations (representing colloids generated from the bentonite as well as the fracture) were initially at 0.8 and 0.7 mg/L before flow, and then decreased to 0.2 mg/L after 4 L, and eventually to less than 0.1 mg/L. The flow did not generate any additional colloid arriving at L4, and served to mainly deplete concentrations that were present before the start of flow. The concentrations of latex colloids arriving at L4 were also extremely low, and were close to detection limits. The apparent background concentrations of fluorescing latex colloids appear to have been increased due to the use of fluorescing solute dyes in previous tests. There appeared to be a small peak of red latex possibly from L3 showing up within the first 500 mL. This is similar to the behaviour of dye from L3 in previous tests. The latex from L1 shows a small peak in the 2000 to 3000 mL range, which is consistent with the travel time of tracer from L1. These latex peaks may represent latex that was released during the period of bentonite expansion that occurred during the 19 day period of no-flow. Following the initial release of colloids, it seems that bentonite erosion became minimal and stopped releasing

colloids in significant enough quantities to reach L4. As in many of the tests in the synthetic fracture, colloid generation could not keep up with the removal rate of flowing water. Figure 31 shows the bentonite distribution during the fracture survey taken 37 days after the start of flow. Again the bentonite concentration distribution did not display any pattern that would suggest transport away from L1 or L3. There appeared to be an increase in bentonite in the lower left side, which corresponds to the lowest elevation in the fracture plane. This would be consistent with the down slope movement of bentonite colloids, which are unlikely to be captured by L4. The concentrations of fluorescing latex colloids were also at background levels during the survey.

In summary, the concentrations of bentonite and latex colloids eluted from L4 and observed at other borehole locations suggested a minimum amount of bentonite erosion and colloid generation.

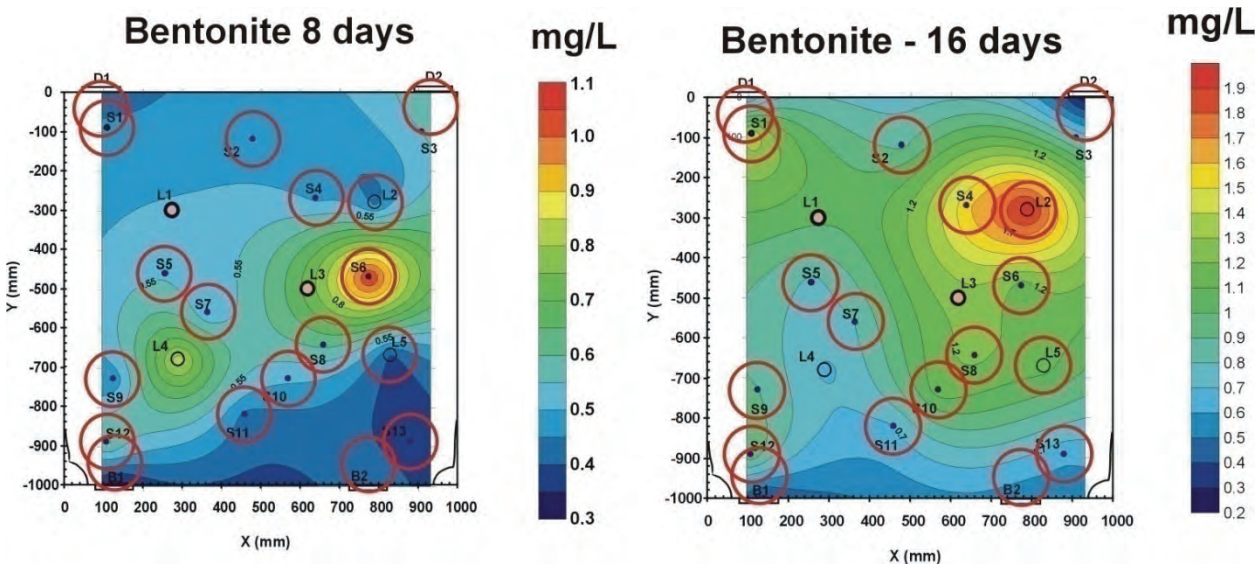

Figure 29: Bentonite Distribution in the Fracture during the Period of No Flow.

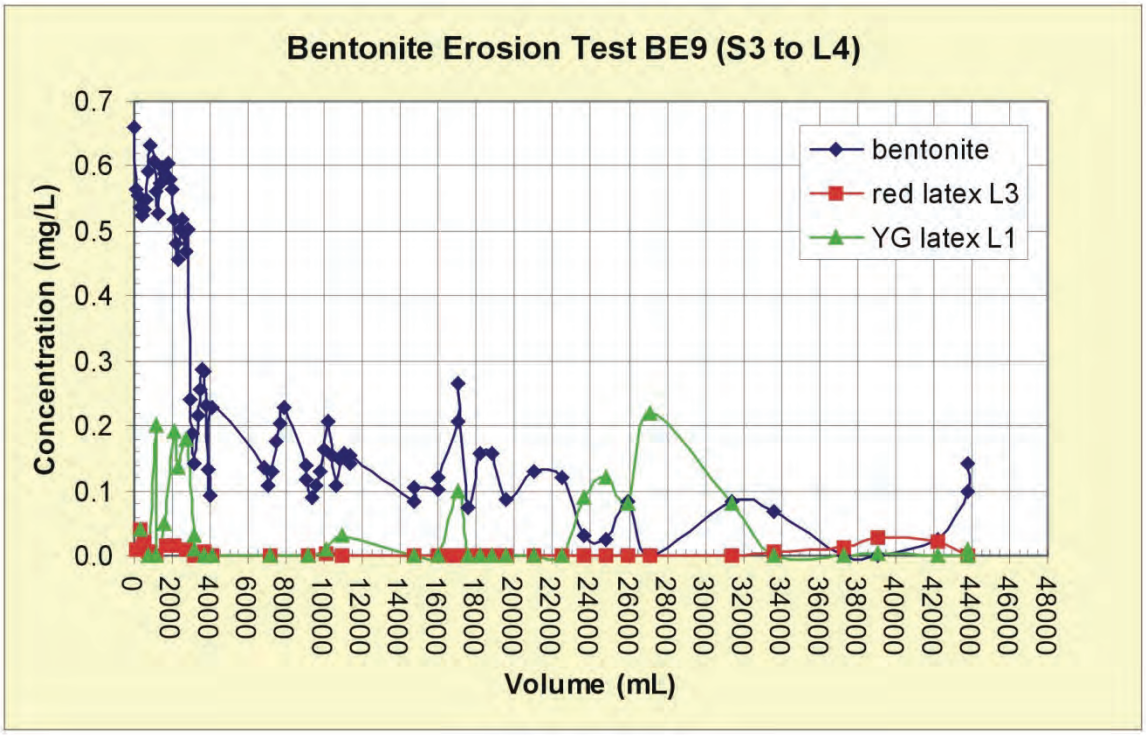

Figure 30: Concentrations of Bentonite and Latex Colloids Eluted from the Fracture

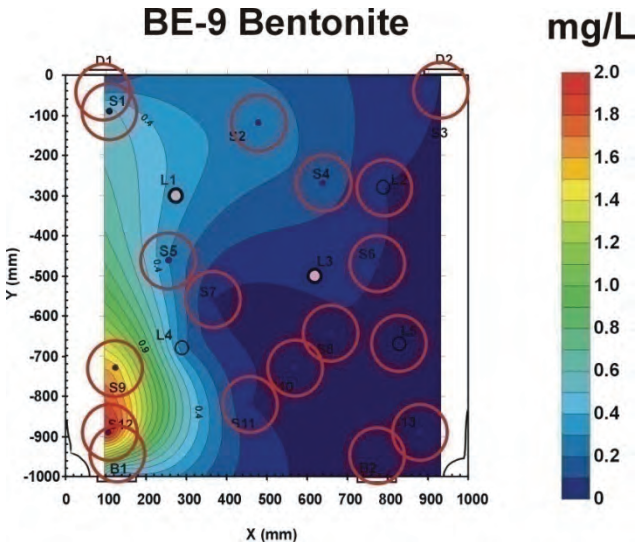

Figure 31: Bentonite Distribution in the Fracture during the Period of Flow.

3.2.3 Solute Tracer Tests after Bentonite Erosion Experiment

The breakthrough curves and percent recoveries of the solute tracer tests performed after the bentonite erosion experiment are shown in Figure 32 and compared to the results of tracer tests performed before the erosion test. Note that in previous studies in the Quarried Block the transport behaviour of iodide, bromide and uranine were similar. Therefore, it is valid to compare the breakthrough curves of different tracers to look for evidence of changes in fracture transport properties. Tracer distributions in the fracture after three tests are compared in Figure 33. A comparison of solute tracer test results indicates significant changes in transport properties after the bentonite erosion tests. Solute tracer for the borehole pair S3 to L4 arrived slightly earlier after bentonite erosion, and displayed 3 peaks instead of 2. For tests between S1 and L4 solute tracer also arrived earlier and displayed 3 peaks instead of one broad peak. Before the bentonite erosion experiment solute tracer remained in the middle of the Quarried Block, but after bentonite erosion solute tracer tended to concentrate in the upper right and lower left corners. After bentonite erosion, solute tracer injected into S2 arrived significantly earlier than before bentonite erosion, and was characterized by 3 sharp peaks instead of 2 broad peaks. Although the first arrival of tracer injected into S6 was similar before and after bentonite erosion, a large fraction of the tracer arrived significantly faster after bentonite erosion. Also, after bentonite erosion the tracer from S6 was found in the lower left region of the fracture around L4, whereas before bentonite erosion it tended to concentrate in the upper part of the fracture (Figure 33).

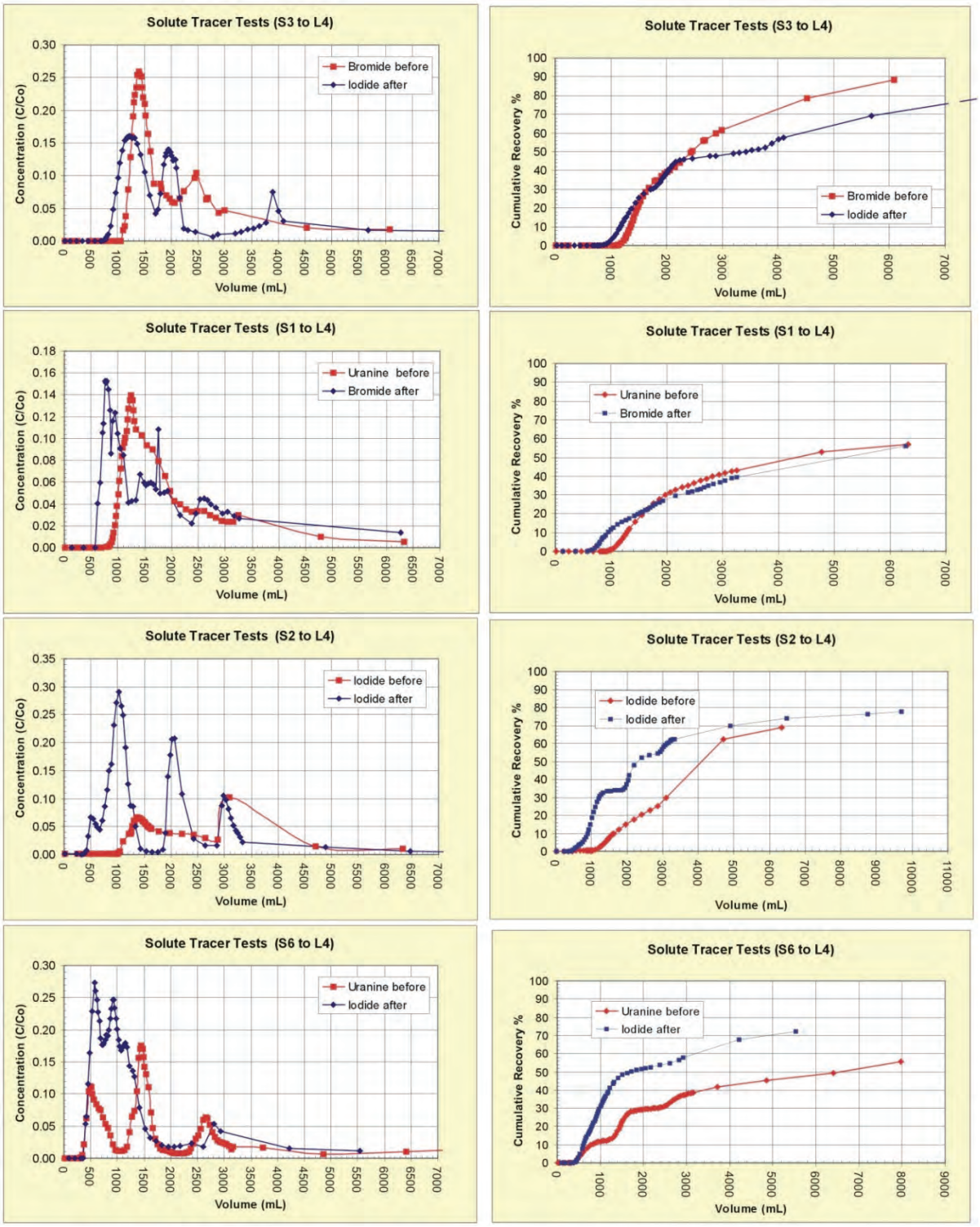

Figure 32: Compare Solute Transport Before and After the Bentonite Erosion Experiment, in the Form of Breakthrough and Percent Recovery Curves.

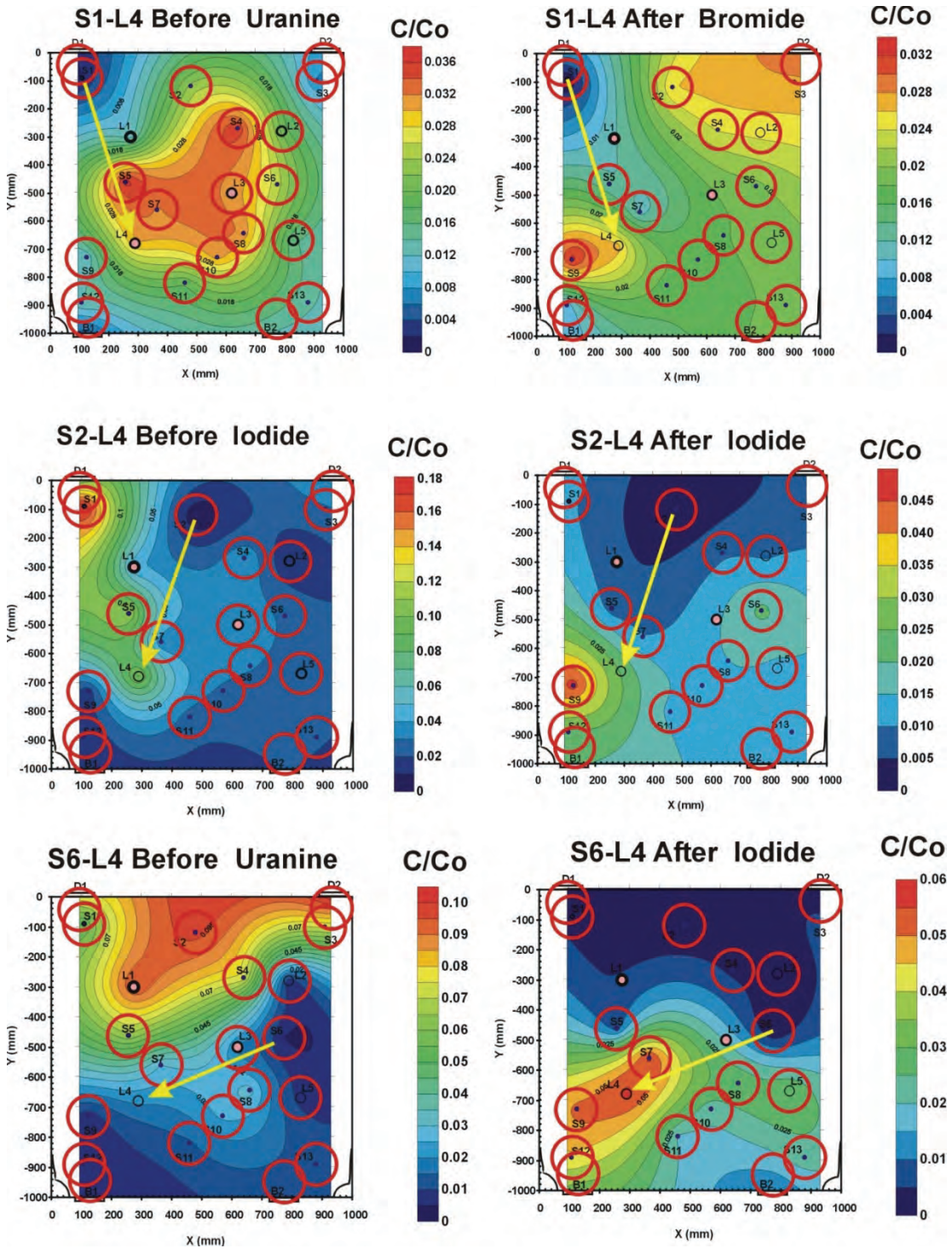

Figure 33: Compare Solute Tracer Distributions in the Fracture Before and After Bentonite Erosion. The Elution Volumes Were Between 3100 and 3300 mL.

3.2.4 Post Test Analyses of Fracture Surface

The low concentrations of colloids (bentonite and latex) extracted from L4 and the other holes used for post-test analyses suggest that only a minimum amount of bentonite colloid transport has taken place. At the completion of the bentonite erosion experiment and the solute tracer tests it was not known whether (1) erosion did not take place or (2) whether erosion did occur and the colloids were trapped. The changes in fracture transport properties suggest that bentonite deposition in the fracture had taken place. The goal of the post-test analyses was to examine the fracture surfaces and the remaining bentonite in the boreholes to discover what actually happened. The specific objectives of the post-test analyses were:

- Determine bentonite mass distribution between what was left in the boreholes, what was extruded from each borehole, and what was deposited during transport.
- Determine the effect of fracture slope and aperture on bentonite extrusion and transport.
- Determine to what extent, if any, bentonite and latex colloids were transported.
- Identify trapping mechanisms (pockets of larger aperture, fracture slope, channelling caused by aperture distribution) that may have prevented colloids from reaching L4 and other boreholes.
- Demonstrate the usefulness of fluorescent latex colloids as tracers to help visualize possible bentonite erosion and subsequent transport.

Observed bentonite morphology after opening: Figure 34 shows the L1 bentonite plug exposed on the upper and lower fracture surface shortly after the fracture was opened. Under UV light the yellow-green fluorescence clearly marked the presence of bentonite from L1. During borehole opening the bentonite plug came free of the borehole and was fixed on the bottom fracture surface where it was anchored by local surface morphology. The stainless steel frit is still attached to the top of the bentonite plug. The gel layer that expanded into the fracture can be seen on the upper and lower fracture surfaces. The morphology of the gel layer includes ridges that formed during the opening of the fracture; much like a thick paint between two surfaces would do when the surfaces are pulled apart. The morphology of the bentonite on the bottom surface also reflects expansion into local areas of larger aperture. Figure 35 shows the L3 bentonite on the upper and lower fracture surfaces. The L3 bentonite remained in the borehole, with small amounts attached to the bottom fracture surface. The view of the top fracture surface only shows the expanded bentonite gel, since the rest of the clay is still in the borehole. The gel on the upper surface contains light coloured rock fragments that were detached from the bottom surface upon opening the fracture. The bottom fracture surface contains a small amount of bentonite gel, whose presence was highlighted by the red fluorescence.

The morphology of both clay plugs displayed features that were seen in the mock-up tests. The expanded clay formed a ring close to the borehole that filled the entire fracture aperture. This was surrounded by a thinner ring that likely did not fill the entire aperture. Once the bentonite was allowed to dry, the outer ring formed a very thin deposit that would be difficult to see without the presence of fluorescent colloids. There was no evidence of mineral separations as was seen in the mock-up tests that had high bentonite erosion rates in the presence of deionized water.

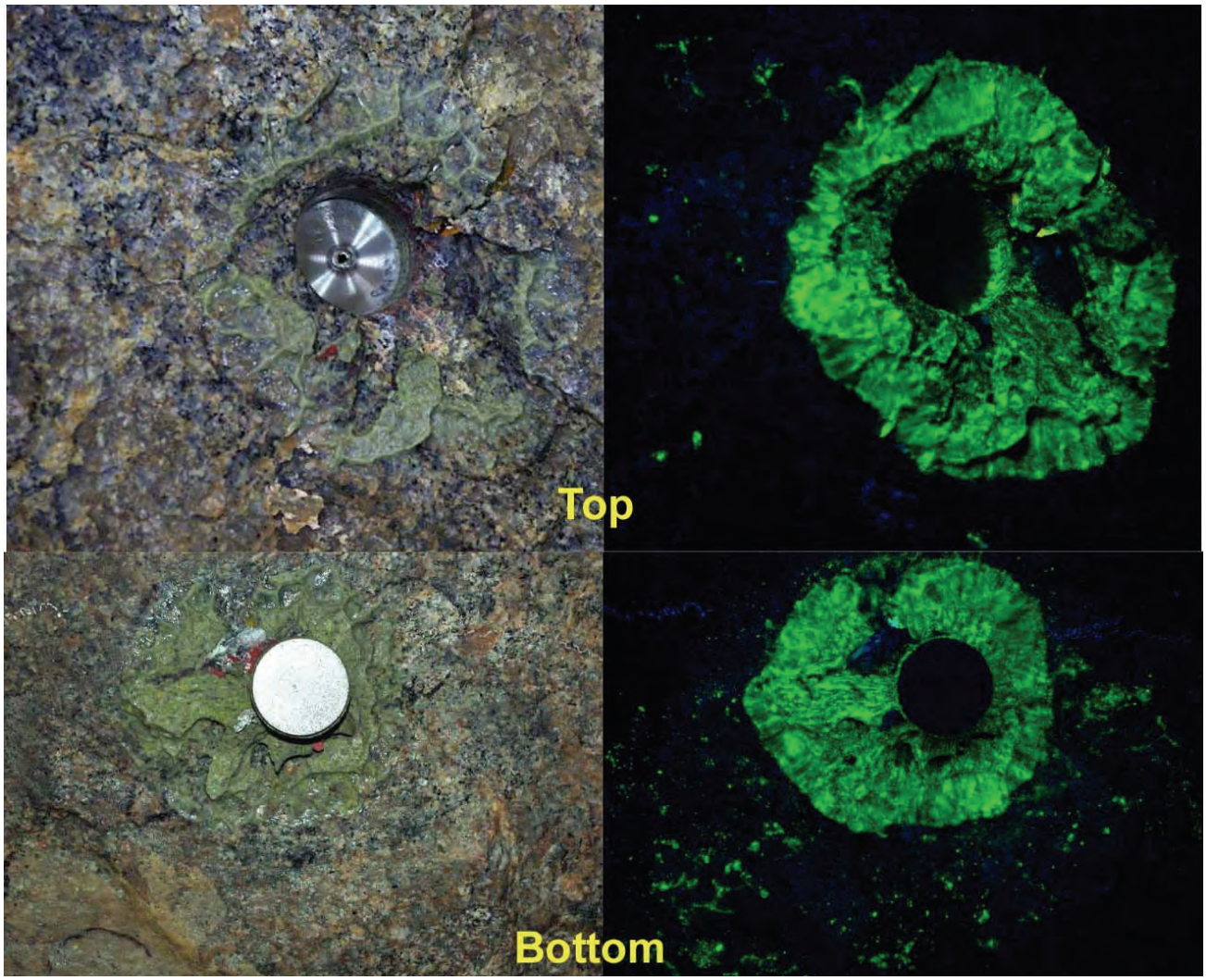

Figure 34: Top and Bottom Views of L1 under Plain Light on the Left and UV Light on the Right.

After about 3000 h of being in contact with synthetic Grimsel water the gel ring around L1 had a diameter of 12.7 ± 0.6 cm, which corresponds to an expansion ratio of 3.34. The gel ring around L3 had a diameter of 13.4 ± 0.6, giving an expansion ratio of 3.62. It is hard to compare these expansion ratios to the tests in the synthetic fracture because we do not know when (or if) the bentonite in the Quarried Block stopped expanding. If one were to extrapolate the expansion rate observed in Test 8 in the synthetic fracture, it would take approximately 1000 h to reach an expansion ratio of 3.6.

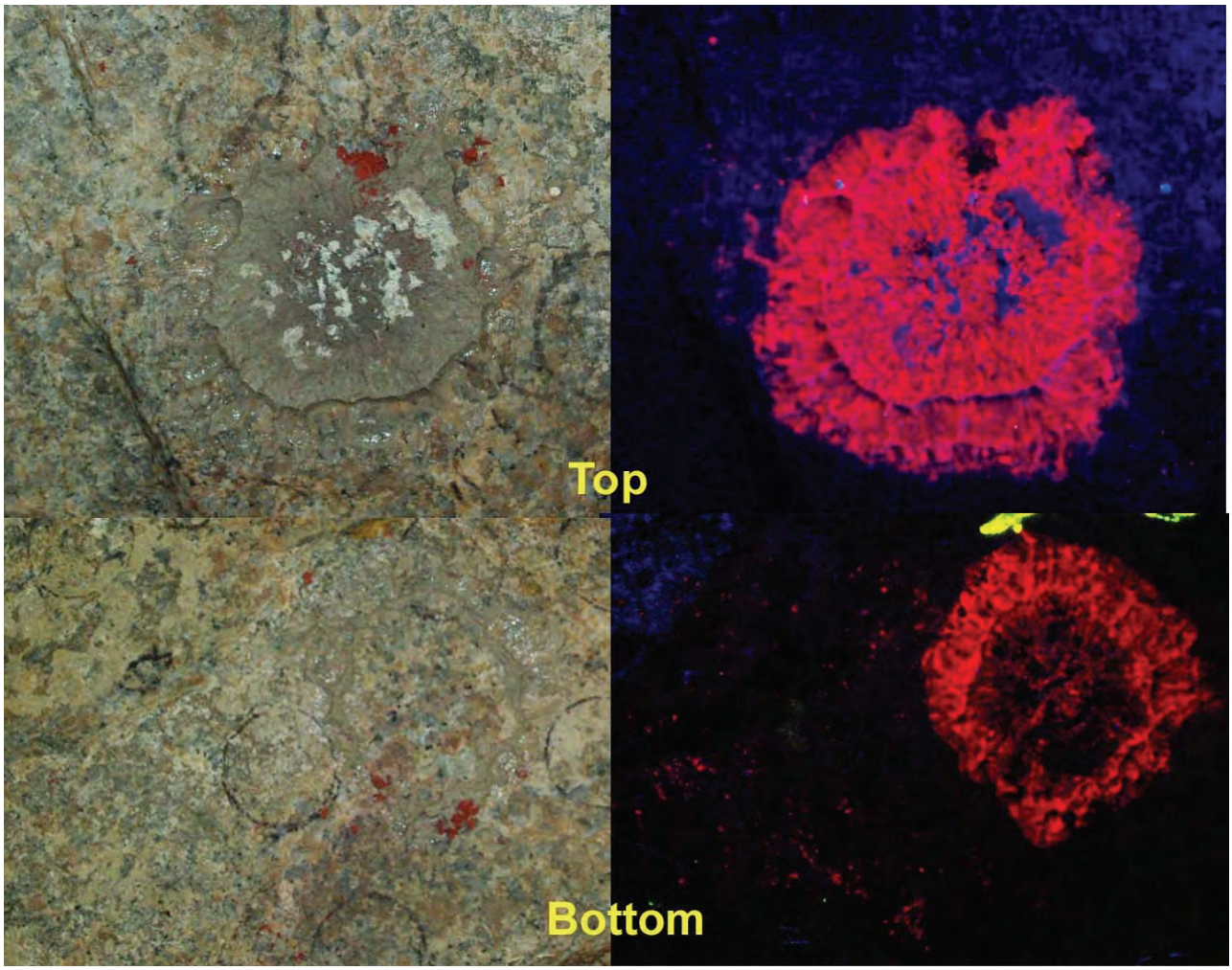

Figure 35: Top and Bottom Views of L3 under Plain Light on the Left and UV light on the Right.

UV images to map extent of bentonite transport and deposition: The fracture surfaces were photographed in UV and visible light, and the photos were digitally adjusted to fit the map of borehole locations in the Quarried Block. Figure 36 shows the distribution of fluorescence on the top fracture surface, while Figure 37 shows the corresponding fluorescence on the bottom fracture surface. Note that the image in Figure 36 has been flipped so that it matches the orientation of the bottom fracture surface in Figure 37. The blue colour in these images is the reflection of light from the UV lamp and should be ignored. The top fracture surface contains slightly more fluorescence than the bottom surface, but the distribution patterns on both surfaces are similar. Bentonite from both plugs shows an erosion and deposition pattern that runs down slope from the bentonite source, just as one would predict from the mock-up tests. No up slope bentonite deposition can be seen. Figure 38 shows a close up of the L1 and L3, with the fluorescence superimposed on a photo take in visible light. The Appendix contains photos showing swab sample locations under UV light. These provide more detail on the distribution of fluorescence on fracture surfaces. The bentonite eroding from L1 appeared to move down slope along 3 paths.

Bentonite appeared to accumulate along the fracture edge with the lowest elevation, as seen in the mock-up tests. The bentonite from L3 also moved down slope along pathways that appeared to be correlated with fracture morphology. The extent of L3 bentonite erosion and transport seem to be less extensive than for L1, probably since there was a pocket of larger aperture around L1.

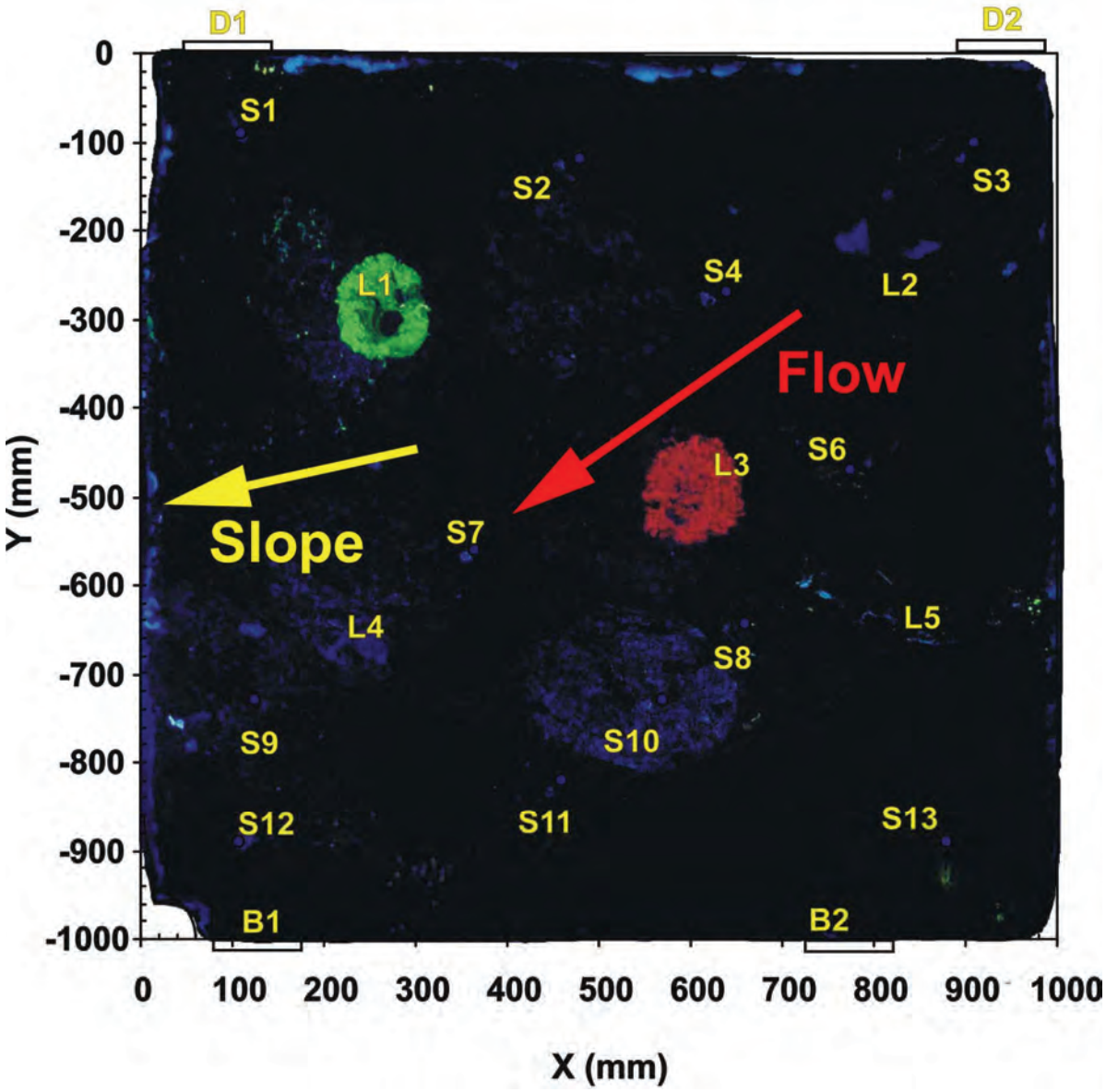

Figure 36: Top Fracture View.

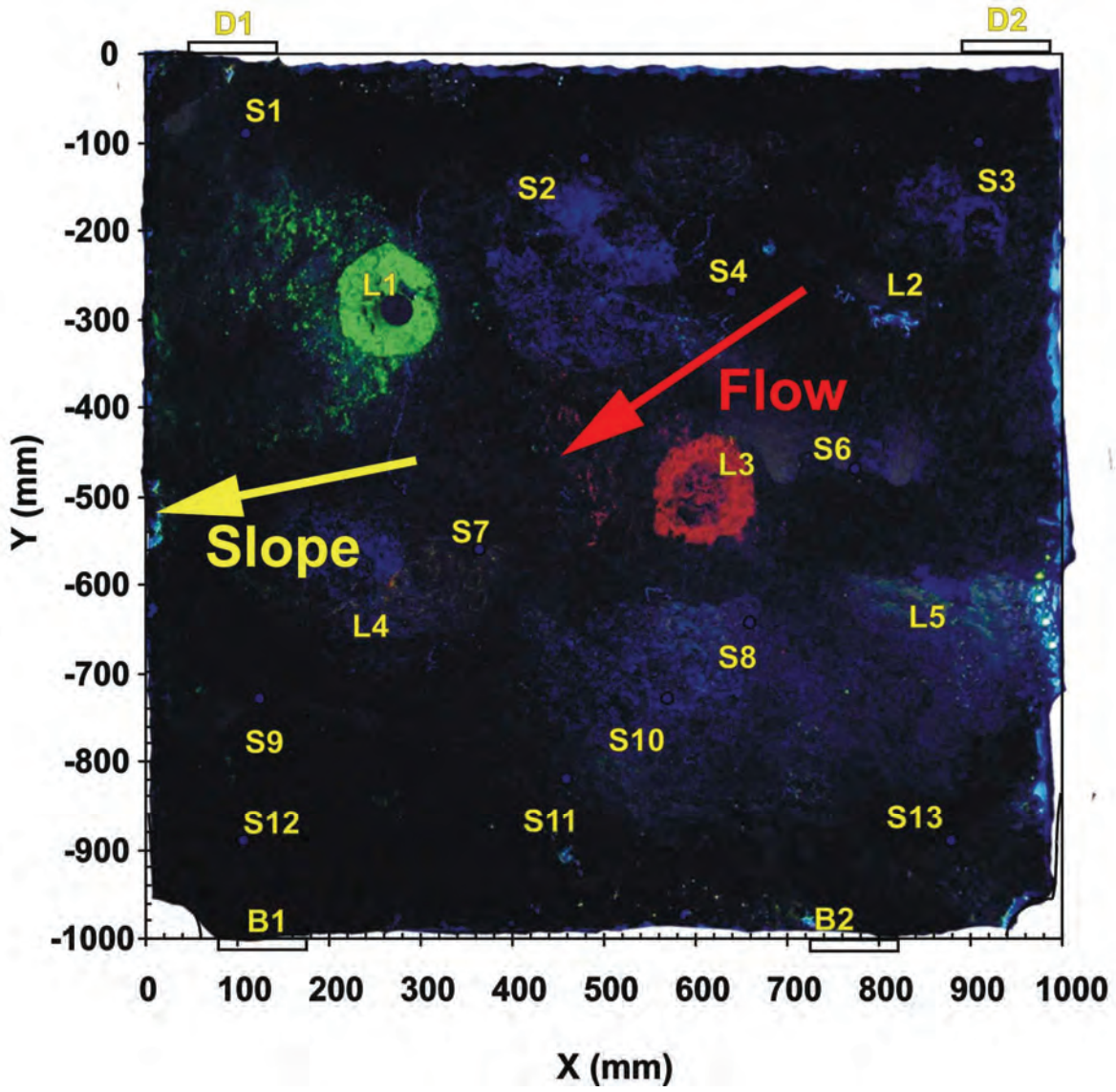

Figure 37: Bottom Fracture View

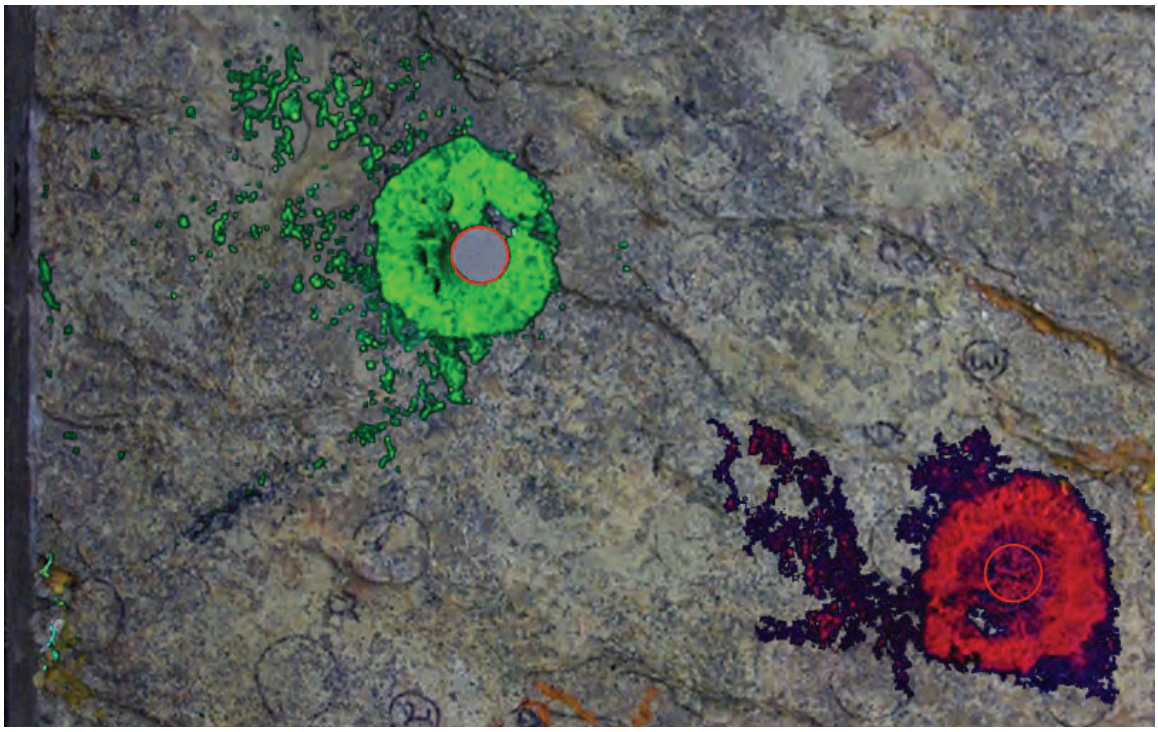

Figure 38: Close Up of L1 and L3, Showing Fluorescence Superimposed On the Bottom Fracture Surface. Red Circles Show Location of Bentonite before Expansion.

Bentonite recovery and Swab sampling of fracture surfaces: The bentonite on the fracture surfaces was allowed to dry before any attempt was made to recover and sample bentonite deposits. The bentonite that had extruded into the fracture was easily removed from the fracture surface and saved for analyses. Parts of the thinner outer rim were also scraped from the fracture surface and saved for analyses. The L1 and L3 bentonite plugs were easily recovered. However, after all of the easily recoverable bentonite mass was removed from the rings surrounding the bentonite plugs, a strong fluorescence was still evident on the fracture surfaces, indicating that some bentonite and latex was fixed to the rock surfaces.

Assuming that the presence of fluorescing colloids on fracture surfaces was an indication of bentonite deposition, selected areas on both fracture surfaces were swabbed under UV light. The removal of fluorescence was used as an indication of complete colloid removal from a given sample area. The intent of this sampling program was to confirm the association of bentonite and fluorescing latex colloids and to estimate the mass of remaining bentonite as a function of surface area. Figures A1 through to A4 in the Appendix identify the regions on the upper and lower fracture surfaces that were sampled by swabbing. Areas without fluorescence were sampled to establish background bentonite concentrations. Measured bentonite concentrations were corrected for background values.

Table 6 summarizes the average surface concentrations (mg/cm^2) of bentonite colloids recovered from fracture surfaces in the vicinities of L1 and L3. The gel type deposit refers

to those areas beneath the inner and outer rings of bentonite that had expanded into the fracture. These samples represent the material left behind after the overlying solids had been removed. The fracture type samples represent areas on fracture surfaces outside of the rings surrounding the bentonite plugs, where apparent bentonite deposition had taken place. The mass concentration of bentonite per surface area in the gel type deposits was about 10 times higher than in the fracture deposits. This is probably because, as indicated by the fluorescence, the gel deposits had a relatively high colloid concentration that was uniformly distributed. The fracture deposits consisted of patches with high and low colloid concentrations. With the exception of gel deposits from L1, the concentrations of bentonite per area within colloid deposits were similar on the upper and lower fracture surfaces.

Table 6: Summary of Swab Analyses

Location	Deposit Type	Average Bentonite (mg/cm^2)	Average Mass Ratio of Red Latex to Bentonite	Average Mass Ratio of Yellow-Green Latex to Bentonite
L1 top	gel	0.18 ± 0.04		0.015 ± 0.005
L1 bottom	gel	0.27 ± 0.06		0.026 ± 0.013
L1 top	fracture	0.04 ± 0.03		0.009 ± 0.004
L1 bottom	fracture	0.04 ± 0.04		0.010 ± 0.004
L3 top	gel	0.11 ± 0.05	0.023 ± 0.003	
L3 bottom	gel	0.12 ± 0.10	0.038 ± 0.034	
L3 top	fracture	0.01 ± 0.01	0.011 ± 0.007	
L3 bottom	fracture	0.03 ± 0.02	0.031 ± 0.073	

gel: surfaces beneath the inner and outer rings after bentonite solids removed.
fracture: areas of apparent bentonite deposition beyond the outer ring.

The original mass ratio of fluorescing latex to bentonite was 0.0023 for both bentonite plugs. The average latex/bentonite ratios are given in Table 6. The average latex/bentonite ratio for fracture deposits from L1 were a factor 4 higher than in the original bentonite, while the ratios in the gel were a factor 7 to 11 higher. The bentonite deposits from L3 were slightly more enriched with respect to latex. The ratios in their fracture deposits were a factor 5 to 13 higher while the average ratios in the gel were a factor 10 to 17 higher. As with the mock-up tests, a higher fraction of latex was mobilized compared with the mobilized fraction of bentonite.

The observed concentrations of bentonite colloids in the fracture deposits were actually small. Using an approximate area of 770 cm^2 for the extent of fracture deposits around L1, the combined mass of bentonite colloids from upper and lower fracture surfaces that was released from L1 was estimated to be 0.057 g, based on average surface concentrations. Similarly the amount of bentonite colloids released from L3 was 0.011 g, based on an approximate surface area of 270 cm^2.

Bentonite mass balance: The bentonite masses (as room dried weights) recovered from fracture surfaces are presented in Table 7, along with the original mass of each bentonite plug. In the case of L1, 70 percent of the original bentonite mass was recovered from the plug that was stuck to the bottom fracture surface. About 12.7 percent had extruded into a high aperture cavity near L1. The total amount of gel recovered from the upper and bottom fracture surfaces was 13.9 percent. The total unaccounted mass of L1 bentonite was 1.40 g, or 3.3 percent of the total mass. For comparison, the estimated amount of bentonite deposited in the fracture was only 0.06 g. The recovered L3 plug represented 83.7 percent of the total mass. The total recovered gel from both fracture surfaces was 13 percent. The total unaccounted mass of 1.38 g was 3.3 percent of the total mass. The estimated mass of bentonite deposited in the fracture was 0.011 g. Note that for both bentonite plugs, the highest mass of gel was recovered from the fracture surface that contained the bentonite plug. Also the fraction of bentonite that formed gel layers was similar for both bentonite plugs. The total mass of bentonite recovered from L4 during the bentonite erosion experiment was 0.005 g, which is insignificant compared to the total bentonite mass in the system.

Table 7: Mass Balance of Bentonite Recovered During Post-Test Analyses

Bentonite Source	Category	Recovered Bentonite Mass (g)	Percent of Original Mass
L1	**original mass in borehole**	42.5	
	gel on top fracture	1.4499	3.4
	gel on bottom fracture	4.4543	10.5
	extruded in cavity beside L1	5.4021	12.7
	plug recovered from L1	29.7333	70.0
	unaccounted mass	1.4034	3.3
	estimated in fracture from swab	0.062	0.1
L3	**original mass in borehole**	41.6	
	gel on top fracture	4.3353	10.4
	gel on bottom fracture	1.0677	2.6
	Plug recovered from L3	34.8004	83.7
	unaccounted mass	1.3846	3.3
	estimated in fracture from swab	0.011	0.0

3.3 DISCUSSION

The bentonite erosion test in the Quarried Block (QB) provided a link between the simple mock-up tests and the geosphere by introducing the variability of a natural fracture and increasing the time scale by a factor of about 4. In the mock-up tests it was relatively easy to visualize the progress of bentonite expansion into the fracture and the generation of

colloids. This would not be the case in the Quarried Block, or in field-scale experiments. Although further complexities and uncertainties would arise when extending QB-scale results to the field scale, the procedures developed for the bentonite erosion experiment could be used as a guide for developing the protocol for field scale tests.

The strategies used to estimate progress and impact of bentonite erosion and colloid generation focussed on monitoring colloid concentrations in water eluted from borehole L4, measuring colloids from neighbouring boreholes, and using solute tracers to evaluate changes in fracture transport properties triggered by bentonite deposition. Evidence gathered during the stagnant and the flow phases of the bentonite erosion experiment suggested that bentonite erosion and colloid generation were very low. During the period of no flow, borehole surveys detected very low bentonite colloid concentrations and only background concentrations of latex colloids. The apparent background concentrations of latex colloids were caused by residual fluorescence from previous dye tests. When flow was started the already low bentonite colloid concentrations decreased further. The measured concentrations of latex colloids were also very low, although the arrival of very small amounts of latex colloids from L1 and L3 were noted at elution volumes suggesting pulse releases at the time flow was initiated. The subsequent drop in latex colloids provided evidence that bentonite erosion had become very small or had stopped altogether. Previous solute tests had demonstrated that if mobile tracers are released at L1 and L3, they will show up at L4 at known elution volumes. The lack of colloids appearing at L4 or detected at the other boreholes suggests that either colloids were not released from the bentonite or they were effectively retained by the fracture. Since latex colloids are assumed to be relatively mobile, their very low concentrations suggested that the release rate of colloids was low. Solute tracer tests performed before and after the bentonite erosion experiment indicated that some bentonite had migrated into the fracture, where it formed deposits that altered the transport properties of the fracture. This observation was noted during the mock-up tests. If bentonite had migrated within the fracture, why was there not significant colloid concentrations detected in the sampled fracture water? Using the mock-up experiment as an analogy, bentonite erosion and transport most likely occurred during the period of no flow. By the time flow was initiated the bentonite gel had stabilized and was no longer releasing significant amounts of colloid. Since the major driving force for bentonite colloid transport during the period of no flow is gravity, one could expect to see bentonite deposits down slope of the bentonite plugs. Therefore, the observations made during the mock-up and bentonite erosion tests provided strong clues as to what the bentonite distribution would look like when the fracture was opened.

The use of fluorescing latex colloids to mark bentonite emplaced in L1 and L3 proved to be very useful. When the Quarried Block was opened the fluorescence from latex colloids clearly marked the extent of bentonite deposition within the fracture at both borehole locations. This would not have been possible without the use of fluorescent colloids. This technique likely would be useful in field-scale tests in which compacted bentonite were placed in contact with water-bearing fractures. The fluorescence could be used to identify bentonite expansion and erosion into the fracture in overcore samples. Using the assumption that latex colloids are more mobile than bentonite and that bentonite erosion would release latex, the latex colloids could serve as a marker for bentonite erosion from a uniquely identifiable location. The low erosion rates of bentonite in the QB tests made it difficult to thoroughly test this assumption. Higher latex/bentonite mass ratios were noted in bentonite deposits than in the original borehole plugs, suggesting that the release of latex colloids from bentonite plugs may have been higher than the release of bentonite colloids. However, bentonite colloids were found wherever fluorescence was noted on the

fracture surface. Therefore, although latex colloids are more mobile than bentonite, their fluorescence can be used as a qualitative marker for the presence of bentonite colloids.

One can attempt to evaluate the effect of fracture geometry, as approximated by the aperture distribution, on bentonite erosion and deposition by comparing the observed fluorescence patterns observed on fracture surfaces with the fracture aperture model developed for the Quarried Block. Figure 39 shows the areas of significant fluorescence around the bentonite plugs at L1 and L3 superimposed on the fracture aperture model. Figure 39A shows the entire aperture model with an image of the lower fracture surface and the L1 and L3 bentonites superimposed over a section of the model. Figure 39 B&C show the region around L1 with and without the fluorescence. Figure 39 D&E show the region around L3 with and without the fluorescence.

At L1 the bentonite had filled the void located just above L1 (Figure 39 C). The mass of bentonite in this void, together with the mass of the recovered bentonite plug, was approximately the same as the mass of bentonite remaining in borehole L3. The expansion of the bentonite ring to the top of the figure may have been limited by a small fracture splay just above L1. The bentonite deposits appear to stream down slope toward the left, cut across the pattern of fracture aperture distribution. The exception may be a lineament that appeared to limit bentonite movement toward S5. However, within the bentonite streams, individual deposits appear to be aligned with the local geometry of aperture distribution. An explanation for the pattern in the down slope deposits could be that during the no flow expansion phase bentonite filled the fracture space, guided by gravity and boundaries established by fracture splays. When flow was initiated, local erosion may have occurred in areas of higher flow associated with larger aperture. Any eroded bentonite was probably deposited locally in areas of lesser flow velocity. In any case, the amount of redistributed bentonite was very small.

The fracture aperture in the vicinity of L3 was smaller and more uniformly distributed compared to L1. This may help to explain why the mass of bentonite gel, which was slightly less than at L1, had a slightly larger expansion diameter. The down slope bentonite deposits at L3 appear bounded above and below by regions of larger aperture, which correspond to fracture splays. These splays likely served as boundaries that may have influenced the down slope movement of bentonite. Although bentonite erosion could have occurred in these regions of larger aperture, the lack of bentonite deposits on the other side of these splays suggests that their main influence was in the form boundaries during the initial period of no flow. Between the splays the aperture distribution was relatively uniform. The overall pattern of down slope bentonite deposits was similar to what was observed in the mock-up tests, except for local variations induced by the fracture geometry.

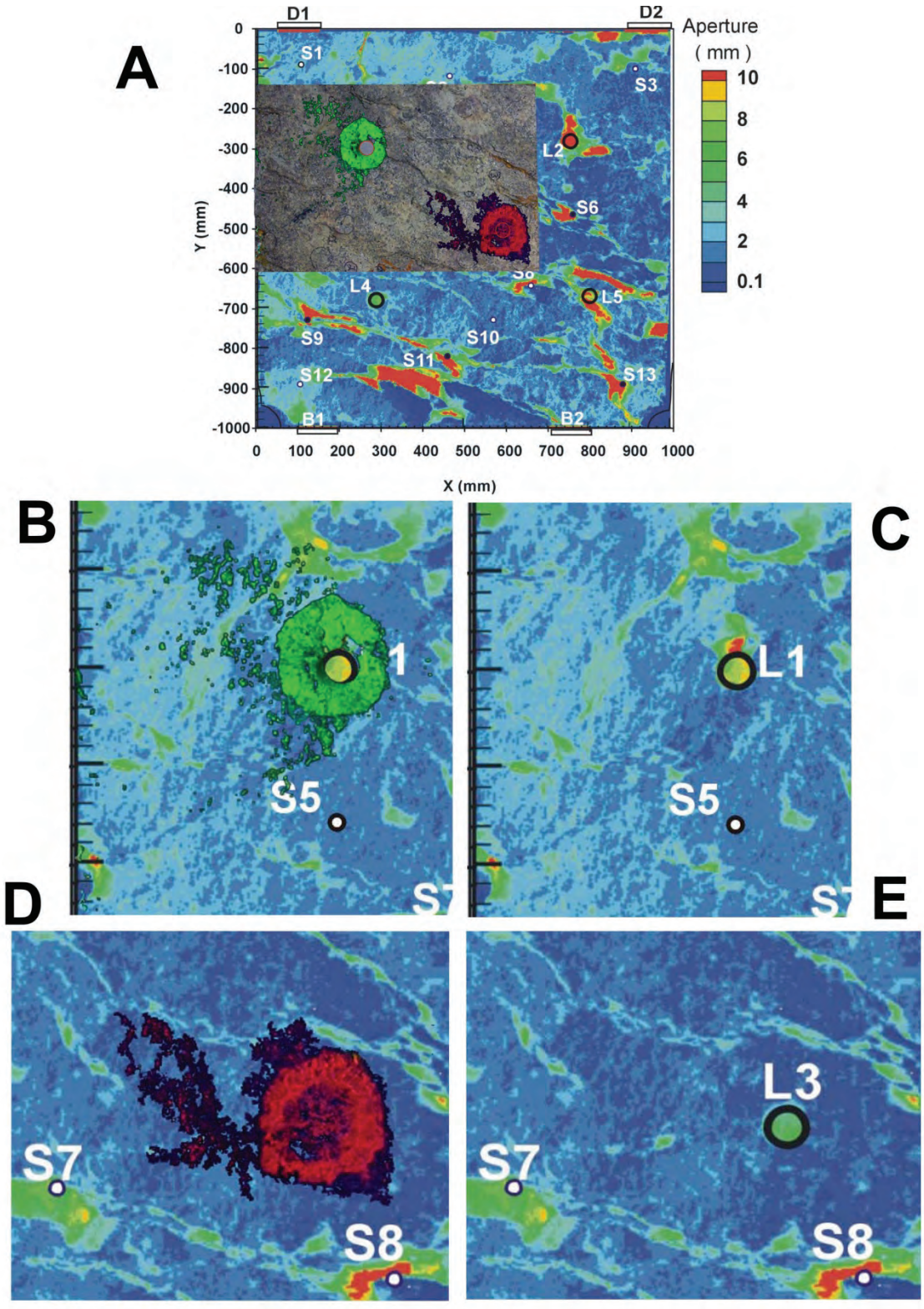

Figure 39: Fluorescence from Bentonite Plugs Superimposed on Fracture Aperture Model. (A) View of Entire Fracture. (B) and (C) L1 With and Without Fluorescence. (D) and (E) L3 With and Without Fluorescence.

The results of the Quarried Block test were remarkably consistent with the mock-up tests. Any differences can be attributed to longer times and different fracture geometries. The bentonite concentrations (0.04 to 0.65 mg/L) eluted from the Quarried Block were lower than observed in the mock-up tests. This could be due to the longer transport distances or that the gel had more time to stabilize in the Quarried Block. However, when flow was started in Test 8, with a longer period of no flow and a sloped fracture, bentonite colloid concentrations dropped to the same levels seen in the Quarried Block. This suggests that colloid removal from the flow system occurs by entrapment in low spots, such as the lower side of the fracture, is an important mechanism for bentonite colloid filtration. Down slope movement and deposition of bentonite colloids was observed in both types of tests. Changes in fracture transport pathways were observed in both tests. This is consistent with a picture of initial bentonite erosion and down slope movement of bentonite followed several hundred hours later by bentonite gel stabilization and attachment to fracture surfaces. The result is the presence of bentonite deposits that resist further erosion and colloid generation, and are able to alter fracture transport properties. The fracture aperture distribution in the Quarried Block had some effect on the shape of the bentonite deposits. However, the effect of fracture slope was consistently more important than aperture distribution.

4. SUMMARY AND CONCLUSIONS

The results of the bentonite erosion experiment in the Quarried Block were consistent with observations made with the mock-up experiments in a simple fracture. Bentonite erosion and colloid generation were found to be affected by water composition, bentonite composition, fracture dip and fracture aperture.

As expected, water chemistry had the greatest impact, with significantly higher bentonite erosion and colloid generation rates observed in deionized water compared to synthetic Grimsel water. The Grimsel water provides a much better approximation of glacial melt water, than does deionized water. Steady state concentrations of bentonite colloids released from Na-rich bentonites in waters representative of glacial melt waters ranged from 0 and 3 mg/L, while steady-state colloid concentrations released from Ca-montmorillonite varied from 0.2 to 0.5 mg/L. In the presence of small quantities of divalent salts bentonite gels developed a more stable structure with time that became resistant to further erosion. Transported bentonite colloids formed deposits that become resistant to erosion and altered flow properties within the fracture. When water flow was initiated there was a significant increase in bentonite erosion and colloid generation in dilute water. However, in the presence of synthetic Grimsel water, water flow had a minimal effect on colloid generation.

Gravity is an important force that drives bentonite transport in fractures and promotes bentonite erosion. As a result, fracture slopes had a significant influence over bentonite colloid transport and deposition under the water compositions used in this study.

Bentonite expansion into the synthetic fracture with a larger aperture (5 mm compared to 1 mm) was more extensive, due to less wall resistance for a given fracture volume and possibly because of gravity driven erosion. The effect of aperture distribution in the Quarried Block had a minor effect on bentonite deposition patterns.

The size distribution of transported bentonite colloids depended upon water chemistry, bentonite composition, and fracture slope. Average sizes ranged between 200 and 500 nm in dilute water and increased to between 300 and 1400 nm in Grimsel water. When a fracture slope was present the larger colloids were trapped in the lower part of the fracture, leaving transport mainly to the very small 10 nm colloids. Fracture slopes enhance colloid entrapment and reduce colloid and contaminant transport that is upward or across the sloping fracture.

The results of the Quarried Block tests indicate that in waters containing millimolar amounts of dissolved salts (representative of glacial melt water) the bentonite that expands into an open fracture is likely to form stable deposits that do not release significant concentrations of bentonite colloids.

The fraction of bentonite mass loss due to erosion or colloid generation in the presence of Grimsel type groundwater is very small. Although 13 to 14 percent of the bentonite expanded into the fracture in the form of gel deposits, less than 0.15 percent of the original bentonite mass was observed in the form of deposited or transported bentonite colloids. This amount is insignificant given the uncertainty in the overall bentonite mass balance (~ 3 to 5 %)

ACKNOWLEDGEMENTS

The work described in this report was carried out by AECL with funding from NWMO Technical Program, under Contract GS04, and from SKB as part of the Colloid Transport Project F91P1.

REFERENCES

Bessho, K. and C. Degueldre. 2009. Generation and sedimentation of colloidal bentonite particles in water. Applied Clay Science, 43, 253-259.

Boek E S, P.V. Coveney, and N.T. Skipper. 1995. Monte Carlo molecular modelling studies of hydrated Li-, Na- and K-smectites: Understanding the role of potassium as a clay swelling inhibitor. Journal American Chemical Society, 117, 12608–12617.

Brown H.G. 2002. Glacier meltwater hydrochemistry. Appl. Geochem. 17, 855-883.

Degueldre, C., P. Aeberhard, P. Kunze, and K. Bessho. 2009a. Colloid generation/elimination dynamic processes: Toward a pseudo-equilibrium? Colloids and Surfaces A: Physiochem. Eng. Aspects, 337, 117-126.

Degueldre, C., J. Raabe, and S. Wold. 2009b. Applied Geochemistry, 24, 2015-2018.

Derjaguin, B. and L. Landau. 1941. Theory of the stability of strongly charged lyophobic sols and of the adhesion of strongly charged particles in solutions of electrolytes. Acta Physico Chemica URSS, 14, 633.

García-García, S., C. Degueldre, S. Wold and S. Frick. 2009. Determining pseudo-equilibrium of montmorillonite colloids in generation and sedimentation experiments as a function of ionic strength, cationic form, and elevation. Journal of Colloid and Interface Science, 335, 54-61.

Jansson, M. 2009. Bentonite erosion laboratory studies. SKB Technical Report TR-09-33.

Lajudie, A., J. Raynal, J-C. Petit and P. Toulhoat. 1995, Clay-based materials for engineered barriers: A review. In Materials Research Society Symposium Proceedings, V 353.

Liu , J. and I. Neretnieks. 2006. Physical and chemical stability of the bentonite buffer, SKB Report R-06-103.

Liu, L., L. Moreno and I. Neretnieks. 2009. A dynamic force balance model for colloidal expansion and its DLVO-based application. Langmuir 25, 679-687.

Missana, T., Alonso, U., Turrero, J. M. 2003. Generation and stability of bentonite colloids at the bentonite/granite interface of a deep geological radioactive waste repository. Journal of Contaminant Hydrology 61, 17-31.

Möri, A., W.R. Alexander, H. Geckeis, W. Hauser, T. Schäfer, J. Eikenberg, T.H. Fierz, C. Degueldre, and T. Missana. 2003. The colloid and radionuclide retardation experiment at the Grimsel Test Site: Influence of bentonite colloids on radionuclide migration in a fractured rock. Colloids and Surfaces A: Physicochemical and Engineering Aspects Vol. 217, No. 1-3, p. 33-47.

Rao, S.N. and P.K. Mathew. 1995. Effects of exchangeable cations on hydraulic conductivity of a marine clay. Clays and Clay Minerals, 43, 433-437.

Sjöblom, R., P. Kalbantner, H. Bjurström and R. Pusch. 1999. Application of the general microstructural model to erosion phenomena -- mechanisms for the chemical-hydrodynamic conversion of bentonite to a pumpable slurry in conjunction with retrieval. Engineering Geology 54, 109-116.

SKB. 2006. Buffer and backfill process report for the safety assessment SR-Can. Technical Report, TR-06-18.

Vilks, P. and N.H. Miller. 2009. Bentonite and Latex Colloid Migration Experiments in a Granite Fracture on a Metre Scale to Evaluate Effects of Particle Size and Flow Velocity. NWMO TR-2009-26, Toronto, Ontario.

Vilks, P. and N.H. Miller. 2006. Laboratory Bentonite Colloid Migration Experiments to Support the Aspo Colloid Project. Ontario Power Generation Supporting Technical Report 06819-REP-01300-10123-R00, Toronto, Ontario.

Zbik, M.S., W.N. Martens, R.L. Frost, Y-F. Song, Y-M. Chen, and J-H. Chen. 2008. Transmission X-ray Microscopy (TXM) Reveals the Nanostructure of a Smectite Gel. Langmuir 2008, 24, 8954-8958.

APPENDIX A: LOCATIONS OF SWAB SAMPLES

CONTENTS

A.1 LOCATIONS OF SWAB SAMPLES

Figures A1 to A4 show the locations of the swab samples superimposed on images of the fracture surface photographed under UV light. The fluorescence shown is that observed before swab sampling took place. The geometry of each swabbed area was determined by the visible wetted area photographed under visible light immediately after the swab sample was taken.

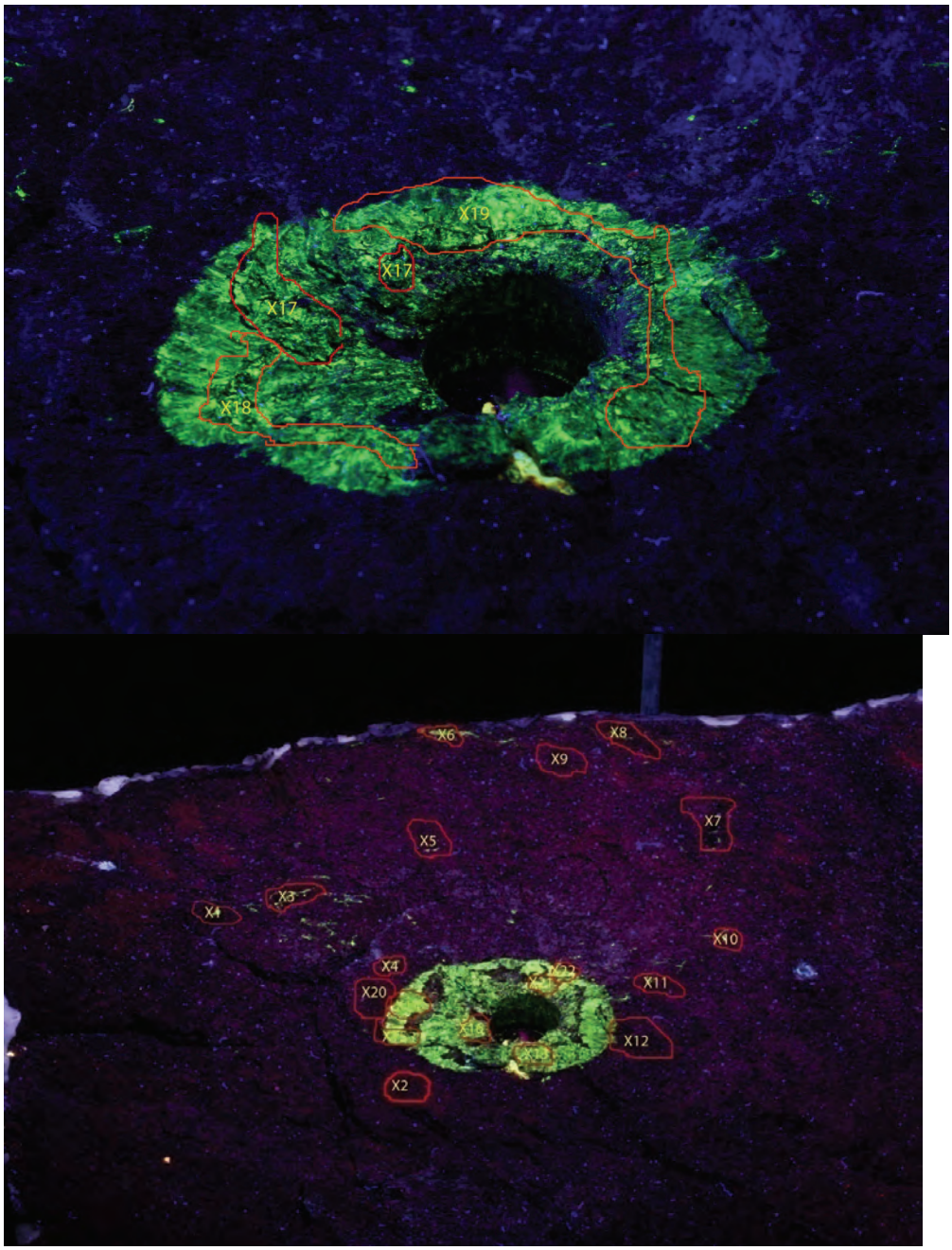

Figure A- 1: L1 Top Sample Locations

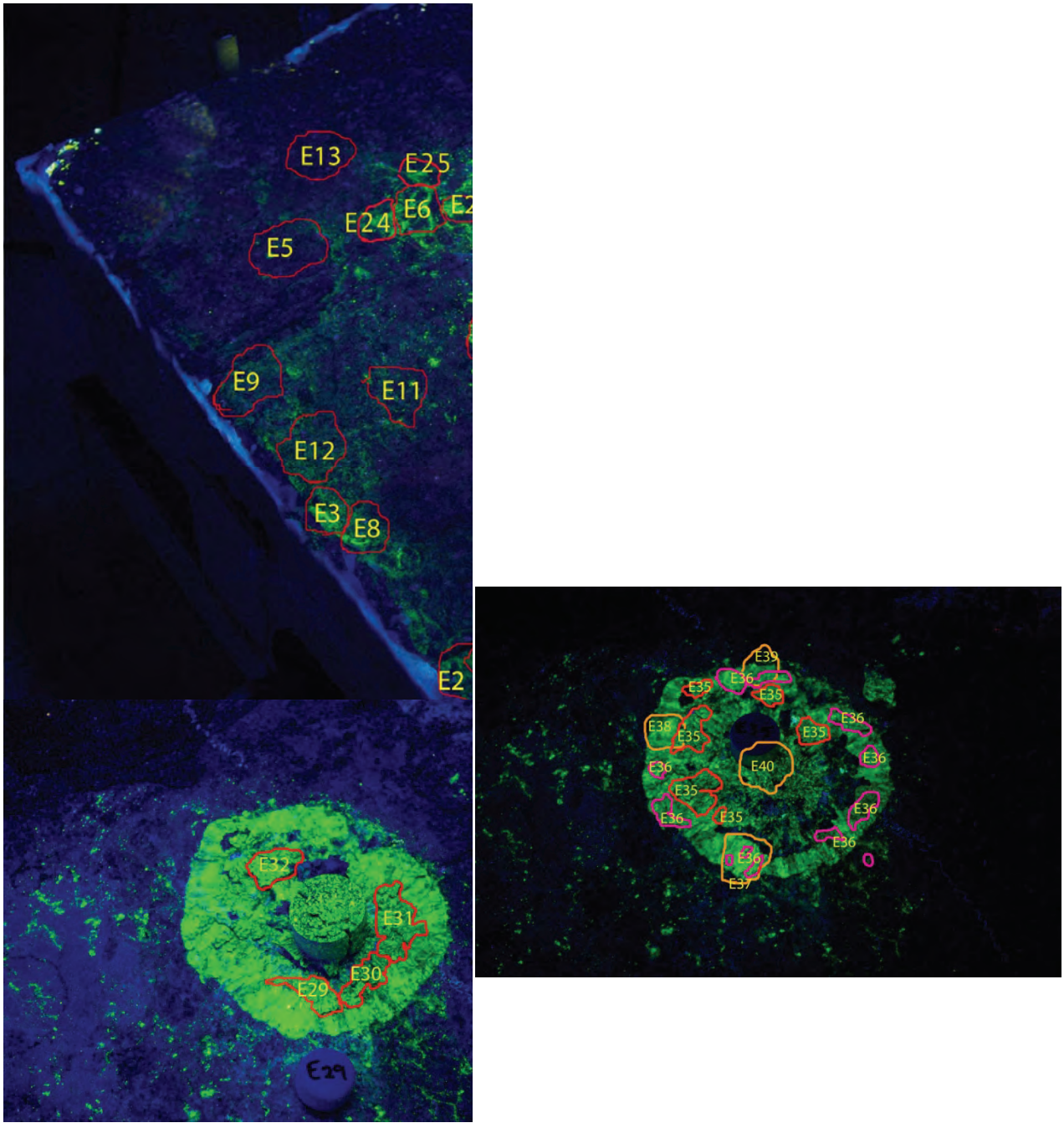

Figure A- 2: L1 Bottom Sample Locations

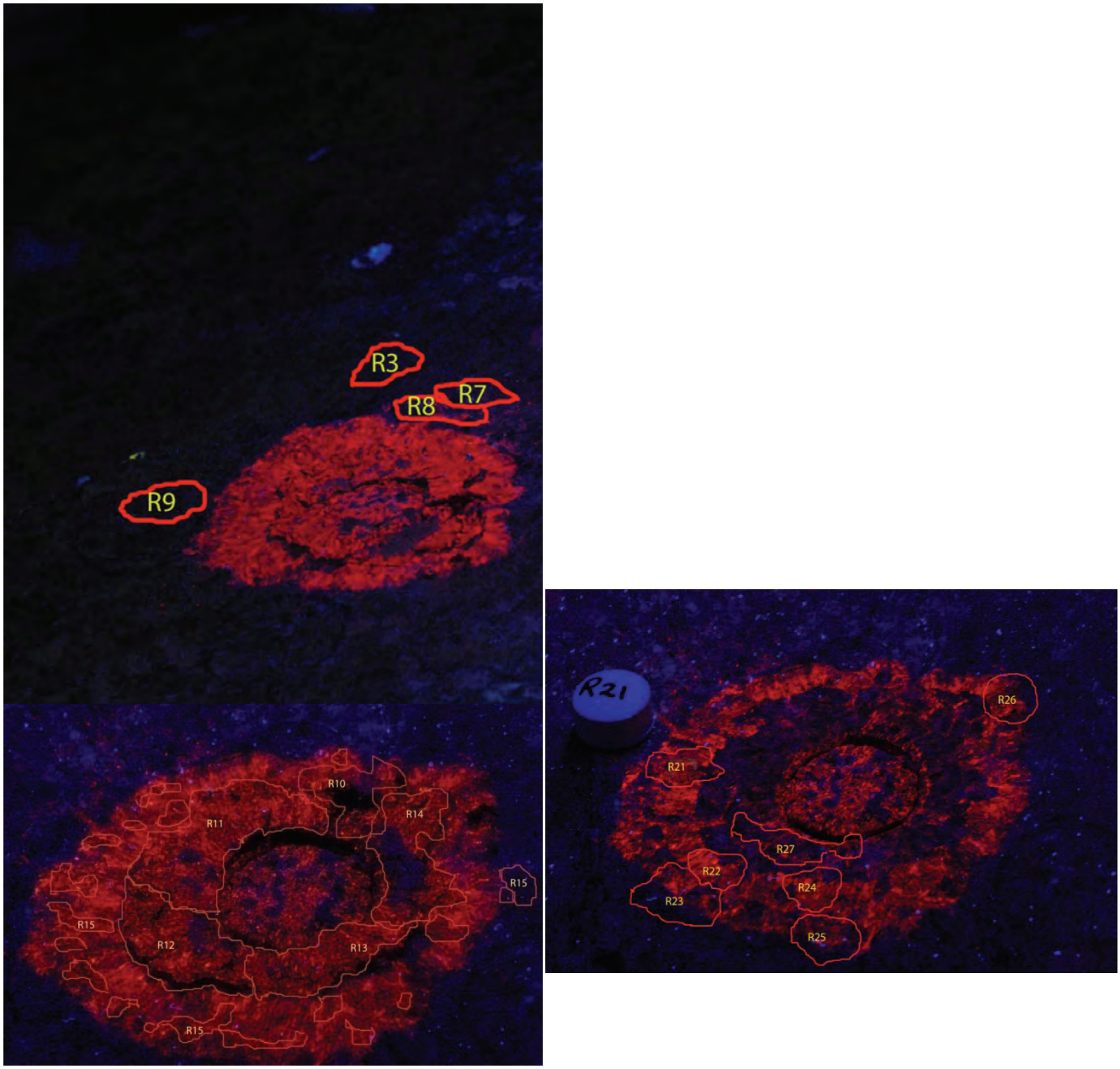

Figure A- 3: L3 Top Sample Locations

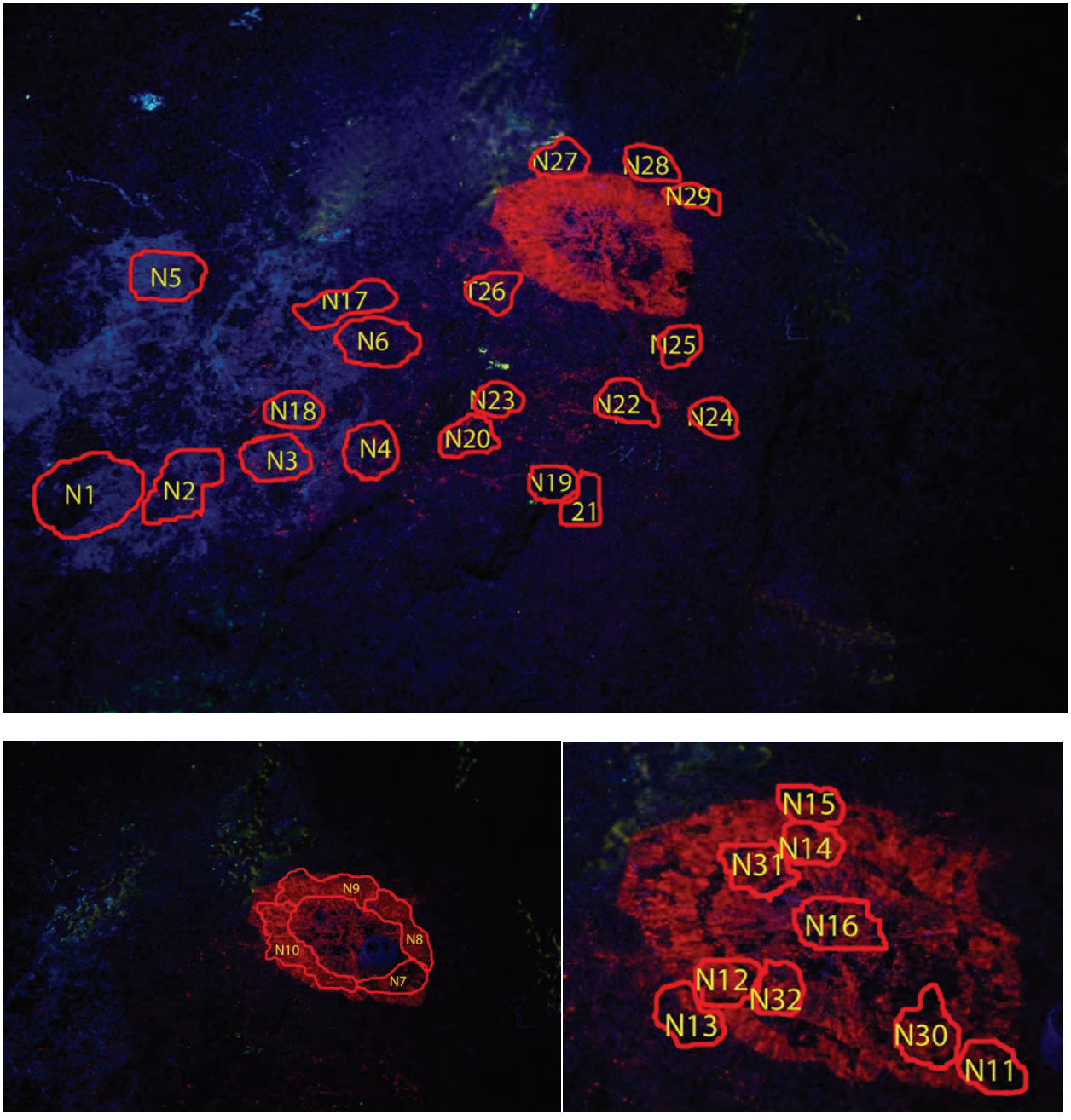

Figure A- 4: L3 Bottom Sample Locations